NAV1.1 AND NAV1.6: ELECTROPHYSIOLOGICAL PROPERTIES, EPILEPSY-ASSOCIATED MUTATIONS AND THERAPEUTIC TARGETS

Reesha R. Patel

Submitted to the faculty of the University Graduate School in partial fulfillment of the requirements
for the degree
Doctor of Philosophy
in the Program of Medical Neuroscience,
Indiana University

July 2016

Accepted by the Graduate Faculty, Indiana University, in partial fulfillment of the requirements for the degree of Doctor of Philosophy.

_____

Theodore R. Cummins, Ph.D., Chair

Doctoral Committee

_____

Andy Hudmon, Ph.D.

_____

Michael R. Vasko, Ph.D.

May 25, 2016

_____

Patrick L. Sheets, Ph.D.

_____

Xiaoming Jin, Ph.D.

DEDICATION

This work is dedicated to my loving and supportive parents, Rajni and Smita Patel, brother, Shaun Patel and husband, Sandeep Mehta.

ACKNOWLEDGMENTS

This dissertation would not have been possible without the support of many people, to whom I would like to express my deepest gratitude. The encouragement, kindness and support you have given me truly made my graduate experience memorable.

First and foremost, I would like to thank my graduate advisor, Dr. Theodore Cummins. My scientific achievements are credited to his constant encouragement, guidance and patience. He is truly an inspirational scientist, and I am incredibly grateful to have worked under his mentorship.

I would also like to thank my committee members: Dr. Andy Hudmon, Dr. Patrick Sheets, Dr. Michael Vasko and Dr. Xiaoming Jin. Their guidance has shaped my scientific thinking, steered the direction of my research aims and made the successful completion of this dissertation possible.

I am especially grateful for all the members of the Cummins lab, past and present: Dr. Yucheng Xiao, Dr. Zhiyong Tan, James Jackson, Adrianne Jackson, Cindy Barbosa, Zifan Pei, Claudia Pan, Emily Mason, Dr. John Theile and Dr. Weihua Song. Their continual support greatly influenced my scientific accomplishments and the atmosphere they created truly made coming to lab fun. I am honored to have worked with them.

I would also like to acknowledge collaborators for the work presented in this dissertation. Dr. Xioming Jin and Dr. Xingjie Ping provided essential guidance in conducting multielectrode array experiments. Nickolay and Tatiana Brutevetsky provided striatal neuron cultures critical for examining the effects of cannabidiol on neuronal excitability.

Outside of scientific guidance, there have been many people who have helped make this dissertation possible including the administrative staff of the Stark Neurosciences Research Institute, the Indiana School of Medicine Biomedical Gateway (IBMG) program and the Graduate school: Dr. Gerry Oxford, Nastassia Belton, Diana Kelley, Amy Lawson, Monica Henry, Dr. Simon Rhodes and Debra Barker. I am especially grateful to Dr. Joseph Bidwell for his encouragement in applying to and joining the IBMG program and Dr. Gerry Oxford for his support throughout graduate school.

I would like to thank all my fellow graduate students and in particular: Aarti Chawla, Cindy Barbosa, Lauren Federici, Zifan Pei and Derrick Johnson, without you the days would have felt much longer.

Most importantly, none of this would have been possible without the unconditional love of my family. I am incredibly fortunate to have them and cannot express enough gratitude to them for everything they have done for me. My mom and dad, Rajni and Smita Patel, have given me unwavering support in all of my

endeavors and continuously encouraged me to achieve my highest potential. My brother and role model, Shaun Patel, introduced me to the field of neuroscience, has always encouraged me to challenge myself and supported me through both my accomplishments and failures despite having torn down all of his Lego masterpieces when we were younger. My dog, Anaya Patel, has the unique ability to remind me that there is always time for a walk and a belly rub might make up for a wasted day on failed experiments. And last but not least, my husband, Sandeep Mehta, stayed with me through graduate school, agreed to spend the rest of our lives together and has always given me nothing but endless support and love.

Reesha R. Patel

NAV1.1 AND NAV1.6: ELECTROPHYSIOLOGICAL PROPERTIES, EPILEPSY-ASSOCIATED MUTATIONS AND THERAPEUTIC TARGETS

Voltage-gated sodium channels (VGSCs) are critical for the initiation and propagation of electrical signals in neurons; consequently they are significant regulators of neuronal excitability. They are exquisitely tuned and aberrations in their activity can lead to pathophysiological conditions. This dissertation highlights the roles of two prominent brain isoforms of VGSCs, Nav1.1 and Nav1.6. These isoforms have distinct localization in the brain. Specifically, Nav1.1 is predominantly expressed in the soma and proximal axon initial segment (AIS) of GABAergic neurons, while Nav1.6 is found at the distal AIS and nodes of Ranvier of both GABAergic and excitatory neurons. Several mutations have been identified in Nav1.1 and recently mutations in Nav1.6 have been discovered in patients with distinct epileptic phenotypes that respond poorly to current anti-epileptics. There is a need to better understand mechanistically how mutations in these channel isoforms lead to epilepsy in order to identify more efficacious treatment strategies. Therefore, the aims of this dissertation were to 1) examine the differential biophysical properties of Nav1.1 and Nav1.6, 2) determine the biophysical consequences of epilepsy-associated mutations in Nav1.1 and Nav1.6 and examine the effects of cannabinoids on wildtype and mutant channel activity and 3) test the effects of selective inhibition of Nav1.1 versus Nav1.6 on epileptiform activity. To address these aims, whole-cell electrophysiology and mutlielectrode array recordings were used. The

results demonstrate that 1) Nav1.1 and Nav1.6 have important differences in their biophysical properties that may be important in the fine-tuning of neuronal excitability, 2) epilepsy-associated mutations in Nav1.1 and Nav1.6 alter several biophysical properties of the channels but have differential effects on resurgent current generation suggesting a divergence in the mechanism by which they induce epileptogenesis and cannabidiol can inhibit aberrant channel activity and reduce neuronal excitability and 3) pharmacological inhibition of Nav1.6, but not Nav1.1, abolishes epileptiform activity. Overall, this dissertation provides insight into the distinct contributions of Nav1.1 and Nav1.6 to physiological and pathophysiological firing activity and their ability to be targeted for therapeutic purposes. This knowledge is critical for understanding the potential role of VGSCs in epilepsy syndromes and identifying possible drug targets for more efficacious treatment strategies.

Theodore R. Cummins, Ph.D., Chair

TABLE OF CONTENTS

LIST OF TABLES

LIST OF FIGURES

LIST OF ABBREVIATIONS

4-AP	4-aminopyridine
ACSF	Artificial cerebrospinal fluid
AEA	Anandamide
AED	Anti-epileptic drug
AP	Action potential
BACE1	β-site APP-cleaving enzyme 1
CBD	Cannabidiol
CNS	Central nervous system
DRG	Dorsal root ganglion
EGFP	Enhanced green florescent protein
EIEE	Early infantile epileptic encephalopathy
FHF	Fibroblast homologous factors
GEFS+	Generalized epilepsy with febrile seizures plus
HEK293T	Human Embryonic Kidney Cells with SV40 Large T-Antigen
LFP	Local field potential
MPL	1-methyl-2-pyrrolidinone
SMEI	Severe myoclonic epilepsy in infancy
TTX	Tetrodotoxin
VGSC	Voltage-Gated Sodium Channel
WT	Wildtype

I. INTRODUCTION

A. Overview

Epilepsy is one of the earliest brain disorders to be described in an ancient Babylon text on medicine, *Sakikku* – meaning 'all diseases,' over 3,000 years ago, yet it still remains one of the most prevalent neurological disorders affecting over 3 million people in the US alone and 65 million people worldwide according to Citizens United for Research in Epilepsy (CURE). Epilepsy is the development of repeated, unprovoked episodes of abnormal electrical activity manifesting as episodes of convulsions or loss of consciousness called seizures. It is a frequently debilitating condition that results from an imbalance in the excitatory and inhibitory activity in the brain. The etiology of epilepsy has been linked to infection, trauma, genetic mutations, and other disorders of the brain. This dissertation focuses on genetic mutations identified in brain isoforms of voltage-gated sodium channels, Nav1.1 and Nav1.6, resulting in distinct phenotypes classified as early infantile epileptic encephalopathy 6 (EIEE6) and early infantile epileptic encephalopathy 13 (EIEE13), respectively.

Voltage-gated sodium channels (VGSCs) are critical for the initiation and propagation of electrical signals in neurons; consequently they are significant regulators of neuronal excitability. Their activity is exquisitely tuned and aberrations in their activity lead to pathophysiological conditions. Several hundreds

of mutations have been identified in the *Scn1a* gene coding Nav1.1 and with the advancement of whole-exome sequencing, mutations in *Scn8a* coding for Nav1.6 recently have been identified. Our current understanding of the expression of these channels in the brain along with the biophysical consequences of the many Nav1.1 mutations and few Nav1.6 mutations that have been characterized in heterologous expression systems provides insight into possible mechanisms by which they lead to changes in neuronal excitability, setting up a circuit susceptible to abnormal, hyper-synchronous activity. One potential mechanism that has not yet been examined is alterations in resurgent sodium current generation by epilepsy-associated mutant channels. Resurgent sodium current is an atypical, near threshold current that occurs immediately following an action potential and is predicted to enhance neuronal excitability. This dissertation examines the biophysical consequences of epilepsy-associated mutations in Nav1.1 and Nav1.6 with a specific focus on resurgent sodium current.

Despite the development of new anti-epileptic drugs (AEDs), approximately 20 to 40% of patients with a seizure disorder are refractory to treatment [1]. EIEE6 and EIEE13 are intractable epilepsy syndromes that respond poorly to classic AEDs. In the case of EIEE6, classic AEDs that target VGSCs are contraindicated and may exacerbate seizures. Alternative therapeutic strategies are being pursued including: Nav1.1 activators, ketogenic diets, and exogenous cannabinoids. Cannabidiol (CBD) has received much attention for its potential to treat intractable pediatric epilepsies, but still lacks scientific validation of its efficacy. The molecular mechanisms by

which CBD exerts anti-epileptic effects are largely not known. This dissertation examines how both endogenous and exogenous cannabidnoids modulate wildtype and mutant VGSC activity and how selective targeting of specific VGSC isoforms alters epileptiform activity.

Overall, this dissertation provides insight into the biophysical properties of brain isoforms of voltage-gated sodium channels, their potential contribution to physiological and pathophysiological firing activity, and their ability to be targeted for therapeutic purposes. This knowledge is critical for understanding the potential role of VGSCs in genetic and acquired epilepsy syndromes and identifying possible drug targets for more efficacious treatment strategies.

B. Brief history of the discovery of voltage-gated sodium channels

Neurons, and other excitable cells, can communicate through electrical signals termed action potentials. Seminal work by Hodgkin and Huxley set the foundation of our understanding of the underpinnings of action potentials. In 1939, Hodgkin and Huxley inserted a glass microelectrode into the giant squid axon, directly measuring the potential across the membrane, and recorded the first intracellular action potential [2]. They found that the during the action potential the interior of the nerve becomes substantially more positive then the exterior and later attributed this to an increase in the permeability of the membrane to sodium ions [3]. To further study current voltage relationships of the ionic currents, they and

others created a new technique called voltage-clamp, which allowed them to maintain the membrane at a specific potential. In a series of landmark papers, Hodgkin and Huxley described and quantitatively detailed the voltage-dependent ionic currents underlying the action potential – the Hodgkin and Huxley model [4-7]. This foundational work later led to the idea proposed by Hille, Armstrong and others in the 1960s that sodium and potassium are conducted by specific ion channels [8-11].

Selective block of channels by a puffer fish toxin, tetrodotoxin (TTX), and tetraethylammonium suggested that sodium and potassium ions must pass through separate aqueous pores [10, 12, 13]. This was confirmed with development of the patch clamp technique by Erwin Neher and Bert Sakmann in 1976 - in which a glass pipette is pushed against the cell membrane forming a tight seal with a resistance in the Gigaohm range, pulled away from the cell creating a membrane vesicle at the tip of the pipette, after which the membrane patch is ruptured to allow recording from single channels [14, 15]. The functional properties of the channel and molecular models of the function of VGSCs were further established in the 1970s by Hille, Armstrong, Bezanilla and others [16].

In 1980, the voltage-gated sodium channel α subunit was first purified from the electric eel (*Electrophorus electricus*) [17]. The channels were then identified with scorpion toxins by photoaffinity labeling revealing a large α subunits of 260 kDa [18]. Cloning and sequencing cDNA encoding the α subunits of sodium channels

established their primary structure and showed that mRNA encoding the α subunit is sufficient for expression of functional channels [19-21]. In recent years, the first glimpse into the three dimensional structure of these channels was uncovered with the crystal structure of a related homo-tetrameric bacterial sodium channel [22]. Since their discovery, these channels have been extensively studied, and while our understanding of them has come a long way there is still much we do not know.

C. Voltage-gated sodium channels

1. Brief Description

Voltage-gated sodium channels consist of a large α subunit (~260 kDa) that can associate covalently and non-covalently with auxiliary proteins including β subunits (~30-40 kDa) of which there are four: Navβ1 – Navβ4. The alpha subunit is made up of approximately two thousand amino acid residues that form a complex tertiary structure consisting of four homologous domains (DI-DIV) linked by intracellular loops wherein each domain contains six transmembrane segments (S1-S6) (Figure 1A) [19]. The S1 to S4 segments within each domain come together to form the voltage sensing module. Specifically, the S4 segment contains multiple (four to eight) positively charged, basic residues (mostly arginines but also lysines) that allow it to 'sense' changes in potential across the membrane, and therefore it is often referred to as the voltage sensor [19]. The S5-S6 segments and the outer loop between them known as the P loop form the pore-forming module and selectivity

filter. The three-dimensional structure of the channel, modeled in part from the crystal structure of the bacterial sodium channel, suggests that the four domains arrange symmetrically with the voltage sensing module lying outside the pore-forming modules (Figure 1B) [23]. In a simplistic scheme, VGSCs primarily transition between three states as a result of movement of the voltage sensors and consequent conformational changes in the channel. At resting, hyperpolarized potentials channels are predominately in a closed state and upon depolarization channels transition to an open state to conduct sodium ions after which the channels enter an inactivate state (Figure 1C).

2. Activation and ion conduction

Rapid, voltage-dependent activation of VGSCs, resulting in opening of the channel upon depolarization, is due to outward movement of the DI-DIII voltage sensors. The first description of this by Hodgkin and Huxley was insightful and still remains accurate. They demonstrated the steep voltage-dependence of activation of sodium channels and attributed it to the movement of three 'electrically charged particles' across the membrane [24]. Cloning and sequence analysis of the sodium channel gave insight into the structure of these channels and the hypothesis that the S4 segments, due to the many basic residues it contains, might act as a voltage sensor [19]. Later, mutagenesis studies demonstrated that indeed mutating the positive residues in the S4 segments leads to a decrease in the steepness of the voltage-dependence of activation curve [25, 26]. The movement of the voltage

sensors has been described by a 'sliding helix' or 'helical screw' model in which the S4 segment rotates around its axis as it moves outward which is coupled to a rolling motion of the S1-S3 segments around the S4 sensor [27-29]. Other models have also been proposed which differ in the distance and nature of how the S4 segment moves [30]. Ultimately, outward movement of the voltage sensor results in opening of the activation gate formed by the portion of the S6 segment from each domain at the intracellular surface of the channel [22]. The rapid activation property of VGCSs is unique and allows for the steep upstroke of the action potential with the specific movement of sodium ions through the pore at nearly the rate of free diffusion [31].

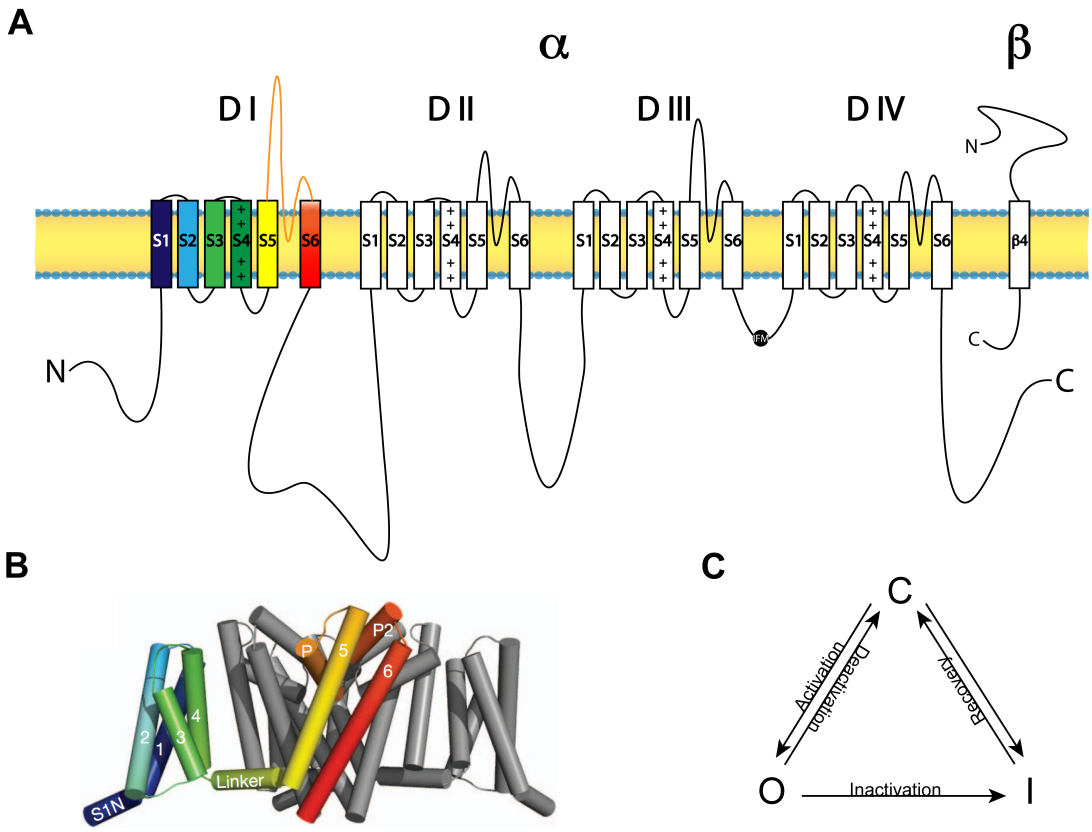

Figure 1. Voltage-gated sodium channels A, Linear schematic of the structure of voltage-gated sodium channels. B, Three-dimensional side view of the channel from the crystal structure of a bacterial voltage-gated sodium channel. C, Simplistic state transition model. This figure was created using Adobe Illustrator CS5. The three-dimensional structure pictured in panel B was taken with permission (see Appendix A) from Payandeh *et al.*, Nature, 2011.

The crystal structure of the bacterial sodium channel revealed four major parts to the pore including: a large extracellular funnel, a narrow ion selectivity filter, a large central cavity followed by the activation gate [22]. Several studies utilizing different methodological approaches demonstrated that the extracellular linker between S5-S6 segments, referred to as the P-loop, form the outer funnel and selectivity filter while the S6 segments come together to form the pore [31]. The selectivity of VGSCs for sodium ions arises from the selectivity filter creating a seamlessly hydrated path for the specific size and charge of sodium.

3. Inactivation

Within 1-2 milliseconds after opening, sodium channels typically undergo a process termed inactivation [4, 6] wherein the intrinsic inactivation particle binds the channel pore prohibiting sodium ions from passing which is commonly described by a hinged lid mechanism (Figure 2A). The first clues regarding the nature of the inactivation particle came from experimental application of proteolytic enzymes to the intracellular surface of the channels resulting in loss of inactivation which suggested that the inactivation particle is proteinaceous in composition and part of an intracellular region of the α subunit [11, 25, 32]. Antibodies targeting the DIII-DIV linker prevented inactivation and helped to further narrow the location of the inactivation particle [33, 34]. The inactivation particle was identified as three, highly conserved hydrophobic residues (isoleucine-phenylalanine-methionine) within the DIII-DIV linker; the phenylalanine residue being essential [35, 36]. The

binding site of the inactivation particle has been suggested to be coordinated by specific residues within the S3-S4 linker of both DIII and DIV [37, 38]. Another region of the channel important for inactivation, specifically in stabilizing inactivation and preventing channel reopening, is the C-terminal tail region proximal to the membrane [39, 40]. The process of inactivation is initiated and limited by movement of the DIV-S4 voltage sensor due to the subsequent conformational change in the channel exposing the binding site for the inactivation particle [41-43]. This property of voltage-gated sodium channels is critical for action potential repolarization in the absence of potassium channels and is responsible for the refractory period following an action potential spike - regulating firing frequency.

An alternative type of inactivation, referred to as slow inactivation, occurs on a longer timescale and is mediated by a structurally distinct process than fast inactivation [44]. Slow inactivation is considerably less well understood than fast inactivation. Structurally, it has been proposed to be the result of 'collapse' or rearrangement of the pore [45], although whether this is collapse of the inner or outer pore is controversial. Long depolarizations are needed to induce slow inactivation and recovery from slow inactivation can be on the orders of seconds or minutes. The functional role of slow inactivation on firing activity is not completely understood, but it has been suggested to be important in regulating excitability [46].

4. Diversity of isoforms

There are nine voltage-gated sodium channel α subunits: Nav1.1 – Nav1.9 [47]. These channels have distinct functional as well as pharmacological characteristics. One such pharmacological characteristic is their sensitivity to tetrodotoxin (TTX), which has been used to classify these channels into two major groups: those that are TTX-sensitive (Nav1.1, Nav1.2, Nav1.3, Nav1.6 and Nav1.7) with IC50 values in the low nM range and those that are TTX-resistant (Nav1.5, Nav1.8 and Nav1.9) with IC50 values in the μM range. These channels also have distinct expression patterns. Nav1.1, Nav1.2, Nav1.3 and Nav1.6 are predominantly expressed in the central nervous system (CNS). Nav1.4 is primarily expressed in skeletal muscle while Nav1.5 is primarily found in cardiac muscle. Nav1.7, Nav1.8 and Nav1.9 are primarily expressed in the peripheral nervous system. These channels are also expressed in tissues outside of their predominant locations to varying degrees.

5. Post-translational regulation

VGSCs are highly regulated proteins that can undergo extensive post-translational modifications throughout the intra- and extracellular regions of the channel. There is a large body of data indicating that Nav1.2 and Nav1.5 activity can be regulated by a multitude of post-translational modifications and second messenger proteins including: phosphorylation, palmitoylation, methylation and

calmodulin. Phosphorylation, the covalent addition of a phosphoryl group to serine, threonine or tyrosine residues mediated by various kinases, can modulate VGSC activity. Protein kinase A has been found to both increase and decrease peak sodium current [48-50]. Protein kinase C decreases sodium current and slows the rate of inactivation [51, 52] while Fyn kinase decreases peak sodium current, increases the rate of inactivation and shifts the voltage-dependence of inactivation to more hyperpolarizing potentials [53]. Other kinases have also been found to modulate VGSC activity [54, 55]. Less studied post-translational modifications such as palmitoylation, the covalent attachment of a lipid palmitate group to cysteine, serine or threonine residues catalyzed by thioesteraes, and methylation, the attachment of a methyl group to arginine or lysine residues, have also been found to modulate VGSC activity. Pharmacologically inhibiting palmitoylation of Nav1.2 slows the rate of inactivation as well as the recovery from inactivation [56]. Methylation of Nav1.5 increases peak sodium current by increasing surface expression of the channel [57]. Numerous other post-translational modifications have also been proposed to modulate VGSC activity and still others have not been explored.

Beyond post-translational regulation, many other interacting proteins or second messenger proteins, activated downstream of primary signaling molecules, can directly bind to the channel and modulate their activity. A major second messenger is calcium, which can lead to the activation of calmodulin. Calmodulin has been found to bind to different regions of VGSCs in the presence and absence of

calcium [58, 59]. Depending on the state of the calmodulin, region of interaction, and VGCS isoform, calmodulin can alter various properties of VGSCs [60].

Much less is known about modulation of Nav1.1 and Nav1.6. While Nav1.1, Nav1.2 and Nav1.6 are highly conserved; they exhibit clear differences in their functional properties. It is likely that these two isoforms are differentially modulated but this needs to be further explored. These modifications by signaling pathways and second messenger modifications can be altered in disease states and may be involved in episodic disorders such as epilepsy [61].

D. Resurgent sodium current

1. Mechanism

Resurgent sodium current is the result of unbinding of an open-channel blocker at intermediate repolarizing potentials following depolarization. After depolarization and channel opening, and under specific conditions, some fraction of the channels can undergo a blocked state that is faster than and distinct from classic fast inactivation. Upon repolarization to negative, intermediate potentials the blocker unbinds allowing the flow of resurgent current after which the channels inactivate or deactivate (Figure 2A) [62] . This can allow channels to cycle between open, blocked and unblocked states bypassing fast inactivation, which is responsible for the refractory period following an action potential, permitting rapid firing. As the open-channel blocker is thought to compete with the intrinsic inactivation particle

to bind the channel pore, the rate of fast inactivation is a major determinant of resurgent sodium current generation. This has been demonstrated with both toxins as well as by disease mutations that result in a slower rate of fast inactivation and consequently enhance resurgent sodium currents [63-65]. These currents were first described in cerebellar Purkinje neurons [66].

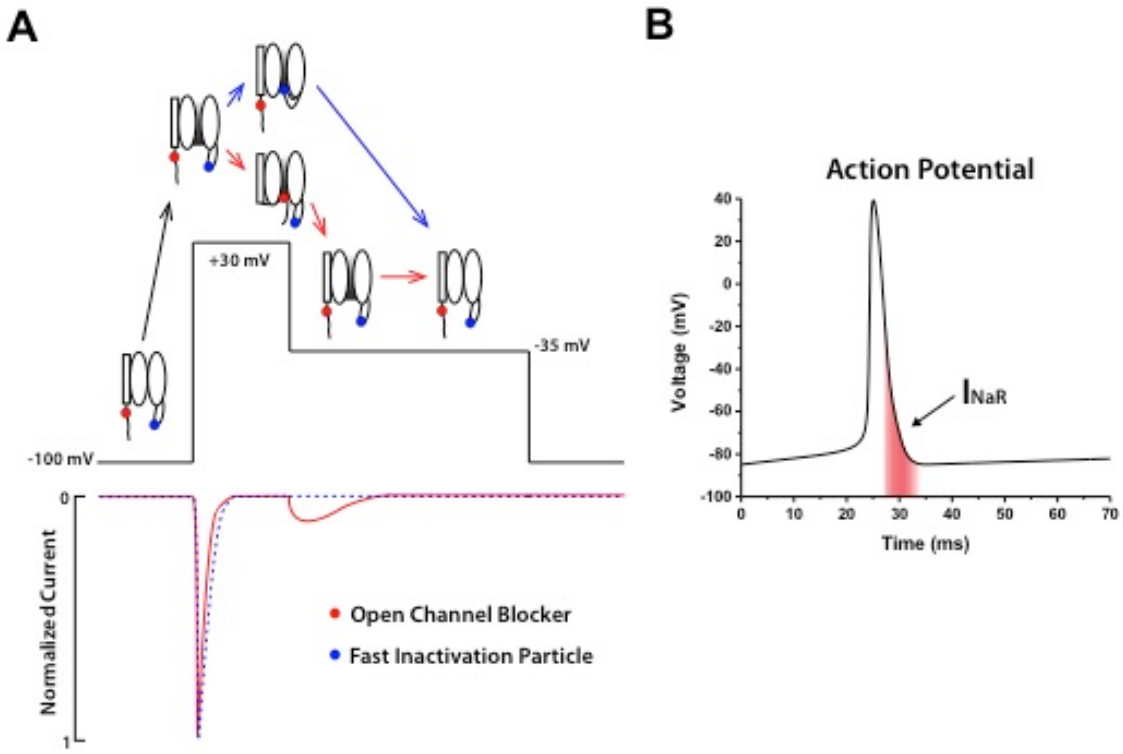

Figure 2. Mechanism of resurgent sodium current generation A, Illustration of channel conformations at each potential step in the voltage protocol. Current produced when channels undergo classic fast inactivation (blue dotted trace) versus current produced when some fraction of the channels undergo open channel block (red trace) can be seen below the corresponding voltage protocol. B, Depiction of where inward resurgent sodium current would occur during a typical action potential.

To date, the only identified endogenous open channel blocker implicated in resurgent current generation is Navβ4. Navβ4 – null mice have complete loss of resurgent sodium current in medium spiny neurons of the striatum [67]. Knockdown of Navβ4 via small interfering RNA in cerebellar granule neurons abolishes resurgent sodium current which can be restored with Navβ4 peptide [68]. Additionally, knockdown of Navβ4 in dorsal root ganglion (DRG) neurons decreased resurgent sodium current while overexpression of Navβ4 increased Nav1.6 mediated resurgent sodium current [69]. Specifically, the membrane proximal C-terminal portion of the Navβ4 subunit, containing several positively charged and hydrophobic/aromatic residues, acts as an open channel blocker. Indeed, intracellular addition of a peptide mimicking this sequence, $Navβ4_{154-167}$ (KKLITFILKKTREK), can recapitulate resurgent sodium currents in heterologous expression systems lacking an endogenous open channel blocker [70, 71]. Intriguingly, co-expression of the VGSC α subunit and Navβ4 is not sufficient to produce resurgent sodium currents in some heterologous expression systems (i.e. HEK293 and ND7/23 cells) suggesting that other modulatory proteins and/or cellular background factors are critical. A requirement for resurgent sodium current generation, at least in Purkinje neurons, is phosphorylation of part of the sodium channel complex [72]. Intracellular application of alkaline phosphatase to outside-out patches from Purkinje neurons abolishes resurgent sodium current and this can be partially rescued with the phosphatase inhibitor vanadate [63, 73]. Interestingly, β toxins, an exogenous open channel blocker, can produce a similar resurgent sodium current [74].

Several studies have identified modulatory proteins and chemical compounds that alter the activity of resurgent sodium current. Fibroblast homologous factors (FHFs), auxiliary proteins of sodium channels, inhibit resurgent current generation by biasing channels to an inactive state [75]. Inflammatory mediators can enhance fast resurgent sodium current as well as resurgent current with slow kinetics generated by TTX resistant Nav1.8 expressed in DRG neurons [76]. It is not entirely clear how inflammatory mediators increase resurgent sodium current generation, but one possibility is that these molecules are acting indirectly via signaling pathways leading to post-translational modification of the channel complex. Indeed, protein kinase C phosphorylation of a serine residue (1479) in Nav1.7 has been shown to increase resurgent sodium current generation [77]. Blood-depressing substance I modestly slows the rate of inactivation of sodium currents isolated from Purkinje neurons, and dramatically increases resurgent sodium current [78]. Navβ4 has been identified to be a target of β-site APP-cleaving enzyme 1 (BACE1). BACE1 knockout in Purkinje neurons demonstrates an increased rate of resurgent sodium current decay compared to wildtype resulting in a slower spontaneous firing rate [79]. Chemical compounds have also been shown to enhance or inhibit resurgent sodium currents. Oxaliplatin, a chemotherapeutic drug, increases Nav1.6 mediated resurgent and persistent sodium current from DRG neurons at cooler (22°C) temperatures, which is thought to mechanistically underlie the cooling-aggravated neuropathy seen with oxaliplatin treatment. [80]. Conversely, anandamide (AEA), an endogenous cannabinoid, can selectively inhibit

resurgent sodium current over peak transient current generated by Nav1.7 in HEK293 cells [81].

2. Functional implications

The brief reopening of channels, due to unbinding of the open-channel blocker, during the repolarization phase of the action potential provides a depolarizing drive to approach threshold for firing additional action potentials. Channels that undergo open-channel block recover faster from apparent inactivation and are available after an action potential spike effectively decreasing the refractory period following an action potential spike [62, 82]. Indeed, sodium currents have been observed to flow during the interval between action potentials [82, 83]. Therefore, these currents are predicted to enhance neuronal excitability. Accordingly, knockdown of Navβ4, preventing resurgent current generation, decreases both spontaneous firing as well as repetitive firing with long depolarization stimuli [67-69]. Modeling studies have corroborated these findings [84-86]. Importantly, while resurgent current facilitates rapid firing and burst firing, it is not sufficient for this spiking pattern. The density and localization of the full complement of ion channels determines the spiking pattern of a neuron.

3. Expression

The major channel that generates resurgent sodium current is Nav1.6. In Purkinje neurons from Nav1.6 – null mice, resurgent sodium current is abolished. However, a major determinant of resurgent sodium current generation is the rate of inactivation, and slowing the rate of inactivation can allow other channel isoforms to generate resurgent currents [63]. Indeed, in some neuronal populations other isoforms predominantly contribute to the generation of resurgent current [87, 88]. These currents have been shown to increase with developmental age. This may be because of the concomitant increase in Nav1.6 expression in many of these neuronal populations. While resurgent sodium currents have so far been observed in many neuronal populations in different brain regions as well as the peripheral nervous system, TTX-sensitive resurgent currents are normally completely absent in other neuronal populations including: mouse spinal neurons, CA3 neurons of the hippocampus and small diameter spinal sensory neurons [89-92]. For this dissertation research it is important to note that many populations of neurons in critical circuits involved in epilepsy have been found to express resurgent current including: striatal medium spiny neurons, perirhinal layer II pyramidal neurons, hippocampal dentate gyrus, ventral CA1 pyramidal neurons, globus pallidus, subthalamic nuclei, and medial entorhinal cortex [92].

E. Expression of brain isoforms of voltage-gated sodium channels

As mentioned above, there are four predominant isoforms of VGSCs expressed in the brain: Nav1.1, Nav1.2, Nav1.3 and Nav1.6. There have been many

studies examining the expression of these brain isoforms of VGSCs that have identified very distinct cellular (i.e. neuronal populations) as well as subcellular (i.e. neuronal compartments) localization of each isoform. Each isoform's function within these different regions is highly specialized as evidenced by disruption of their activity or expression leading to pathological conditions and/or lethality.

Nav1.1 expression has been observed in different neuronal compartments including: soma, dendrites, nodes of Ranvier as well as the axon initial segments in various neuronal populations. Early studies described Nav1.1 as having a somato-dendritic expression pattern [93-96]. Later studies found dense expression of Nav1.1 at the proximal (closer to the soma) axon initial segment, characterizing a distinct microdomain, of retinal ganglion cells, spinal cord motor neurons and parvalbumin positive GABAergic neurons [97-100]. Nav1.1 has also been found at the nodes of Ranvier of some neuronal populations [99, 100].

Nav1.2 is highly expressed in unmyelinated axons and nerve terminals [101, 102]. Early in development Nav1.2 is expressed in the axon initial segment of hippocampal and cortical, principal neurons and cerebellar granule neurons. During development and myelination of axons, Nav1.2 channels are mostly replaced by Nav1.6 [88, 102, 103]. However, expression of Nav1.2 is still retained to varying degrees in the axon initial segment, axons and nerve terminals of mature retinal ganglion cells and cerebellar granule neurons [88, 96, 101, 104]. Recently, Nav1.2

expression was observed in the proximal axon initial segment of somatostatin positive but not parvalbumin positive GABAergic neurons [105].

While Nav1.3 mRNA was detected during prenatal development, its expression diminishes during early postnatal days and is lost in the adult rodent brain [96, 106]. However, Nav1.3 expression is retained in adult human brain, where it is found subcellularly in a somato-dendritic distribution [107]. Interestingly, many studies have reported an upregulation of Nav1.3 expression in many different CNS regions under pathological conditions including: epilepsy, traumatic brain injury and spinal cord injury [108-113].

Nav1.6 is ubiquitously expressed in the brain. In particular, Nav1.6 expression is dense in the axon initial segment and nodes of Ranvier of many neuronal populations [97, 101, 102, 114, 115]. It has also been observed in dendrites and at synapses [114, 116].

F. Epilepsy-associated mutations in Nav1.1 and Nav1.6

Many *de novo* and inherited mutations have been identified in VGSCs that underlie disorders of excitability including paralysis, pain, cardiac arrhythmias and epilepsy. While epilepsy associated mutations have been identified in several VGSC isoforms (Nav1.1, Nav1.2, Nav1.3, Nav1.6 and Nav1.7), in this dissertation the

biophysical consequences of epilepsy-associated mutations in Nav1.1 and Nav1.6 are highlighted and further explored.

1. Nav1.1

Numerous mutations have been identified in Nav1.1; while the majority are protein truncation mutations, many result in missense mutations that occur throughout the channel protein [117]. The protein truncation mutations clearly result in loss-of-function in channel activity. Many studies have examined the biophysical defects of Nav1.1 missense mutations in heterologous expression systems. Mutations associated with Dravet Syndrome mostly result in apparent loss-of-function in channel activity, while mutations associated with generalized epilepsy with febrile seizures plus (GEFS+) have mixed gain- and loss-of-function effects on channel properties [118]. Because Nav1.1 expression is predominantly in GABAergic neurons, loss of Nav1.1 activity leads to decreased excitability of GABAergic neurons and consequently reduced inhibitory tone. Indeed, heterozygous *Scn1a* mice, a model of Dravet Syndrome, show decreased excitability of GABAergic neurons [119, 120]. This is the current major hypothesis for the mechanism underlying Dravet Syndrome, however alternative hypotheses have been proposed [121, 122].

Phenotypically, mutations in Nav1.1 mostly result in GEFS+ or a more severe phenotype known as Dravet Syndrome or severe myoclonic epilepsy in infancy

(SMEI). These patients start to exhibit seizures within the first year of birth that are typically initiated by fever but later progress into many seizure types. Often they develop mild to severe cognitive and behavioral deficits that persist into adulthood [120]. Most are refractory to treatment with classic AEDs and some AEDs, in which the main mechanism of action is to target VGSC activity, can exacerbate seizures in some cases.

2. Nav1.6

Recently, the first epilepsy-associated mutation in Nav1.6 was identified [123]. Since then, several mutations in Nav1.6 have been revealed [124]. Of the mutations that have been characterized in heterologous expression systems, the majority lead to gain-of-function effects on channel properties. Specifically, biophysical defects including enhanced activation, incomplete inactivation and increased persistent current have been observed [123, 125, 126]. Mechanistically, it can be hypothesized that an increase in Nav1.6 activity would lead to increased neuronal activity and consequently hyper-excitability due the ubiquitous expression of Nav1.6.

Mutations in Nav1.6 lead to a phenotypically distinct epileptic encephalopathy from Dravet Syndrome, currently classified as EIEE13. Seizure onset is typically later in patients with EIEE13 compared to those with Dravet Syndrome but still within early life, and seizure type is much more variable [127].

Febrile seizures, a hallmark of Dravet Syndrome, are rare in patients with Nav1.6 mutations. These patients also typically display movement disorders and develop mild to severe cognitive deficits [126]. While the majority of these patients to do not respond well to current treatment strategies, VGSC blockers have shown some efficacy in the management of seizures in some patients with mutations in Nav1.6 [128, 129].

G. Current anti-epileptic drug action

Voltage-gated sodium channels are the target for many drugs used clinically including: local anesthetics, anti-arrhythmias and anti-epileptics. The primary mechanism of action for the most commonly used AEDs such as phenytoin, carbamazepine, lamotrigine and many others is to inhibit VGSC activity [130]. These drugs bind to a common receptor site in the pore of the channel from either entering through the intracellular end of the pore or, in the case of small hydrophobic inhibitors, through a hydrophobic pathway in the membrane [31, 131]. The receptor site is formed by pore-lining amino acid residues in the S6 segments of domains I, III, and IV, thus binding of drug occludes the pore [132-134]. Specifically, two amino acid resides, phenylalanine 1764 and tyrosine 1771 (numbers corresponding to Nav1.2), in the middle of the S6 segment of domain IV has been shown to be critical for drug binding [132]. This region of the channel is highly conserved among VGSC isoforms, therefore making classic AEDs relatively nonselective. Indeed, these drugs are also used to treat many other disorders such as migraine and neuropathic pain

due to their actions on other isoforms of VGSCs as well as other molecular targets [135].

An important property of classic AEDs targeting VGSCs that makes them clinically efficacious is their voltage- and frequency dependent properties. These properties arise due to higher affinity of the drug for the open or inactivated state of the channel rather than the resting, closed state [131]. Thus, with successive depolarizations a greater number of channels become blocked, a property termed frequency-dependent inhibition. This allows for targeting of hyperexcitable neurons. Clinically, it is important to find drugs that will selectively inhibit excessive, abnormal activity while maintaining physiological activity to prevent unwanted drug side effects.

H. Hypothesis and specific aims

Nav1.1 and Nav1.6 are highly expressed VGSC isoforms in the brain that are localized to distinct cellular and subcellular regions. Nav1.1 is prominently expressed in parvalbumin positive GABAergic neurons specifically at the proximal axon initial segment of these neurons. Nav1.6 is more ubiquitously found in the brain in both excitatory and inhibitory neurons and is highly localized in the distal axon initial segment and nodes of Ranvier. Parvalbumin positive GABAergic neurons characteristically fire very rapid APs (6.5 – 122 Hz) [136]. We hypothesized that Nav1.1 and Nav1.6 channels have distinct biophysical properties that differentially

contribute to the critical properties of sodium channels necessary for fast firing including: slow development of inactivation during depolarizing potentials in the inter-spike interval, rapid recovery of channels after an AP spike, and incomplete inactivation during APs; making both isoforms necessary for a fast firing phenotype. Therefore the first aim of this dissertation was to investigate the differential biophysical properties of Nav1.1 and Nav1.6 using whole-cell patch clamp recordings (Aim 1.1). To date, there has been no extensive biophysical comparison of Nav1.1 and Nav1.6, which is critical to understanding how these two channel isoforms could potentially contribute to the fast firing phenotype of parvalbumin positive GABAergic neurons.

Interestingly, resurgent sodium current and Navβ4, a VGSC auxiliary subunit capable of acting as an open channel blocker, expression are correlated with neurons that fire rapidly [137, 138]. This suggests that these currents may be contributing to the fast firing phenotype. Indeed, Navβ4 mediated resurgent sodium current is predicted to increase neuronal firing by (1) providing a depolarizing drive to approach threshold for firing subsequent APs and (2) effectively increasing the number of channels available to open immediately following an AP. The latter is attributed to the ability of Navβ4 to allow channels to bypass fast inactivation and enhance channel recovery [62]. We therefore hypothesized that Navβ4 could protect channels from accumulating into inactivated states, decreasing use-dependent reduction of current and allowing channels to better follow trains of APs.

This led to the second part of the first aim, which was to investigate the effects of Navβ4 peptide on Nav1.1 and Nav1.6 channel properties (Aim 1.2).

Nav1.1 and Nav1.6 channels are crucial for normal physiological function. Disruption of channel activity by mutations in the genes encoding these channels can lead to pathophysiological conditions. There have been hundreds of mutations identified in *Scn1a*, coding Nav1.1, which predominantly result in loss of function in channel activity and lead to an epileptic phenotype. Recently, the first human epilepsy-associated mutation was identified in *Scn8a*, coding Nav1.6, after which several others were identified. Of the Nav1.6 epilepsy-associated mutations characterized in heterologous expression systems, most mutations result in gain of function in channel activity. Resurgent sodium current generation by epilepsy-associated mutant channels has not been examined. As resurgent sodium current is predicted to increase neuronal excitability and may be important for the fast firing ability of parvalbumin positive GABAergic neurons, alterations in this current could be a potential mechanism by which epilepsy-associated mutant VGSCs cause the hyper-excitability underlying the associated epileptic phenotypes. We hypothesized that epilepsy-associated mutations in Nav1.1 and Nav1.6 would alter resurgent sodium current generation. The second aim of this dissertation was to examine the biophysical consequences of epilepsy-associated mutations in Nav1.1 (N1788K and R1648H) and Nav1.6 (N1768D and L1331V) specifically investigating the effects on resurgent current generation (Aim 2).

Our findings in Aim 2 demonstrated that epilepsy-associated mutations in Nav1.6 dramatically enhance resurgent current generation while epilepsy-associated mutations in Nav1.1 do not, leading us to ask if this current can be selectively targeted. Although there are currently no known selective blockers of resurgent current generated by Nav1.1 or Nav1.6, there is evidence that AEA and ajulemic acid, a synthetic derivative of Δ9-tetrahydrocannabinol, can selectively inhibit resurgent current over peak transient current generated by Nav1.7 and Nav1.5, respectively [81, 139]. It is not entirely clear how these compounds are working. We hypothesized that AEA would similarly inhibit Nav1.1 and Nav1.6 generated resurgent sodium current over peak transient current. Additionally, we hypothesized that CBD may also target VGSC activity due to its proposed efficacy in the treatment of pediatric epilepsies and similarity in structure to Δ9-tetrahydrocannabinol. The third aim of this dissertation was to determine whether Nav1.1 and Nav1.6 generated resurgent current and aberrant activity generated by Nav1.1 and Nav1.6 mutant channels can be targeted with AEA or CBD (Aim 3.1).

Moreover, our findings in Aim 2 suggest that epilepsy-associated mutations in Nav1.1 and Nav1.6 work through distinct mechanisms to induce epileptogenesis and will likely require different treatment strategies. Indeed, most VGSC blockers are contraindicated for the treatment of Dravet Syndrome while they show some efficacy in the treatment of severe epileptic encephalopathy due to Nav1.6 mutations. We hypothesized that selective inhibition of Nav1.1 would increase hyper-excitability due to its' prominent expression in parvalbumin positive

GABAergic neurons, while selective inhibition of Nav1.6 may dampen overall excitability due to its ubiquitous expression. Recently, two selective small molecule inhibitors, ICA and LY compounds, of Nav1.3 and Nav1.7, respectively were discovered [140]. The selectivity of these compounds was attributed to three residues in domain IV of the channel, which are correspondingly conserved in Nav1.1 and Nav1.6. Therefore, we hypothesized that these compounds would show similar differential selectivity for Nav1.1 and Nav1.6. We determined the selectivity of the ICA and LY compounds with respect to Nav1.1 and Nav1.6, and examined how selectively inhibiting each isoform alters epileptiform activity induced by 4-aminopyridine in mouse cortical brain slices using multielectrode array recordings (Aim 3.2).

The findings presented in this dissertation further our understanding of the role of VGSCs in the brain. Specifically, it highlights the distinct functional roles of two major VGSC isoforms expressed in the brain, Nav1.1 and Nav1.6 and their contribution to physiological and pathophysiological activity. The implications of these findings on disease and therapy as well as the future directions of this work are further discussed in Chapter V.

II. HUMAN NAV1.6 CHANNELS GENERATE LARGER RESURGENT CURRENTS THAN HUMAN NAV1.1 CHANNELS, BUT THE NAVβ4 PEPTIDE DOES NOT PROTECT EITHER ISOFORM FROM USE-DEPENDENT REDUCTION

This chapter was adapted from a manuscript published in *Plos One*.

doi: 10.1371/journal.pone.0133485

Reesha R. Patel, Cindy Barbosa, Yucheng Xiao and Theodore R. Cummins

R. R. Patel designed experiments, conducted all electrophysiological experiments except those presented in Figure 16, analyzed and interpreted the data and drafted the manuscript.

A. Introduction

VGSCs mediate the inward current underlying the rising phase of the action potential and are consequently key regulators of excitability. These channels are comprised of a principal α subunit encoded by nine genes that associate covalently and non-covalently with one or more auxiliary β subunits encoded by four genes [141]. Three isoforms of VGSCs are highly expressed in the adult rodent central nervous system including: Nav1.1, Nav1.2 and Nav1.6 [142]. In this study, we focused on Nav1.1 and Nav1.6 because of their distinct cellular and subcellular localization. Specifically, Nav1.1 is predominantly found in parvalbumin positive

GABAergic neurons at detectable levels in the soma and proximal axon initial segment [143-145]. In contrast, Nav1.6 is found in both GABAergic and excitatory neurons within the soma, dendrites, nodes of Ranvier and distal axon initial segment [116, 144]. The axon initial segment is a key feature of neurons containing a high density of VGSCs and is the site of AP initiation [146-148]. These two channel isoforms are thought to have minimal overlap within the axon initial segment suggesting that they have distinct functions [144, 149]. It has previously been shown that different VGSC isoforms can play specific roles within the axon initial segment [150]. Hu *et al.* found that the high-threshold Nav1.2, expressed in the proximal axon initial segment of excitatory neurons, regulates the backpropagation of APs into somato-dendritic compartments while the low-threshold Nav1.6 determines the threshold for firing an AP that will propagate down the axon. In parvalbumin positive GABAergic neurons, Ogiwara *et al.* found that Nav1.1 is important for the maintenance but not initiation of fast firing. However, the full extent to which Nav1.1 and Nav1.6 contribute to sustaining high frequency firing is unclear.

Interestingly, one of the four auxiliary β subunits of VGSCs, Navβ4, is also enriched at the axon initial segment and nodes of Ranvier in many neuronal populations that have high frequency firing characteristics [138]. The C-terminal tail of Navβ4 has been proposed to act as an open-channel blocker that blocks the channel in the open state and upon repolarization unbinds to elicit a resurgence of sodium current, termed resurgent sodium current, after which the channels

inactivate or deactivate [68, 70]. Resurgent sodium current is thus an atypical sodium current that occurs near threshold potentials immediately following an action potential spike. These currents were first identified in cerebellar Purkinje neurons, a type of parvalbumin positive GABAergic neuron, and since have been observed in many neuronal populations [66, 82, 90, 91, 151]. Castelli *et al.* found that resurgent sodium current generation by pyramidal neurons in the perirhinal cortex could be abolished by focal application of TTX to the proximal axon, likely the axon initial segment. It is predicted that resurgent sodium current generation would enhance cellular excitability by providing a depolarizing drive after an AP spike to approach threshold for firing another AP [84, 86, 152].

To date, there has been no extensive comparison of the biophysical properties of Nav1.1 and Nav1.6, which is critical to understanding how these two channel isoforms could potentially contribute to the high frequency firing characteristics of parvalbumin positive GABAergic neurons. The aims of this study were to 1) directly compare the biophysical properties of human Nav1.1 and Nav1.6, 2) determine whether resurgent sodium currents alter sodium influx in response to different AP waveforms that are characteristic of different cell types and 3) determine if Navβ4 peptide protects channels from undergoing use-dependent reduction. We found that these channel isoforms have distinct biophysical properties that could contribute to different characteristics of VGSCs important for fast firing. Moreover, resurgent sodium current generation increases sodium influx in response to different duration AP waveforms, and while Navβ4 peptide enhances

apparent recovery from inactivation, it does not protect channels from undergoing use-dependent reduction. These findings provide novel insight into the potential roles of these two channel isoforms as well as the potential role of Navβ4 peptide in maintaining a fast firing phenotype.

B. Materials and methods

1. cDNA constructs

Optimized human constructs for Nav1.1 and Nav1.6 were designed in-house, purchased from Genscript (Piscataway, NJ) and subsequently hNav1.1 was subcloned into pTarget using XhoI and SalI restriction sites and hNav1.6 was subcloned into pcDNA3.1+ using KpnI and XbaI restriction sites. The amino acid sequences for the synthesized, human Nav1.1 and Nav1.6 cDNA constructs correspond with BAC21102.1 and NP_055006.1 in the NCBI database, respectively.

2. Cell cultures and transfections

The use of HEK293T cells [153] was approved by the Institutional Biosafety Committee and followed the ethical guidelines for the National Institutes of Health for the use of human-derived cell lines. HEK293T cells were grown under standard tissue culture conditions (5% CO2; 37°C) with DMEM supplemented with 10% fetal bovine serum. HEK293T cells were transiently transfected using the calcium

phosphate precipitation method. Briefly, a calcium phosphate-DNA mixture (4.5 μg channel construct and 0.5 μg enhanced green florescent protein (EGFP)) was added to cells in serum-free media for 4-5 hours and subsequently washed with fresh media. 12-24 hours post-transfection, cells were split onto laminin-coated glass coverslips. Cells were identified by expression of EGFP using a fluorescent microscope and whole-cell patch clamp recordings were obtained 36-72 hours post-transfection.

3. Whole-cell patch clamp recordings

Whole-cell patch clamp recordings were obtained at room temperature (~23°C) using a HEKA EPC-10 amplifier, and the Pulse program (v 8.80, HEKA Electronic, Germany) was used for data acquisition. Voltage-clamp data (except for that obtained with AP waveforms) were digitized at 20kHz and filtered at 5kHz. Electrodes were fabricated from 1.7mm capillary glass and fire-polished to a resistance of 0.9-1.3MΩ using a Sutter P-97 puller (Sutter Instrument Company, Novato, CA). All voltage protocols were started 5 minutes after obtaining a gigaΩ seal and entering the whole-cell configuration, which controlled for time-dependent shifts in channel properties and allowed time for diffusion of Navβ4 peptide when used. Voltage errors were minimized to less than 5mV using series resistance compensation and passive leak currents were cancelled by P/-5 subtraction. The bath solution contained in (mM): 140 NaCl, 1 $MgCl_2$, 3 KCl, 1 $CaCl_2$, and 10 Hepes, adjusted to a pH of 7.30 with NaOH. The pipette solution contained in (mM): 140

CsF, 10 NaCl, 1.1 EGTA, and 10 Hepes, adjusted to a pH of 7.30 with CsOH. Fluoride was used in part because it increased the stability of the recordings over time. Fluoride can also reduce persistent sodium current components [154], which enhanced our ability to compare resurgent current amplitudes. To induce resurgent currents in HEK293T cells, 200μM Navβ4 peptide (KKLITFILKKTREK-OH) (Biopeptide Co., San Diego, CA), a peptide that corresponds to part of the sequence of the C-terminal tail of the full-length Navβ4 subunit, was included in the pipette solution when specified. Resurgent currents are not detectable in HEK293T cells without Navβ4 peptide in the pipette solution.

4. Modeling AP waveforms

Fast spiking interneurons have substantially narrower AP waveforms than pyramidal neurons [155, 156], therefore we developed fast and slow AP waveforms to elicit currents in voltage-clamp experiments. The AP waveforms were initially generated in the NEURON simulation environment [157] using previously developed computational models of pyramidal and fast-spiking GABAergic neurons [158]. The slow (pyramidal) and fast (fast spiking GABAergic) waveforms were then digitally modified to have identical initial membrane potentials, peak potentials and after-hyperpolarization potentials. Thus, the major differences were the rate of rise, the rate of repolarization and the overall duration of the AP. The mid-height duration of the fast AP waveform (modeled at 37 °C) was 0.29ms and that of the slow AP waveform was 1.0ms, which are similar to the durations measured for fast

spiking cortical interneurons and cortical pyramidal neurons (Table 1) [155]. Since voltage-clamp experiments were carried out at room temperature (~23°C), the waveforms were adjusted to account for channel gating at room temperature. Mammalian sodium channel kinetics as well as AP duration have temperature coefficients (Q10s) of approximately 2 [159-161]. Therefore, AP waveforms were slowed by a factor of 2.5 (Q10 = 2). Parameters for modeled (37°C) and actual (23°C) action potential waveforms are summarized in Table 1. Trains of action potentials were created by concatenation of 20 single action potential waveforms. The initial trains had a spike frequency of 100Hz. These were modified to also generate 25Hz trains by lengthening the interspike interval using linear voltage ramps. To account for recording at room temperature, the 25 and 100Hz trains were scaled using a Q10 of 2. The effective frequencies after scaling were 8 and 33Hz (Fig. 3). The scaled AP waveforms and trains of APs were then used as voltage command waveforms to elicit sodium currents. Data collected from AP voltage command waveforms represent an average of five traces. Data obtained with 33Hz AP waveform trains were acquired at 6.6kHz and filtered at 3.3kHz and those obtained with 8Hz waveform trains were acquired at 4kHz and filtered at 2kHz.

Table 1. Modeled Action Potential Parameters.

	Slow AP		Fast AP	
	Modeled 37°C	**Actual 23°C**	**Modeled 37°C**	**Actual 23°C**
Max rate of rise (V/s)	542.5	180.8	1234.0	411.3
Max rate of decay (V/s)	-109.5	-36.5	-367.5	-122.5
Overshoot Amplitude (mV)	39.3	39.3	39.3	39.3
Width at -20mV (ms)	1.0	3.0	0.29	0.87
Peak AHP (mV)	-84.9	-84.9	-84.9	-84.9

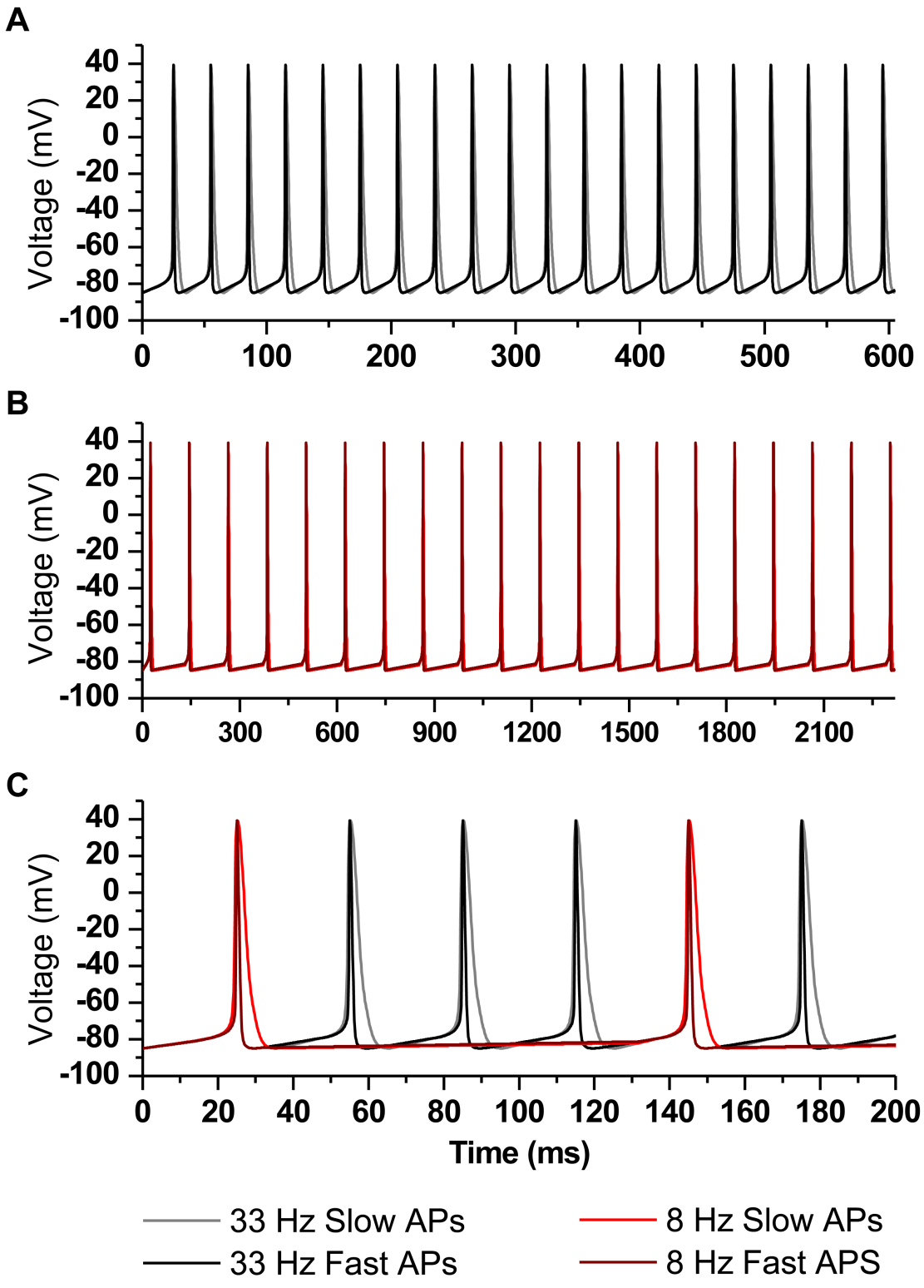

Figure 3. Waveform command protocol for trains of 33Hz and 8Hz of fast and slow action potentials.

5. Data analysis

Electrophysiological data were analyzed using Pulsefit (v 8.67 HEKA Electronic, Germany), Microsoft Excel, Origin (v 8.0, OriginLab Corp, Northhampton, MA), and Prism (v 6.0, Graphpad Software Inc., La Jolla, CA). Steady-state activation and inactivation curves were fit to a Boltzmann function to obtain midpoint and slope values. Quantification of the area under the curve was measured from 20ms to 35ms and baseline was set to zero. All data points are presented as mean ± SEM and *n* is the number of experimental cells from which recordings were obtained. Statistical significance was assessed using an unpaired t-test or a one-way ANOVA as indicated.

C. Results

1. hNav1.1 and hNav1.6 have differential biophysical properties

To compare the biophysical properties of human Nav1.1 and Nav1.6 (hNav1.1 and hNav1.6), we transiently transfected HEK293T cells with each channel isoform and obtained whole-cell patch clamp recordings. hNav1.1 and hNav1.6 have a similar current-voltage relationship for peak sodium current (Fig. 4A,B). Correspondingly, these two channel isoforms show no differences in their voltage-dependence of steady-state activation (Fig. 4C). Gating parameters are summarized in Table 2. We then examined the kinetics of deactivation by applying a brief

(0.5ms) depolarizing step pulse to +10mV followed by a repolarizing step to voltages ranging from -60mV to -100mV for 50ms eliciting tail currents that were fit to a single exponential function (Fig. 4D, *inset*). Representative traces of deactivation tail current can be seen in Figure 4D. The time constants for the kinetics of deactivation were similar for both channel isoforms across all voltages tested (Fig. 4E).

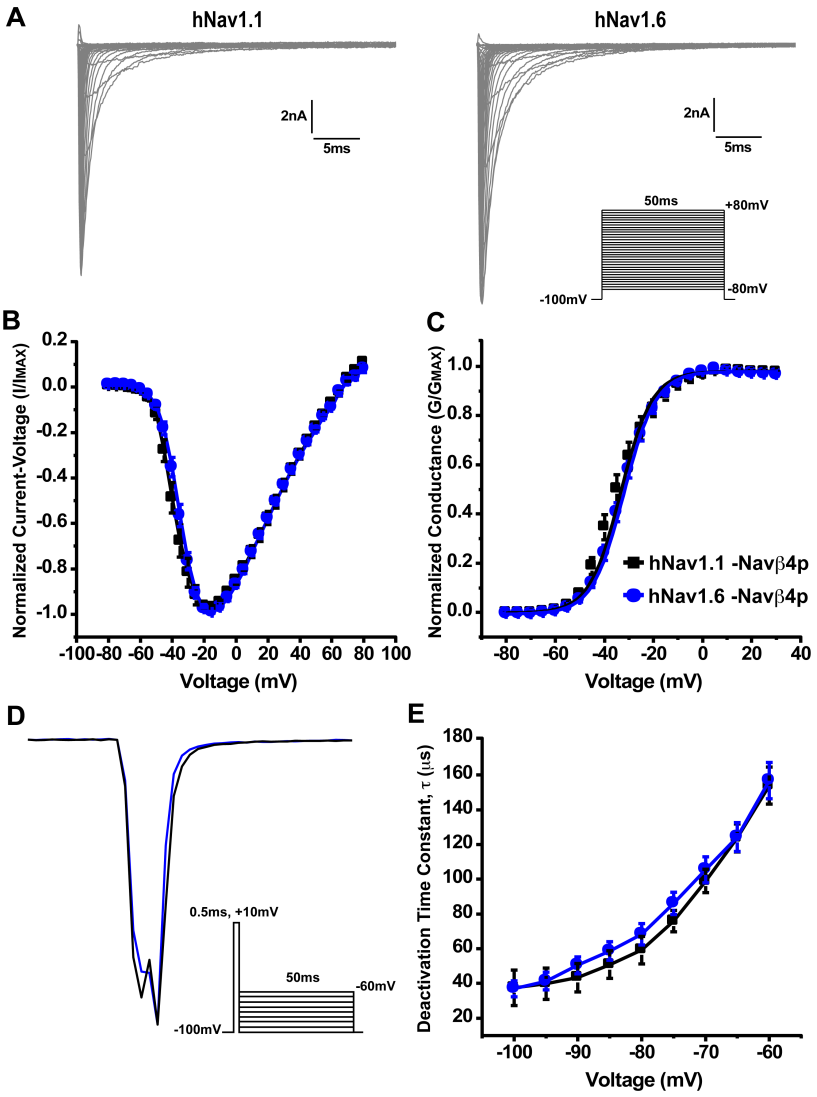

Figure 4. No differences in the current-voltage relationship, voltage-dependence of steady-state activation and deactivation kinetics of hNav1.1 and hNav1.6. A, Representative current traces recorded from hNav1.1 (left) and hNav1.6 (right) expressed in HEK293T cells. The currents were elicited by applying 50ms step-depolarization to potentials ranging from -80mV to +80mV from a holding potential of -100mV. *Inset,* Protocol used to obtain current-voltage traces. B, Normalized peak current-voltage relationship for hNav1.1 (black squares; n=14) and hNav1.6 (blue circles; n=14). C, Voltage-dependence of steady-state activation shows no difference in conductance between hNav1.1 and hNav1.6. D, Representative traces showing hNav1.1 (black) and hNav1.6 (blue) deactivation tail currents at -70mV. *Inset,* Protocol used to elicit deactivation tail currents. E, Time constants of channel deactivation were similar for hNav1.1 and hNav1.6 at voltages ranging from -100mV to -60mV. Time constants were obtained by a brief 0.5ms depolarization to +10mV followed by a series of repolarizations to potentials from -100mV to -60mV eliciting tail currents that were fit to a single exponential function.

Table 2. Summary of activation and inactivation gating parameters.

	Activation		**Inactivation**		
	V1/2	Slope	V1/2	Slope	n
hNav1.1	-34.8 ± 1.8	6.7 ± 0.3	-67.2 ± 1.7	4.7 ± 0.1	14
hNav1.6	-32.6 ± 1.1	6.5 ± 0.1	-71.9 ± 1.3*	5.9 ± 0.1*	14

* $p < 0.05$ Compared to hNav1.1

Next, we examined the voltage-dependence of steady-state inactivation by holding cells at voltages ranging from -120mV to +30mV for 500ms and then applying a 20ms test pulse to +10mV to determine the fraction of current available (Fig. 5A, *inset*). hNav1.6 had a small but significant hyperpolarizing shift in the midpoint (-72 ± 1mV; *n* = 14) of the voltage-dependence of steady-state inactivation curve compared to hNav1.1 (-67 ± 2mV; *n* = 14) (Fig. 5A, Table 2). To explore what was underlying the shift in inactivation we examined the development of closed-state inactivation, which reflects the direct transition of channels from a closed into an inactivated state. Development of closed-state inactivation was measured using a voltage protocol in which cells were held at -100mV and stepped to a prepulse potential ranging from -100mV to -50mV for increasing durations immediately followed by a test pulse to 0mV to assess the fraction of current inactivated during the prepulse (Fig. 5C, inset). The data were plotted (peak current amplitude as a function of inactivation duration) and fit to a single exponential function to determine the time constants for development of closed state inactivation as seen in Figure 5B. We found that hNav1.6 had statistically smaller tau values for development of closed state inactivation at voltages ranging from -80mV to -60mV compared to hNav1.1 (Fig. 5C). Specifically, at voltages near typical resting potentials in neurons such as -70mV, hNav1.1 (τ = 56.5 ± 12.1ms; *n* = 9) had a slower rate of closed-state inactivation development compared to hNav1.6 (τ = 26.0 ± 2.0ms; *n* = 8), which would allow it to be more resistant to inactivation during slow sub-threshold depolarizations [162]. This would result in greater channel

availability for hNav1.1 to open once the membrane is depolarized to threshold potentials for firing an AP.

We also compared recovery from fast inactivation (repriming), a property that can limit the channels ability to sustain high firing frequencies. To do this, we held cells at -100mV and applied a prepulse to 0mV for 20ms to induce fast inactivation and then allowed the channels to recover for increasing durations at potentials ranging from -100mV to -70mV before applying a test pulse to 0mV for 20ms to measure the available channels (Fig. 6A, *inset*). Representative traces of recovery from fast inactivation at -70mV are depicted in Figure 6A. Each test pulse current was normalized to the maximal current at each time point and plotted as a function of time for each recovery voltage (Fig.7). Time constants for repriming kinetics were estimated using single exponential fits and these time constants are plotted as a function of recovery voltage in Figure 6B. We found that hNav1.1 and hNav1.6 had similar time constant values for recovery from inactivation at voltages ranging from -100mV to -80mV. However, at -70mV hNav1.6 (τ = 22.3 ± 1.1ms; n = 17) had significantly faster repriming kinetics compared to hNav1.1 (τ = 33.1 ± 2.1ms; n = 19). It is important to note that the maximal fraction recovered was greater for hNav1.1 compared to hNav1.6 at recovery voltages from -90mV to -70mV (Fig. 6C), consistent with the differences observed in the voltage-dependence of steady-state inactivation.

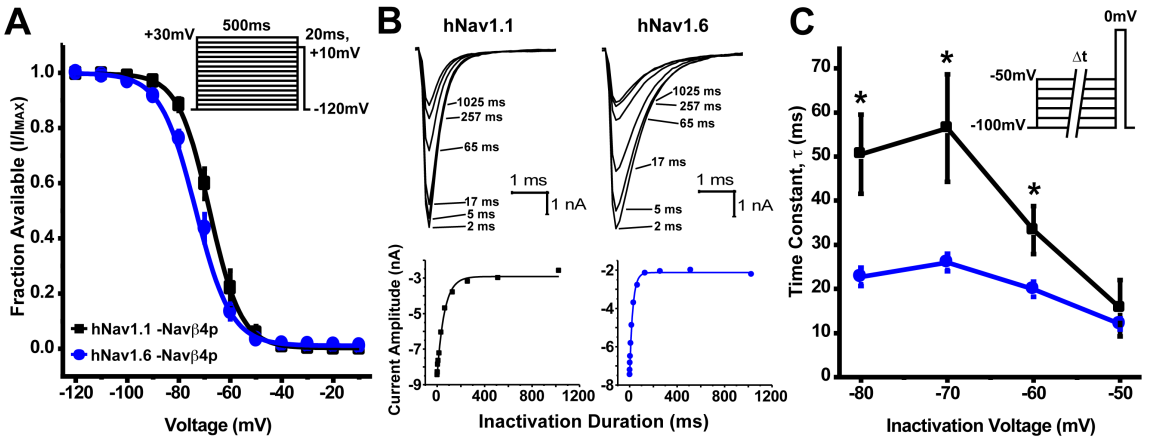

Figure 5. Voltage-dependence of steady-state inactivation and kinetics of development of closed-state inactivation are different for hNav1.1 and hNav1.6. A, To examine the voltage-dependence of steady-state fast inactivation a series of 500ms steps from -120mV to +30mV followed by a 20ms step pulse to +10mV was used to measure channel availability. Midpoints of the voltage-dependence of steady-state fast inactivation were estimated by fitting data with a Boltzmann function and was more hyperpolarized for hNav1.6 (blue circles; n = 14) compared to hNav1.1 (black squares; n = 14)(Unpaired t-test, $p < 0.05$). Table 2 summarizes gating parameters. *Inset*, Protocol used to measure steady-state inactivation. B, Top: Representative family of current traces generated by hNav1.1 (left) and hNav1.6 (right) showing the rate of development of inactivation at -70mV. Bottom: Plots for the time course of development of inactivation for the peak current from the corresponding cell above. C, Time constants for development of closed-state inactivation are smaller for hNav1.6 (blue circles; n = 8) compared to hNav1.1 (black squares; n =9) (Unpaired t-test, *$p < 0.05$). Time constants were determined by single exponential fits to time courses measured using the voltage protocol depicted in the inset.

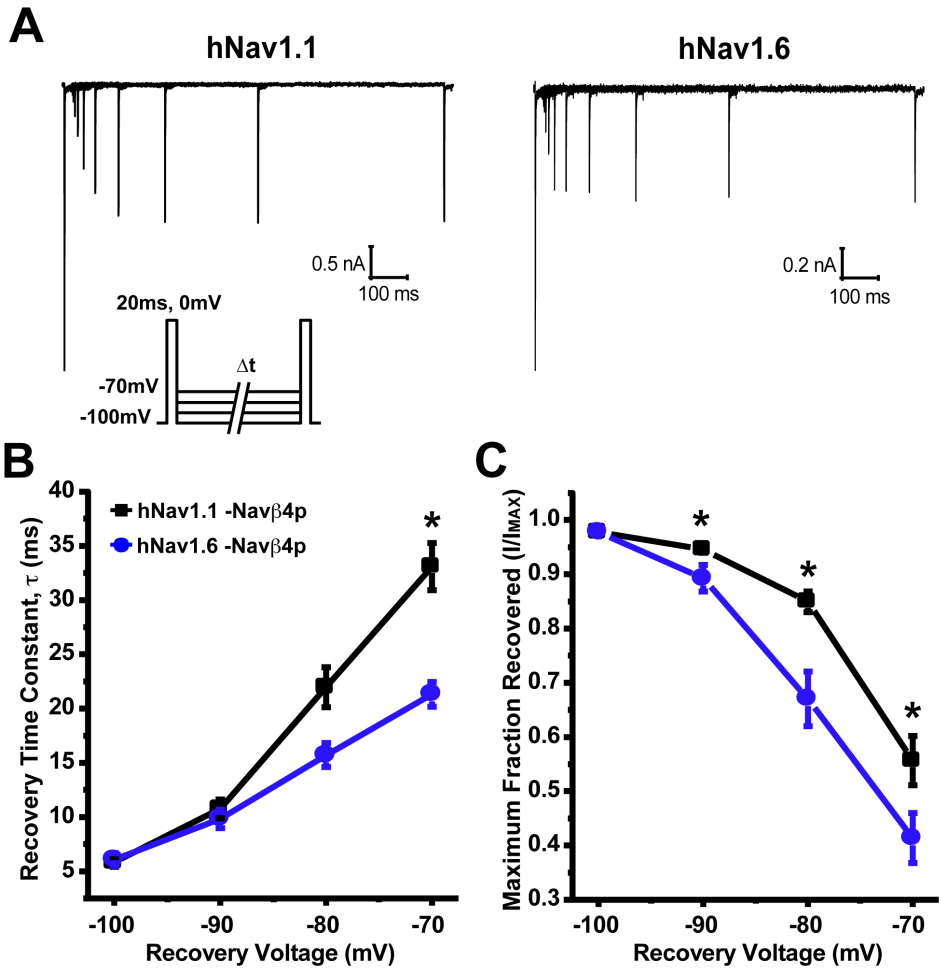

Figure 6. Rate and fraction of recovery from fast inactivation are different for hNav1.1 and hNav1.6. A, Representative traces of recovery from fast inactivation measured by first inducing fast inactivation from a holding potential of -100mV with a 20ms step pulse to 0mV and then applying a 20ms test pulse to 0mV subsequent to various recovery times at -70mV. *Inset,* Protocol used to measure recovery from fast inactivation. B, hNav1.6 (blue circles; n = 17) has a smaller time constant for recovery at -70mV compared to hNav1.1 (black squares; n = 19). C, Maximal fraction recovered from fast inactivation was greater for hNav1.1 at voltage ranging from -90mV to -70mV compared to hNav1.6 (Unpaired t-test, *$p < 0.05$).

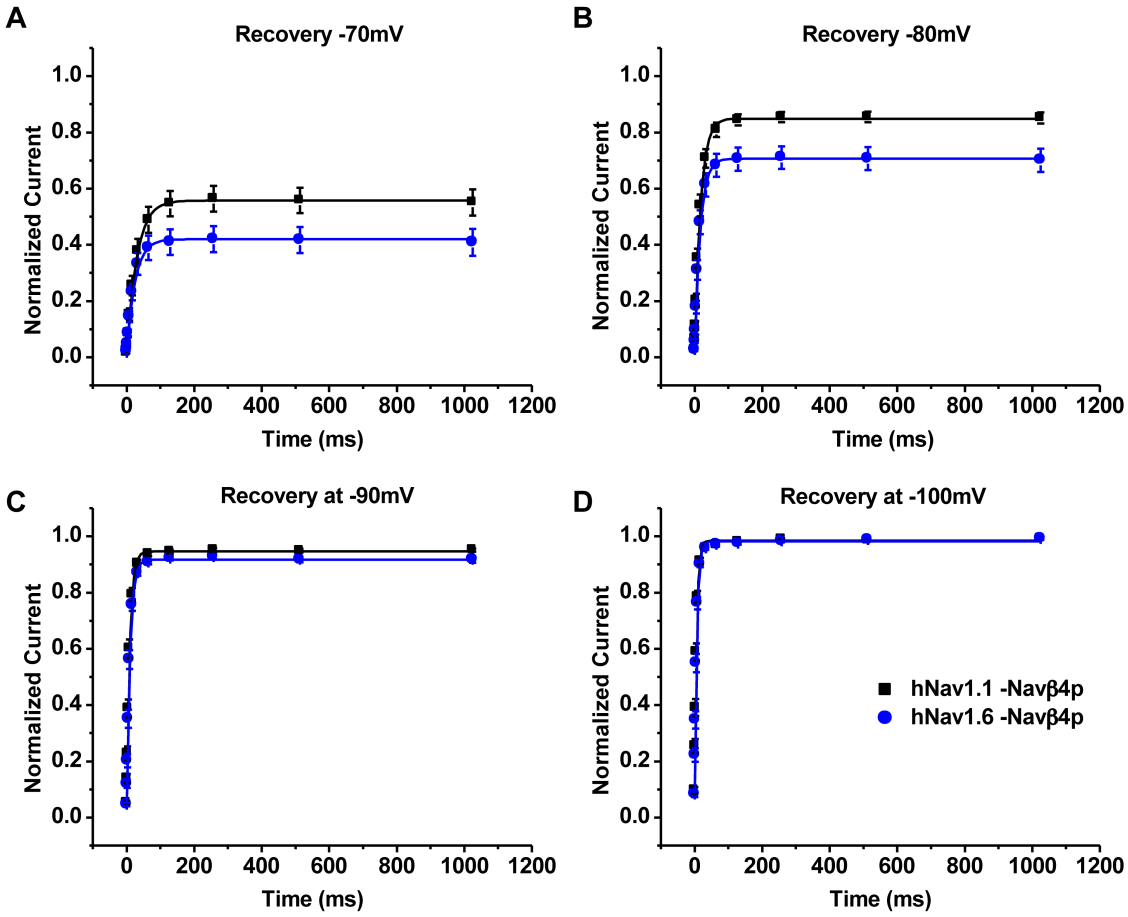

Figure 7. Time courses of recovery from fast inactivation at voltages ranging from -70mV to -100mV.

2. hNav1.6 has a greater propensity to generate resurgent currents than hNav1.1

We next asked whether there was an intrinsic difference in the ability of hNav1.1 and hNav1.6 to generate resurgent sodium currents. We examined resurgent current generation by hNav1.1 and hNav1.6 in HEK293T cells by inclusion of a peptide (Navβ4 peptide) corresponding to a portion of the C-terminal tail of the Navβ4 auxiliary subunit in the pipette solution, which has been previously shown to induce resurgent currents in this cell type [163-165]. Figure 8A shows a family of representative resurgent current traces generated from cells expressing either hNav1.1 or hNav1.6 obtained by applying an initial depolarizing step to +60mV for 20ms from a holding potential of -100mV followed by a 50ms step to repolarizing voltages ranging from +25mV to -80mV (Fig. 8B). Resurgent currents were quantified by dividing the peak resurgent current amplitude measured after 1.5ms into the repolarizing step (to prevent contamination by tail currents) by the peak transient current measured with a 20ms test pulse at +10mV and are shown as a percentage of the peak transient current amplitude. hNav1.6 demonstrated a greater propensity to generate resurgent currents within voltages ranging from -45mV to +25mV compared to hNav1.1 (Fig. 8C). The peak resurgent current was more than 2-fold greater for hNav1.6 (15.9 ± 2.4%; n = 15) compared to hNav1.1 (7.4 ± 1.3%; n = 15) and occurred at -35mV and -45mV, respectively.

One of the major determinants of resurgent current generation is the rate of inactivation because the Navβ4 peptide is thought to directly compete with the ability of the intrinsic fast inactivation gate to bind the channel. Therefore, we examined the kinetics of fast inactivation of peak transient sodium currents by fitting the decay phase of macroscopic currents elicited with test potential steps to voltages ranging from -20mV to +20mV with a single exponential function. Figure 8D shows representative normalized traces elicited by a voltage step from -100mV to -10mV demonstrating the slower decay phase of hNav1.6 compared to hNav1.1. We found that hNav1.6 has significantly larger time constants for kinetics of inactivation compared to hNav1.1 at all the voltages tested (Fig. 8E). The slower kinetics of inactivation for hNav1.6 corresponded to its greater ability to generate resurgent currents. We did not observe any differences in the kinetics of inactivation with and without of Navβ4 peptide for either channel isoform (Fig. 9).

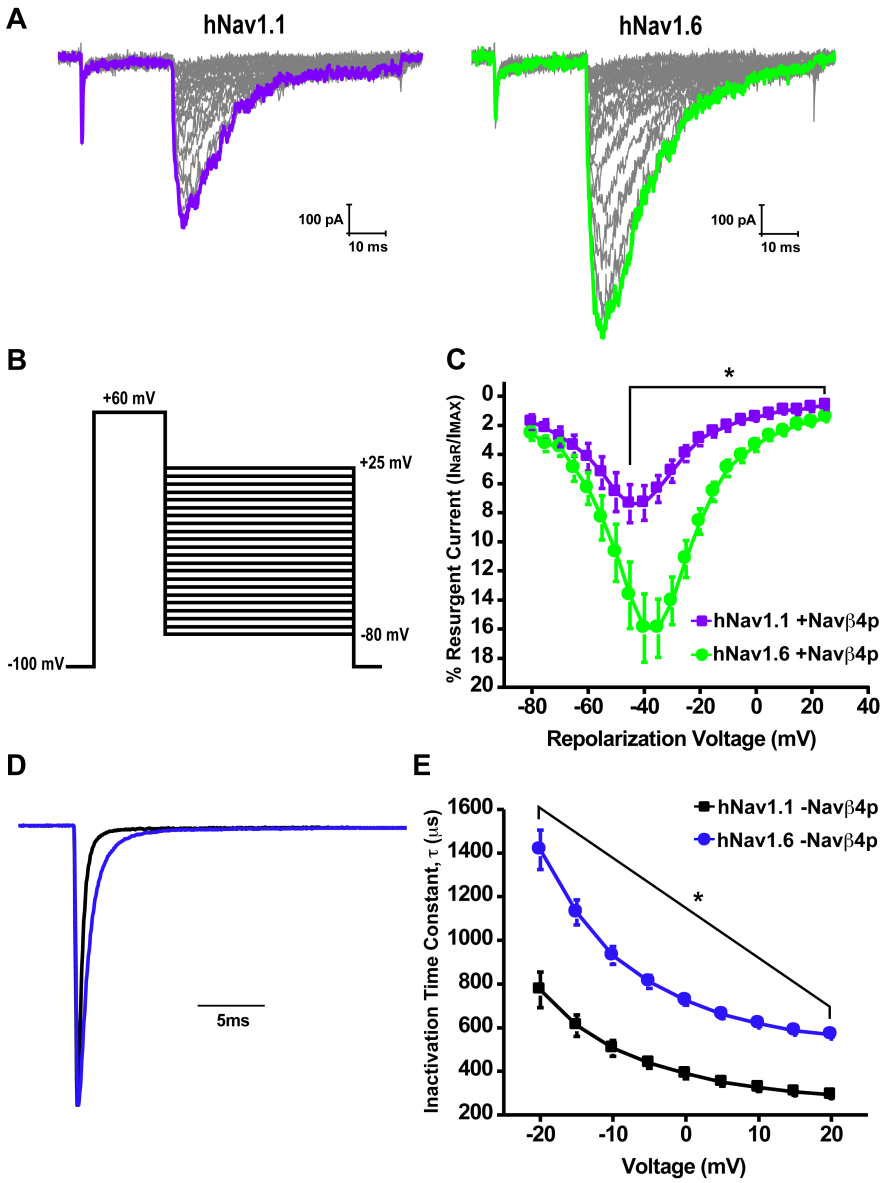

Figure 8. Resurgent current generation is increased and kinetics of inactivation are slowed for hNav1.6 compared to hNav1.1. A, Representative family of resurgent current traces from hNav1.1 (left) and hNav1.6 (right) with Navβ4 peptide in the pipette solution. Currents were elicited by depolarization to +60mV for 20ms followed by repolarization to potentials ranging from +25mV to -80mV for 50ms. B, Protocol used to measure resurgent currents. C, Current-voltage curve of peak resurgent current normalized to peak transient current measured at +10mV by hNav1.1 (purple squares; *n* = 15) and hNav1.6 (green circles; *n* = 15). D, Representative normalized current traces elicited by a step depolarization from -100mV to -10mV by hNav1.1 (black) and hNav1.6 (blue) without Navβ4 peptide in the pipette solution. E, Averaged decay time constants measured at potentials ranging from -20mV to +20mV from hNav1.1 (black square; *n* = 14) and hNav1.6 (blue circles; *n* = 14) (Unpaired t-test, *p < 0.05).

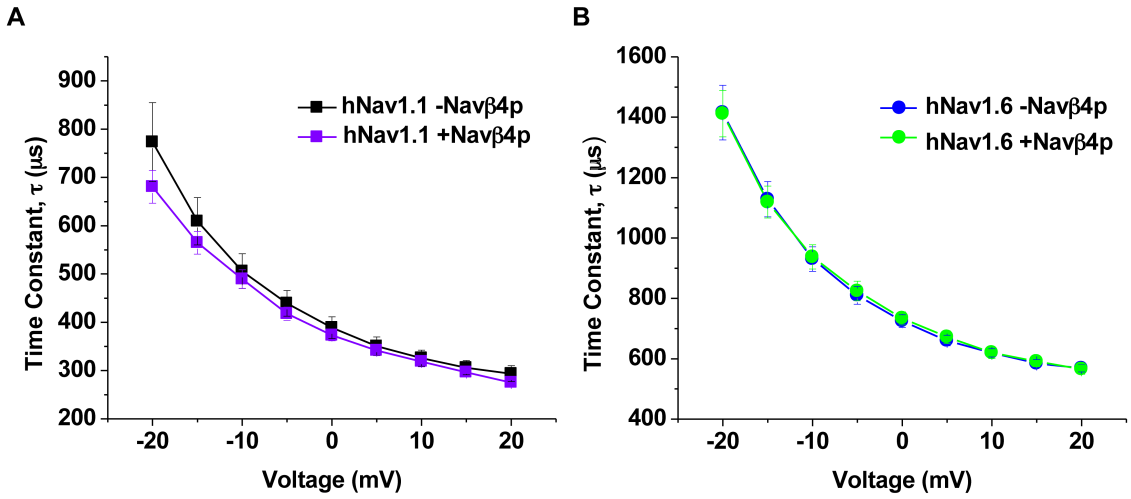

Figure 9. No different in the kinetics of fast inactivation in the presence and absence of the Navβ4 peptide for hNav1.1 and hNav1.6.

3. Sodium influx through hNav1.1 and hNav1.6 in response to slow and fast AP waveforms is altered in the presence of Navβ4 peptide

AP waveforms vary with cell type and one of the major differences is the width of the action potential [137, 166]. It is unknown if and where during the AP waveform resurgent sodium current generated by hNav1.1 or hNav1.6 would result in an increase in sodium influx. We therefore wanted to examine the influence of resurgent current generation on sodium influx in response to a slow and fast AP waveform. To do this, we first modeled AP waveforms from fast-spiking GABAergic (fast AP) and pyramidal (slow AP) neurons using the simulation program NEURON (Fig. 10A) [27]. We adjusted the initial resting membrane potential, peak amplitude and the after-hyperpolarization potential of the AP waveforms to be identical in order to focus on implications of the difference in the AP width observed between these two different types of neurons. We then used the AP waveform as a voltage command waveform to elicit sodium currents.

Figure 10C,E show the responses of hNav1.1 and hNav1.6 to the fast AP waveform (superimposed for comparison in a dotted line) as an average of normalized traces plotted versus time. Note that not all traces reach a value of one because the peak does not occur at the same exact time in each cell, therefore after averaging the normalized traces from each cell the averaged peak value is less than one. The second peak, or hump, in the decaying phase of the sodium current is likely generated by the fraction of channels that do not undergo fast inactivation during

the upstroke of the action potential. hNav1.1 mediated sodium influx was significantly decreased between 25.2 and 25.5ms and increased during the second non-inactivating component of the current between 26.1 and 28ms by Navβ4 peptide, as highlighted by the grey shaded boxes. Similarly, hNav1.6 mediated sodium influx in the presence of Navβ4 peptide was significantly decreased between 25.4 and 25.6ms and increased between 26.0 and 27.3ms. The decrease in sodium influx likely reflects binding of Navβ4 peptide to the channel while the unbinding of Navβ4 peptide increased the duration of the second non-inactivating component. Responses to the slow AP waveform exhibited a smaller second non-inactivating component compared to the fast AP waveform. However, just as with the fast AP waveform, Navβ4 peptide significantly increased sodium influx during the second non-inactivating component for hNav1.1 between 27.3 and 31.4ms and hNav1.6 between 27.7 and 30.4ms, increasing both the duration of sodium influx and amplitude of the second non-inactivating component (Fig. 10D,F). Unlike with the fast AP waveform, the sodium influx in response to the slow AP waveform did not show the same decrease in current following the initial peak in the presence of Navβ4 peptide. Overall, there was a statistically greater sodium influx mediated by hNav1.6 compared to hNav1.1 as measured by the area under the curve in the presence and absence of Navβ4 peptide with both the slow and fast AP waveforms (Fig. 10B; Fig. 11).

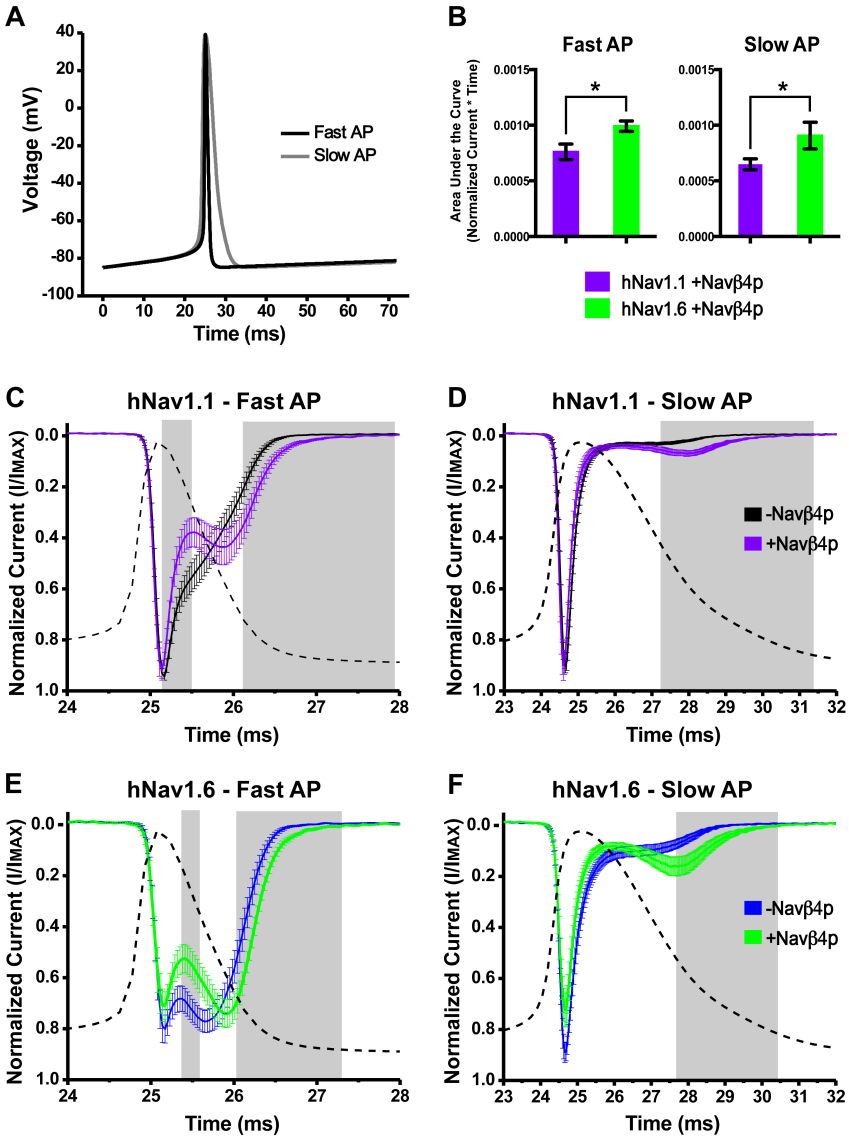

Figure 10. Sodium influx in response to fast and slow AP waveforms are altered in the presence of the Navβ4 peptide. A, Fast and slow voltage command waveforms modeled using NEURON. B, Area under the curve for currents elicited by the fast (left) and slow waveform (right) from cells expressing hNav1.1 (purple bars) and hNav1.6 (green bars) measured between 20 and 35ms (Unpaired t-test, *p < 0.05). Currents generated in response to fast and slow AP waveforms were normalized and then averaged. C, hNav1.1 generated sodium current in response to a fast voltage command waveform in the absence (black traces; *n* = 17) and presence (purple traces; *n* = 14) of Navβ4 peptide. D, Response of hNav1.1 to a slow voltage command waveform. E, hNav1.6 generated sodium current in response to a fast voltage command waveform in the absence (blue trace; *n* = 14) and presence (green trace; *n* = 15) of Navβ4 peptide. F, Response of hNav1.6 to a slow voltage command waveform. Grey boxes represent regions of statistically significant differences (Unpaired t-test, p < 0.05).

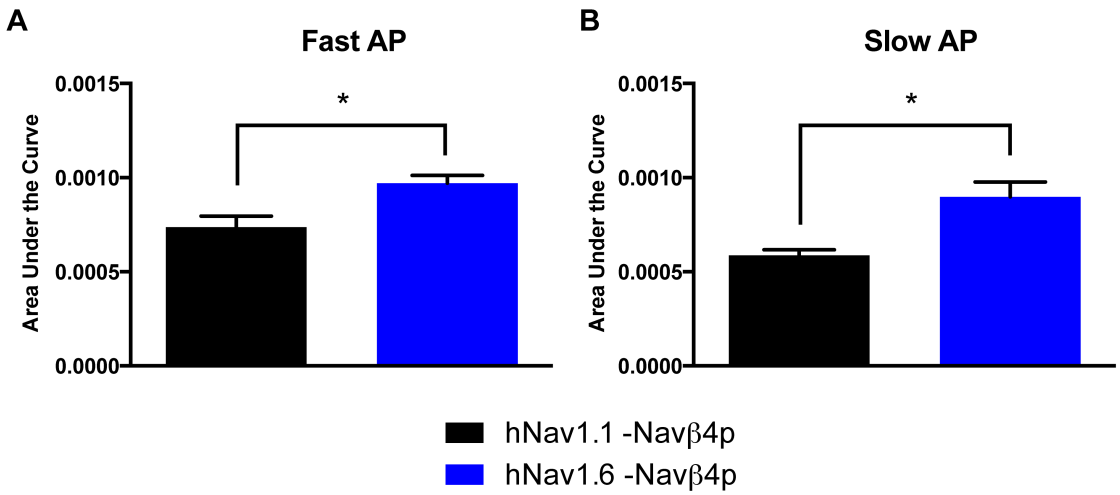

Figure 11. Sodium influx in response to a fast and slow action potential waveform in the absence of the Navβ4 peptide is greater for hNav1.6 compared to hNav1.1.

4. Navβ4 peptide mediated open-channel block allows channels to recover faster

The open-channel blocker responsible for mediating the generation of resurgent current is thought to allow channels to bypass classic inactivation and enhance recovery [62]. We therefore tested whether Navβ4 peptide mediated open-channel block allows channels to recover faster. To do this we used two different voltage command protocols (adapted from Raman and Bean, 2001) in which we applied either a brief, 5ms pulse to +30mV or a longer, 40ms pulse to -30mV to accumulate channels in an open-blocked or inactivated state, respectively, and subsequently allowed channels to recover at -70mV for increasing durations before applying a test pulse to 0mV to measure the fraction of channels available (Fig. 12A,B). We found that both hNav1.1 and hNav1.6 channels have smaller time constants following recovery from an open-blocked state (hNav1.1: τ = 7.0ms; hNav1.6: τ = 6.2ms) compared to an inactivated state (hNav1.1: τ = 26.1ms; hNav1.6: τ = 28.5ms) (Fig. 12C,D). It is important to note that we did not observe any differences in the time course for recovery with these two protocols in the absence of Navβ4 peptide (Figure 13), which indicates that in the absence of Navβ4 peptide the two distinct depolarizing pulses (5ms at +30 mV versus 40ms at -30 mV) induce similar inactivation states for the sodium channels.

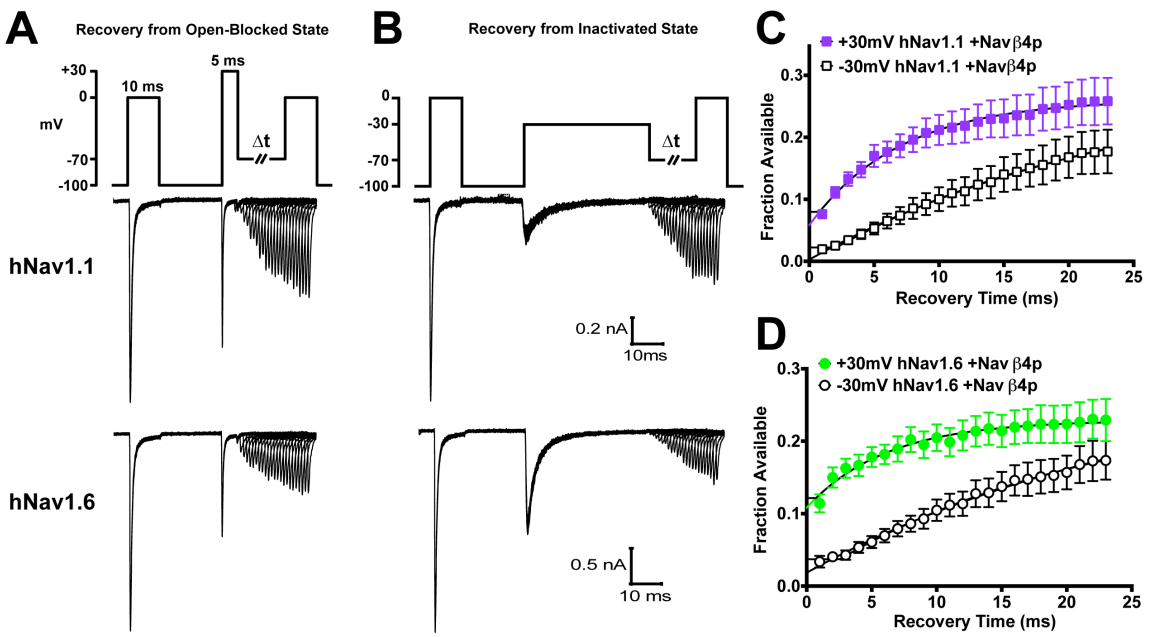

Figure 12. Recovery of channels is faster from open-blocked versus inactivated states for hNav1.1 and hNav1.6. A, Recovery at -70mV for increasing durations following a brief, 5ms pulse to +30mV to allow channels to enter an open-blocked state (top). Representative traces for the time courses of recovery generated by hNav1.1 (middle) and hNav1.6 (bottom). B, Recovery at -70mV for increasing durations following a 40ms pulse to -30mV to allow channels to enter an inactivated state. Representative traces for the time courses of recovery generated by hNav1.1 (middle) and hNav1.6 (bottom). C and D, Summary data showing the fraction available after a 5ms pulse to +30mV (filled) versus a 40ms pulse to -30mV (open) plotted against the recovery time for hNav1.1 (squares; n = 21) and hNav1.6 (circles; n = 14). Fraction available was calculated by normalizing the peak current elicited by the test pulse to the peak current elicited by a step depolarization from -100mV to 0mV at the beginning of the protocol. Data are fit to a single exponential function.

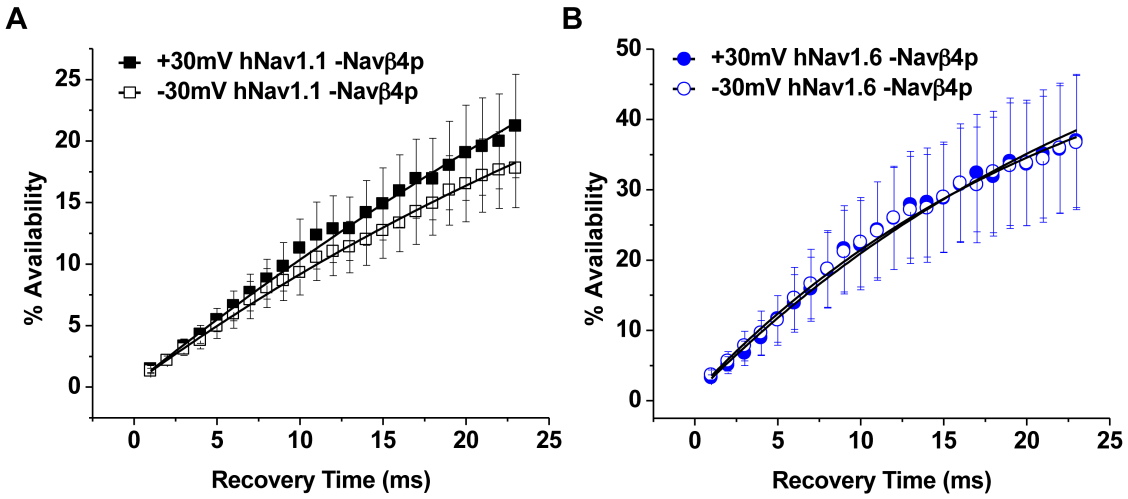

Figure 13. Recovery from open-blocked (+30mV) and inactivated (-30mV) states is not different in the absence of Navβ4 peptide for hNav1.1 and hNav1.6.

5. Navβ4 peptide does not protect hNav1.1 or hNav1.6 from use-dependent reduction with 10Hz step-pulses

Since Navβ4 peptide mediated open-channel block enhances recovery, we predicted that the presence of the open channel blocker would allow channels to better follow a 10Hz step-pulse stimulus by protecting channels from undergoing use-dependent reduction that is entering accumulating in inactivated states will trains of stimuluation. We used a protocol in which we assessed the peak current with an initial 20ms step pulse to -10mV from -80mV followed by 19 step-depolarizations (at 10 Hz) from -80mV to either +30mV or +60mV for 20ms before a final test pulse to -10mV for 20ms to determine the remaining channels available (Fig. 14A,B, *inset*). Two depolarization voltages were used because Navβ4 peptide binds more stably to the channel at higher depolarization voltages [167]. We calculated the percent current reduced between the initial and final test pulses and found that hNav1.6 undergoes approximately 15% more use-dependent reduction compared to hNav1.1 (Fig. 14B). The presence of Navβ4 peptide did not alter use-dependent reduction with 10Hz step-pulses to +30mV or +60mV by either channel isoform.

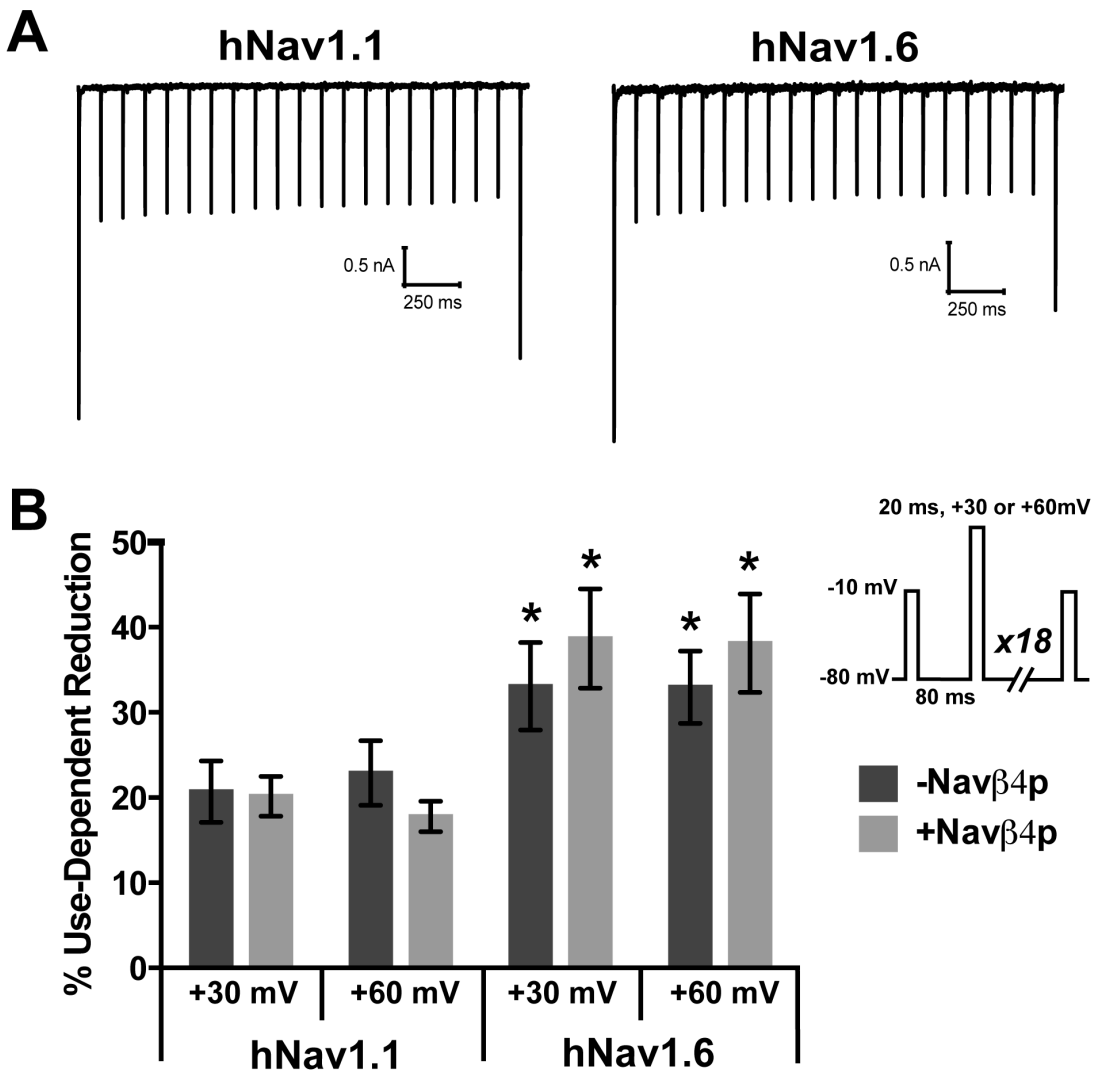

Figure 14. The Navβ4 peptide does not effect use-dependent reduction of hNav1.1 or hNav1.6 with 10Hz stimulation. A, Representative traces of use-dependent reduction traces generated by hNav1.1 (left) and hNav1.6 (right) when pulsed at +30mV. Use-dependent reduction was examined with an initial and final 20ms step pulse to -10mV from -80mV to assess the current available before and after 19 consecutive step depolarization from -80mV for 80ms to +30mV or +60mV for 20ms. B, Percent inhibition was calculated between the initial and final currents for cells in the absence (dark grey bars) and presence (light grey bars) of Navβ4 peptide (*n* = 8-9). *Inset,* Abbreviated protocol used to measure use-dependent reduction. *p < 0.05 compared to corresponding hNav1.1 group.

One possibility is that the use-dependent reduction in current was independent of fast inactivation processes, but rather reflected slow inactivation of hNav1.1 and hNav1.6 channels. To evaluate entry into slow inactivated states during the 10Hz trains, we measured the fraction of channels that recover from fast inactivation after the 10Hz stimulus protocol by applying a 20ms step pulse to -120mV following the last step depolarization to +60mV (allowing channels to recover from fast but not slow inactivation) and used a subsequent test pulse to -10mV to measure channel availability. We found that both hNav1.1 (91.56 ± 1.6 % availability) and hNav1.6 (112.3 ± 7.4 % availability) nearly or completely recovered during this brief recovery pulse, suggesting channels (particularly hNav1.6 channels) are not undergoing slow inactivation.

The lack of an effect of Navβ4 peptide on use-dependent reduction was surprising since Navβ4 peptide allows from fraction of the channels to bypass classic fast inactivation and increasing recovery from apparent inactivation. In order to further explore this, we also used trains of action potential waveforms, a more physiological stimulus, to elicit use-dependent reduction. Figure 15A shows the command waveform for the train of 20 slow APs at 33Hz and representative traces generated in response to the command waveform by hNav1.1 and hNav1.6. Voltage command waveforms for 33Hz fast AP and 8Hz slow and fast AP trains can be seen in Figure 3. The higher frequency trains elicited more use-dependent reduction than low frequency trains (one-way ANOVA; $p < 0.05$). However, addition of Navβ4 peptide did not significantly impact use-dependent reduction with either

hNav1.1 or hNav1.6 at any combination of frequency and AP waveform type (Fig. 15B).

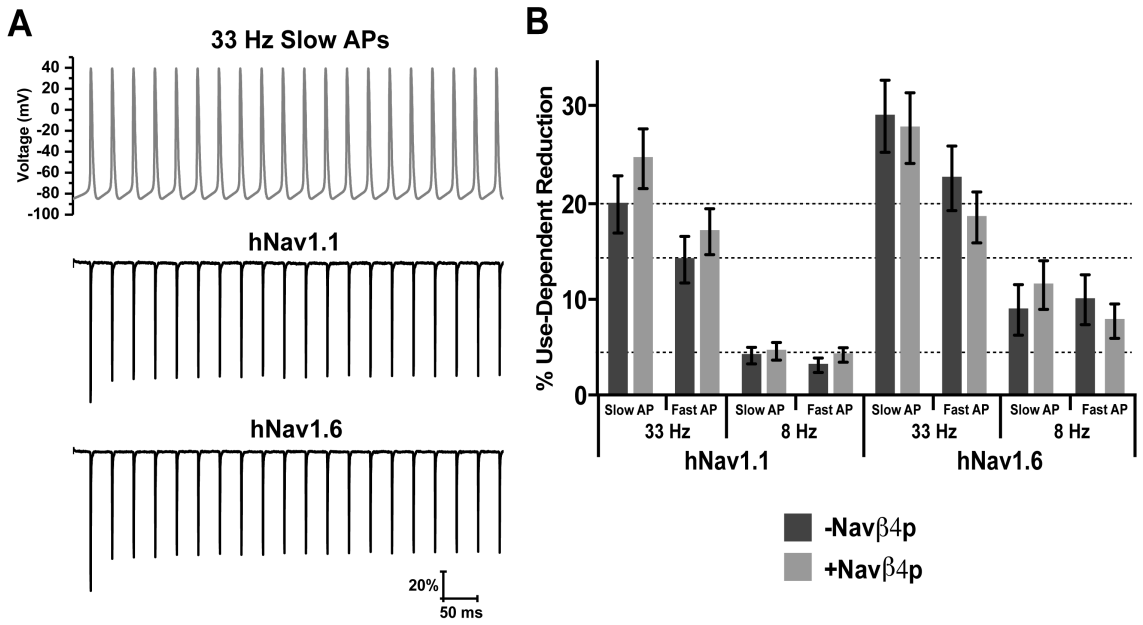

Figure 15. The Navβ4 peptide does not effect use-dependent reduction of hNav1.1 or hNav1.6 with 8 or 33Hz trains of slow or fast AP waveforms. A, Top: Voltage command waveform of 33 Hz slow APs comprising of a total of 20 APs. Below are representative traces of the response from cells expressing hNav1.1 (middle) and hNav1.6 (bottom) to the voltage command waveform. B, Percent reduction between the first and last current elicited by each frequency and waveform type in the absence (dark grey bars) and presence (light grey bars) Navβ4 peptide (*n* = 13-20).

D. Discussion

In this study we show that hNav1.1 and hNav1.6 exhibit distinct biophysical properties. hNav1.6 has a more hyperpolarized voltage-dependence of steady-state inactivation, faster development of closed-state inactivation, slower kinetics of open-channel inactivation and a greater propensity to generate resurgent currents. The presence of Navβ4 peptide mediated resurgent current generation by hNav1.1 and hNav1.6 allowed for a greater influx of sodium in response to a fast and slow AP waveform with an overall greater sodium influx mediated by hNav1.6. However, Navβ4 peptide did not protect against use-dependent reduction of either channel isoform.

The localization of Nav1.1, Nav1.6 and Navβ4 in the axon initial segment of parvalbumin-positive GABAergic neurons suggests their importance in sustaining high frequency firing. Three critical properties of VGSCs in cells with a fast-firing phenotype that likely contribute to fast firing include: slow development of inactivation during depolarizing potentials in the inter-spike interval, rapid recovery of channels after an AP spike and incomplete inactivation during APs [168, 169]. Our data indicate that Nav1.1 and Nav1.6 exhibit interesting differences in these potentially crucial biophysical properties suggesting that both channel isoforms are likely to be important for a fast firing phenotype. The slower development of closed-state inactivation that we observed with Nav1.1 should allow it to be more resistant to inactivation during slow subthreshold depolarizations in

the interspike interval compared to Nav1.6. Consequently, more Nav1.1 channels would be available to open once the membrane voltage reaches threshold for firing an AP. In contrast, we would predict that Nav1.6 contributes more to the rapid recovery of channels after an AP spike and incomplete inactivation during APs due to its greater propensity to generate resurgent current since Navβ4 mediated block allows channels to bypass classical inactivation and enhances recovery of the channels. Moreover, Nav1.6 showed faster repriming kinetics at -70mV although Nav1.1 had an overall greater fraction of recovery at voltages ranging from -90mV to -70mV.

Firing frequency correlates strongly with AP width [137, 166]. The width of the AP in many neurons is primarily controlled by repolarization mediated by potassium channels [169, 170]. Our data shows that the width of the AP waveform can greatly alter sodium current kinetics generated by Nav1.1 and Nav1.6. Both channel isoforms produced a larger second non-inactivating component in response to a fast AP waveform, which is consistent with observations in neurons [155, 169]. However, Nav1.6 showed a much greater second non-inactivating component compared to Nav1.1 in response to the fast AP possibly due to its slower rate of inactivation. The duration of the second non-inactivating component in response to the fast AP is increased by Navβ4 peptide for both isoforms although Nav1.6 carried the greatest overall sodium influx. Sodium currents in response to the slow AP waveform produced a smaller second non-inactivating component with both channel isoforms, but Navβ4 peptide increased both the duration as well as the

amplitude of the second non-inactivating component. Since the second non-inactivating component occurs during the down stroke of the AP waveform, we would predict that Navβ4 peptide would increase the number of non-inactivated (open) channels available immediately following an AP spike, which may enable burst firing [84]. Notably, the Navβ4 peptide produced a longer duration of increased sodium influx in response to the slow AP compared to the fast AP. This may reflect the ability of Navβ4 peptide to play a more prominent role in neurons with slow AP waveforms. Indeed, in neurons with fast AP waveforms, where the Kv3 family of channels predominantly mediate repolarization, VGSCs channels are primarily protected from inactivation by the fast kinetics of Kv3 channels that force VGSCs to transition directly from open into closed states rather than by open-channel block producing resurgent current [169]. Dynamic clamp studies have shown that Kv3 currents and resurgent sodium currents can synergize to protect channels from inactivation during the interspike interval of spontaneously firing Purkinje neurons [85]. Our data shows that Navβ4 peptide mediates a decrease in sodium current during the initial repolarization phase of the fast waveform (see Fig. 10C, E). A decrease in sodium flux at this point during a fast AP would likely also synergize with Kv3 currents and contribute to shorter AP durations.

Auxiliary β subunits of VGSCs are known to modulate the biophysical properties of principal α subunits [164, 171]. Navβ4 mediates the generation of resurgent sodium currents and allows channels to bypass classic inactivation. Though Nav1.6 has a greater intrinsic ability to generate resurgent currents, *Scn8a*

knockout animals demonstrate that the contribution of Nav1.6 to resurgent current generation can vary between neuronal populations suggesting that other factors can influence which isoform is predominantly generating resurgent current [87, 91, 172, 173]. It has previously been shown that there is a good correlation between resurgent current amplitude and the rate of inactivation, suggesting that Navβ4 competes with the intrinsic inactivation particle to bind the channel pore [63, 163]. Resurgent currents are expected to correlate with enhanced recovery of VGSCs from inactivation [84]. We found that Navβ4 peptide can correspondingly enhance recovery from an open-blocked versus inactivated state. We therefore predicted that Navβ4 peptide would protect channels from undergoing use-dependent reduction, which is the result of channels accumulating into an inactivated state and that this would be greater for Nav1.6 compared to Nav1.1. Unexpectedly, we found that Navβ4 peptide does not protect either Nav1.1 or Nav1.6 from use-dependent reduction with a 10Hz stimulus. Furthermore, stimulation with trains of fast or slow action potentials also did not uncover a detectable difference in use-dependent reduction in the presence of Navβ4 peptide. Therefore, at least under our experimental conditions, Navβ4 peptide does not appear to compete with the intrinsic mechanisms for use-dependent current reduction. This might be explained in part by proximity of the inactivation particle compared to the diffuse Navβ4 peptide to the channel and thus may not hold true for the full-length Navβ4 (which unfortunately does not produce resurgent sodium currents in HEK293T cells). It is important to note, full-length Navβ4 is a critical mediator for the generation of resurgent current in DRG neurons as knockdown and overexpression of Navβ4

decreases and increases resurgent current, respectively [69]. Mutating key positively charged residues in the C-terminal of Navβ4 prevents the increase in resurgent current [69], suggesting the appropriate use of the Navβ4 peptide to study resurgent current generation. We therefore tested the full-length Navβ4 in a DRG expression system and did not observe any differences in use-dependent reduction of Nav1.6 currents (Fig. 16), suggesting that our results are not a mere artifact of the peptide. Indeed, in a recent study comparing striatal neurons from Navβ4 null and wildtype mice, no difference was observed in the number of APs evoked by high-frequency stimulation trains for the two genotypes [67]. However, recent evidence indicates that A-type isoforms of FHFs mediate fast-onset long-term inactivation of sodium channels in hippocampal neurons [174]. FHFs and Navβ4 have been proposed to differentially regulate neuronal activity [75], and thus we cannot rule out the possibility that Navβ4 might reduce use-dependent current reduction in some neurons by competing with the effect of FHFs on sodium channel inactivation.

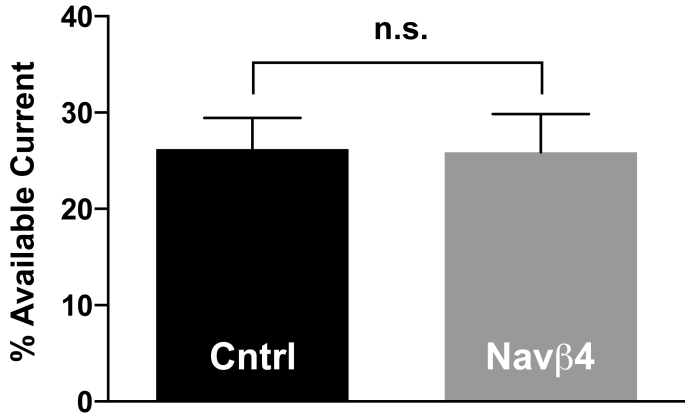

Figure 16. No difference in the use-dependent reduction of Nav1.6 generated currents in DRG for control (black; *n* = 17) and full-length Navβ4 (grey; *n* = 11). N.s., not significant; unpaired t-test. Data generated by Cindy Barbosa.

Subcellular regions within a neuron serve different functions: dendrites provide graded electrical potentials that sum in the soma, the axon initial segment typically initiates action potentials and the nodes of ranvier and axon propagate the action potentials. As mentioned in the introduction of this chapter, Nav1.1 and Nav1.6 are reported to have distinct subcellular distributions. While the molecular determinants of this differential localization are not known, the distinct biophysical properties of these channels may be 'tuned' for specific contributions in different cellular regions as well as neuronal populations as has been shown with Nav1.2 and Nav1.6 in the proximal and distal axon initial segment of excitatory, pyramidal cells [150].

Our data shows that hNav1.6 undergoes more use-dependent reduction compared to hNav1.1 and this is consistent with the proposal that Nav1.1 likely plays a major role in maintenance of fast firing, especially in inhibitory neurons. hNav1.6 currents exhibit slower rates of open-channel inactivation (Fig. 8E), larger resurgent currents (Fig. 8C) and quicker recovery from open-channel inactivation (Fig. 6B) than hNav1.1 currents, indicating that open-channel inactivation is not a major determinant of the use-dependent reduction that we observed. Although slow inactivation might contribute to use-dependent current reduction under some conditions [175, 176], our data and that of others indicate that Nav1.6 channels are less susceptible to slow inactivation than Nav1.1 channels [167]. hNav1.6 channels do exhibit enhanced closed-state inactivation compared to hNav1.1 channels (reflected by a more negative voltage-dependence of inactivation and more rapid

development of closed-state inactivation for hNav1.6), suggesting that closed-state inactivation may play an important role in the use-dependent current reduction that we measured.

E. ABERRANT EPILEPSY-ASSOCIATED MUTANT NAV1.6 SODIUM CHANNEL ACTIVITY CAN BE TARGETED WITH CANNABIDIOL

This chapter is adapted from a manuscript published in *Brain*.

Reesha R. Patel, Cindy Barbosa, Tatiana Brustovetsky, Nickolay Brustovetsky and Theodore R. Cummins

R. R. Patel designed experiments, conducted all electrophysiological experiments, analyzed and interpreted the data and drafted the manuscript.

A. Introduction

There are over 700 mutations identified in brain isoforms of VGSCs in patients with distinct epileptic phenotypes. The majority of these mutations occur in the *Scn1a* gene encoding for Nav1.1 and result in a phenotype known as Generalized Epilepsy with Febrile Seizures Plus (GEFS+) or a more severe form of this termed Dravet Syndrome. The majority of mutations lead to protein truncation and amino acid substitutions that occur throughout the channel protein. Functionally, they are primarily thought to cause loss of channel activity. In accordance with the prominent role of Nav1.1 in parvalbumin positive GABAergic neurons, the prevailing hypothesized mechanism underlying Dravet Syndrome is the loss of Nav1.1 channel activity leading to decreased excitability of GABAergic neurons and

consequently a disinhibition in circuit excitability [145, 177-180]. Indeed, selective deletion of Nav1.1 in parvalbumin positive GABAergic neurons can lead to seizures and mimic a Dravet Syndrome phenotype [179, 181-183]. Moreover, Higurashi *et al.* have observed reduced excitability of GABAergic neurons differentiated from pluripotent stem cells derived from a human patient with Dravet Syndrome [184]. However, it is important to note that recent data from human patient-derived induced pluripotent stem cells challenges this hypothesis and suggests that rather there is an overall upregulation of VGSC activity leading to increased excitability of both excitatory and inhibitory neurons [121, 122]. Recently, there have been mutations identified in *Scn8a* (coding for Nav1.6) in patients with a severe EIEE [123, 124, 185-188]. Of the Nav1.6 mutations characterized in heterologous expression systems, it has been found that most of these mutations result in gain-of-function in channel properties [123, 189], although putative loss-of-function effects on channel properties have also been reported for Nav1.6 mutations [187, 190, 191]. Mutations in these two isoforms cause phenotypically distinct syndromes and understanding the functional consequences of these mutations can provide invaluable insight into the potential role of these channels in physiological and pathophysiological conditions.

Approximately 30% of people with epilepsy are refractory to treatment; therefore there is a great need for the development of alternative anti-epileptic medications. CBD has recently received attention for its potential efficacy in the treatment of childhood epilepsies [192], although more studies are needed to

confirm this finding. Resurgent current is an atypical current predicted to enhance neuronal excitability [84, 193]. Mechanistically, these currents arise from channel reopening during the repolarization phase of the action potential due to unbinding of an open-channel blocker [92]. Therefore, these currents provide a depolarizing drive to approach threshold for firing additional action potentials. These currents have been observed to be dysregulated in both acquired and inherited disorders of excitability. Resurgent currents are increased in a kindling model of temporal lobe epilepsy as well as by mutations in VGSCs associated with pain, myotonia and cardiac arrhythmias [64, 80, 194, 195]. Targeting resurgent sodium current is a potentially novel therapeutic strategy for the treatment of multiple epilepsy syndromes. Intriguingly, endogenous, exogenous and synthetic cannabinoids have been shown to target peak transient currents generated by VGSCs [81, 139, 196-198]. In addition, our lab has previously shown that with Nav1.7, which is present in DRG neurons but not expressed in the brain, AEA can selectively inhibit resurgent current over peak transient current [81]. Furthermore, Foadi *et al.* found that a synthetic derivative of Δ9-tetrahydrocannabinol, ajulemic acid, can inhibit resurgent currents generated by Nav1.5, although this isoform is predominantly expressed in the heart.

Here we focused on mutations in Nav1.1 and Nav1.6 because of the severity of the clinical phenotypes associated with these mutations [199]. We asked whether epilepsy-associated mutations in these channel isoforms alter resurgent sodium current generation, and whether we can preferentially inhibit resurgent sodium

current over peak transient current generated by these two channel isoforms. We found that epilepsy-associated mutations in Nav1.6 dramatically enhanced resurgent current generation while mutations in Nav1.1 did not, suggesting that mutations in these channel isoforms are acting by distinct mechanisms to induce epileptogenesis. Moreover, CBD can selectively inhibit resurgent current over peak transient current generated by wildtype Nav1.6 as well as aberrant resurgent and persistent current generated by Nav1.6 mutant channels. We further validated our findings using endogenous sodium currents from striatal neurons and found that indeed CBD inhibits endogenous resurgent and persistent current in neurons. Furthermore, we found that excitability of striatal neurons is reduced in the presence of CBD. Therefore, CBD could be exerting its anti-epileptic effects, at least in part, through its action on aberrant activity in VGSCs.

B. Materials and methods

1. cDNA constructs

Optimized human constructs for Nav1.1 and Nav1.6 (hNav1.1 and hNav1.6) were designed in-house and purchased from Genscript (Piscataway, NJ). cDNA constructs for wildtype Nav1.1 and Nav1.6 channels encode for amino acid sequences corresponding to the accession numbers BAC21102.1 and NP_055006.1 in the NCBI database, respectively. Mutations were introduced into wildtype cDNA constructs (hNav1.1 R1648H, hNav1.1 N1788K, hNav1.1 N1788D, hNav1.6 L1331V,

hNav1.6 N1768D, and hNav1.6 N1768K) using the QuikChange II XL site-directed mutagenesis kit from Agilent Technologies (Santa Clara, CA) according to the manufacture's instructions. Mutant channel constructs were fully sequenced (ACGT, Inc., Wheeling, IL) to confirm the presence of the correct mutation and absence of additional mutations.

2. Cell cultures and transfections

The use of HEK293T cells [153] was approved by the Institutional Biosafety Committee and followed the ethical guidelines for the National Institutes of Health for the use of human-derived cell lines. HEK293T cells were grown under standard tissue culture conditions. HEK293T cells were transiently transfected using the calcium phosphate precipitation method. Briefly, calcium phosphate-DNA mixture (4.5 μg channel construct and 0.5 μg EGFP) was added to cells in serum-free media for four to five hours, after which it was replaced with normal media. 12-24 hours post-transfection, cells were split onto laminin-coated glass coverslips. Cells were identified by expression of EGFP using a fluorescent microscope and whole-cell patch clamp recordings were obtained 36-72 hours post-transfection. Wildtype and mutant Nav1.6 channels were incubated at 29°C overnight to increase protein surface expression.

3. Striatal neuron cultures

Procedures with mice were performed in accordance with the Institutional Animal Care and Use Committee approved protocol. FVB/NJ mice were purchased from Jackson Laboratories (Bar Harbor, ME, USA) and breeding colonies were established. The mice were housed under standard conditions with free access to water and food. Striatal neuronal cultures were prepared from individual striata of postnatal day 1 (PN1) wildtype FVB/NJ mice of both sexes. We used neuronal-glial co-cultures derived from PN1 mouse pups because it is more physiologically relevant and allows for the study of more mature, better developed cells than pure neuronal cultures derived from embryonic animals. For all platings, 35 mg/mL uridine plus 15 mg/mL 5-fluoro-20-deoxyuridine were added 24 hours after plating to inhibit proliferation of non-neuronal cells. Neurons were cultured in a 5% CO2 atmosphere at 37°C in Neurobasal medium with B27 supplement (Life Technologies). Cultures were used for electrophysiological recordings at 7-12 days.

4. Chemicals and solutions

AEA and CBD were purchased from Sigma Aldrich Co. (St. Louis, MO) and Cayman Chemical Company (Ann Arbor, MI), respectively. AEA was dissolved in ethanol to a stock concentration of 138.3mM, aliquoted and stored at -20°C. CBD was dissolved in methanol to a stock concentration of 31.8mM, aliquoted into tubes topped will argon gas and stored at -80°C. A fresh aliquot of drug was used and diluted with the extracellular patch clamp solution to desired concentration for each

experiment. Control data was collected in the presence of the corresponding vehicle used to dissolve the drug.

5. Whole-cell patch clamp recordings

All whole-cell patch clamp recordings were obtained at room temperature (~23°C) using a HEKA EPC-10 amplifier and the Pulse program (v 8.80, HEKA Electronic, Germany) was used for data acquisition. For experiments with HEK293T cells, electrodes were fabricated from 1.7 mm capillary glass and fire-polished to a resistance of 0.9-1.3 MΩ using a Sutter P-97 puller (Sutter Instrument Company, Novato, CA). All voltage protocols were started five minutes after obtaining a gigaΩ seal and entering the whole-cell configuration, which controlled for time-dependent shifts in channel properties and allowed time for diffusion of the Navβ4 peptide. Voltage errors were minimized to less than 5mV using series resistance compensation and passive leak currents were cancelled by P/-5 subtraction. The bath solution contained (in mM): 140 NaCl, 1 MgCl2, 3 KCl, 1 CaCl2, and 10 Hepes, adjusted to a pH of 7.30 with NaOH. The pipette solution contained (in mM): 140 CsF, 10 NaCl, 1.1 EGTA, and 10 Hepes, adjusted to a pH of 7.30 with CsOH. To induce resurgent currents in HEK293T cells, 200μM Navβ4 peptide (KKLITFILKKTREK-OH) (Biopeptide Co., San Diego, CA), a peptide that corresponds to the sequence of part of the C-terminal tail of the full-length Navβ4 subunit, was included in the pipette solution.

For recordings obtained from striatal neurons, pipettes were fabricated from 1.5 mm borosilicate glass and fire-polished to a resistance of 2-4 MΩ. Series resistance was compensated by 70 to 85%. For voltage clamp recordings, the striatal neuron bath solution contained (in mM): 130 NaCl, 30 TEA-Cl, 3 KCl, 1 $MgCl_2$, 1 $CaCl_2$, 0.05 $CdCl_2$, 5 4-aminopyridine and 10 Hepes, adjusted to a pH of 7.3 with NaOH. The pipette solution was the same CsF containing solution mentioned above but did not contain the Navβ4 peptide. For current clamp recordings, the bath solution contained (in mM): 140 NaCl, 3 KCl, 2 $MgCl_2$, 2 $CaCl_2$ and 10 HEPES adjusted to a pH of 7.3 with NaOH. The pipette solution contained (in mM): 140 KCl, 0.5 EGTA, 5 HEPES and 3 Mg-ATP adjusted to a pH of 7.3 with KOH. Recordings were all started two minutes after establishing the whole-cell configuration. Only cells with a stable resting membrane potential more negative than -35mV were used. To eliminate variation between cells, cells were held at -60mV or -80mV.

For all experiments involving drugs, recordings were made in the presence of extracellular bath solution containing either the drug or vehicle control. Each coverslip was recorded from for up to one and half hours before discarding.

6. Data analysis

Electrophysiological data were analyzed using Pulsefit (v 8.67 HEKA Electronic, Germany), Microsoft Excel, Origin (v 8.0, OriginLab Corp, Northhampton, MA), and Prism (v 6.0, Graphpad Software Inc., La Jolla, CA). Steady-state activation

and inactivation curves were fit to a Boltzmann function to obtain midpoint ($V_{1/2}$) and slope values. Time constants for recovery were obtained by fitting data from each cell to a first order exponential function and averaging time constants across cells. Input resistance was calculated from the change in voltage at the end of a 200ms, -200pA current stimulus using the equation V = I/R. All data points are presented as mean ± SEM and *n* is the number of experimental cells from which recordings were obtained. Statistical significance was assessed using an unpaired t-test, one-way ANOVA with Dunnett *post hoc* test or a two-way ANOVA with Bonferroni *post hoc* test.

C. Results

1. Epilepsy-associated mutations in Nav1.1 resulting in GEFS+ or Dravet Syndrome did not alter peak resurgent current

We examined an arginine (R) to histidine (H) mutation at position 1648 in Nav1.1, which is located in the S4 segment of domain IV, identified in patients with GEFS+ (Fig. 17A) [200]. This mutation has been previously characterized in both heterologous expression systems and mouse models and from the reported biophysical defects that this mutation confers we predicted it would alter resurgent current generation [201-205]. Additionally, we examined an asparagine (N) to lysine (K) mutation at position 1788 in Nav1.1, which is located at the end of the S6 segment of domain IV, identified in a patient with Dravet Syndrome (Fig. 17A).

Coincidentally, this mutation occurs at the exact same position as the first epilepsy-associated mutation identified in human Nav1.6 [123] and has not been previously characterized (Fig. 20A). We characterized the biophysical properties of the wildtype and mutant hNav1.1 channels with whole-cell patch clamp recordings from transiently transfected HEK293T cells. Representative families of current traces from wildtype and mutant channels, elicited by applying depolarizing step pulses ranging from –80mV to +80mV for 50ms from a holding potential of -100mV, are shown in Figure 18B. Current density curves were obtained by normalizing peak current at each voltage by the cell capacitance. hNav1.1 R1648H and hNav1.1 N1788K have significantly ($p<0.05$; two-way ANOVA) reduced current densities compared to hNav1.1 WT (Fig. 17C). We next examined the voltage dependence of channel activation and steady-state inactivation (Fig. 17D; Table 3). hNav1.1 N1788K has a significantly ($p<0.05$; one-way ANOVA) more depolarized $V_{1/2}$ of channel activation and steady-state inactivation compared to wildtype hNav1.1 (Table 3). hNav1.1 R1648H did not show significant changes in channel activation but has a significantly ($p<0.001$; one-way ANOVA) hyperpolarized voltage-dependence of steady-state inactivation (-73.0 ± 2.2mV; n = 10) compared to wildtype hNav1.1 (-61.6 ± 1.7mV; n = 20). We also examined persistent current generation by wildtype and mutant channels using a protocol in which incremental step pulses from -80mV to +30mV were applied from a holding potential of -100mV for 200ms (Fig. 17E, *inset*). Persistent current is a non-inactivating (or very slowly-inactivating) current and was measured at the end of a long (200ms) depolarizing step pulse. These currents can amplify subthreshold currents and facilitate

repetitive firing [206, 207]. We found that neither the hNav1.1 R1648H nor the hNav1.1 N1788K mutant channel significantly altered persistent current (Fig. 17E). Additionally, we examined steady-state slow inactivation, recovery from slow inactivation as well as development of slow inactivation. We found no significant effects of hNav1.1 mutant channels on steady-state slow inactivation or development of slow inactivation. hNav1.1 N1788K significantly ($p<0.0001$; one-way ANOVA) slowed recovery from slow inactivation compared to wildtype hNav1.1 (Fig. 18A-C; Table 4). From these findings, it appears that both hNav1.1 R1648H and hNav1.1 N1788K mutants have loss-of-function effects on some channel properties.

We next asked whether epilepsy-associated mutations in hNav1.1 alter resurgent sodium current generation. Resurgent currents are predicted to increase neuronal excitability and therefore alterations in these currents could potentially underlie the hyperexcitability seen in epilepsy. Resurgent currents were observed by applying an initial depolarizing step to +60mV from -100mV and subsequently repolarizing incrementally from +25mV to -80mV (Fig. 17F). Representative families of resurgent current traces from hNav1.1 wildtype and mutant channels can be seen in Fig. 17G. Peak resurgent current was measured after 1.5ms into the repolarization step to bypass fast tail currents. The percent resurgent current was reported after normalizing the peak resurgent current at each repolarizing voltage step to a single measure of the peak transient current amplitude in each cell. The estimate of peak transient current amplitude in each cell was obtained from a

depolarization step to +10mV from -120mV. This provides a consistent and reliable peak transient current value for each cell, and normalizing the peak resurgent current values to this measure of peak transient current greatly helps to control for variability in channel expression in HEK293T cells. We found that there was no significant difference in the normalized magnitude of the peak resurgent current generated by mutant hNav1.1 channels compared to wildtype hNav1.1 (Fig. 17H). Although there appears to be a shift in the voltage-dependence of resurgent current for mutant hNav1.1 channels, these shifts correspond with shifts in channel activation seen in Figure 17D. Therefore, it is plausible that these shifts are a consequence of alterations in channel activation rather than direct effects of the mutation on the channels' ability to generate resurgent current. It was surprising that the hNav1.1 R1648H mutant channel did not alter peak resurgent current since it demonstrated a faster rate of inactivation (data not shown). However, from these data is appears that peak resurgent currents are not altered by epilepsy-associated mutant Nav1.1 R1648H and N1788K channels.

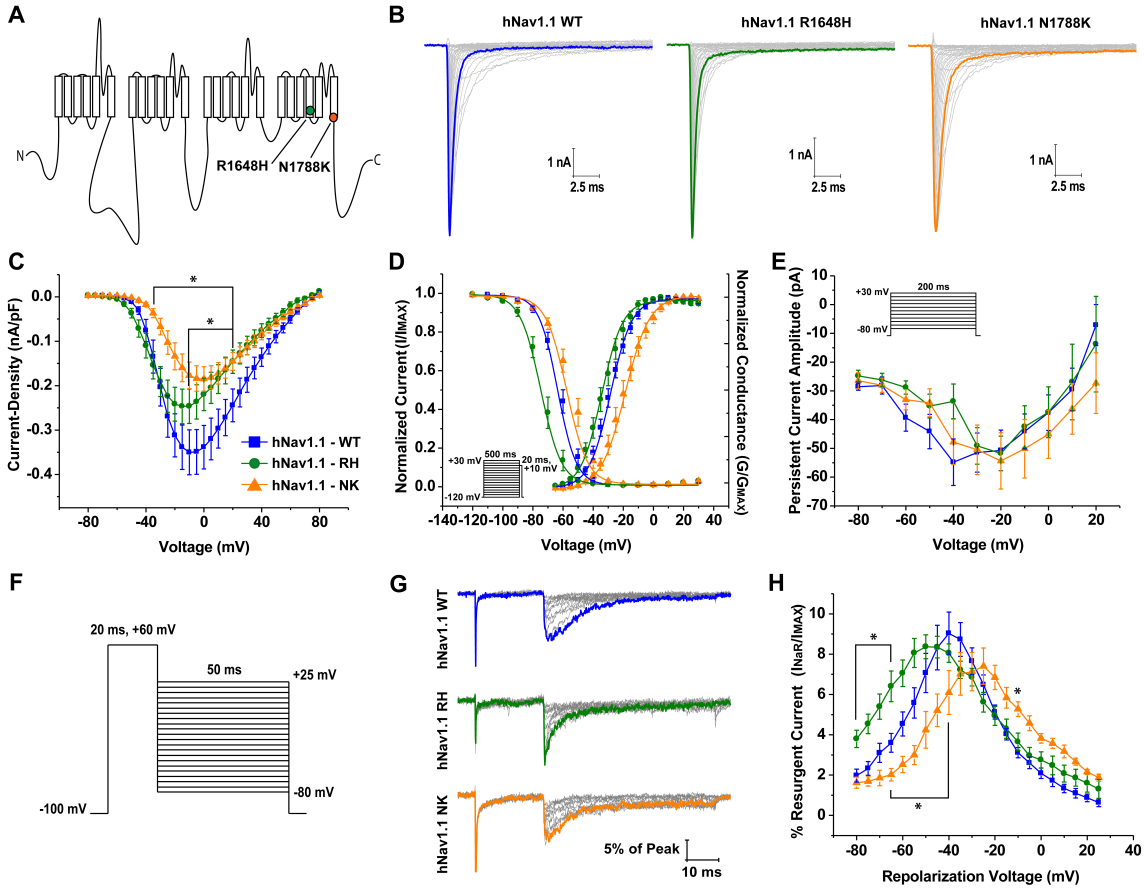

Figure 17. Biophysical characterization of hNav1.1 WT, R1648H and N1788K mutant channels. A, Linear schematic of the structure of the VGSC α- subunit depicting the locations of the hNav1.1 R1648H (green circle) and hNav1.1 N1788K (orange circle) mutations. B, Representative family of current traces generated by hNav1.1 WT, R1648H and N1788K expressing HEK293T cells. Currents were elicited with step depolarizations ranging from -80mV to +80mV for 50ms from a holding potential of -100mV. Peak current traces are bolded. C, Current density – voltage curve for hNav1.1 WT (blue squares), R1648H (green circles) and N1788K (orange triangles). Current density values were calculated by normalizing the peak sodium current at each voltage to the cell capacitance and subsequently averaged across cells. D, Voltage dependence of steady-state activation and inactivation curves fit with a Boltzmann function. Steady-state inactivation was measured using a protocol in which cells were held at a series of voltages ranging from -120mV to +30mV for 500ms followed by a 20ms step pulse to +10mV to measure channel availability (*inset*). E, Persistent current amplitude plotted as a function of voltage. Persistent current was measured at 180ms into current traces elicited by step depolarizations ranging from -80mV to +30mV from a holding potential of -100mV (*inset*). F, Step depolarization from -100mV to +60mV for 20ms to open channels allowing them to undergo open-channel block and subsequently repolarizing to a series of potentials ranging from +25mV to -80mV for 50ms to allow the blocker to unbind. G, Representative family of resurgent current traces generated by hNav1.1

WT (top), R1648H (middle) and N1788K (bottom). Peak resurgent current traces are bolded. H, Percent resurgent current plotted as a function of the repolarization voltage for hNav1.1 WT (blue squares; *n* = 29), R1648H (green circles; *n* = 17) and N1788K (orange triangles; *n* = 11). Percent resurgent current was calculated by normalizing peak resurgent current at each voltage to peak transient current measured with a single step pulse from -120mV to +10mV. *, $p<0.05$; two-way ANOVA.

Table 3. Summary of gating parameters of hNav1.1 and hNav1.6 wildtype and mutant channels.

	Activation		Inactivation		
	$V_{1/2}$ (mV)	slope	$V_{1/2}$ (mV)	slope	*n*
hNav1.1 WT	-28.9 ± 1.5	6.7	-61.6 ± 1.7	5.0	20
hNav1.1 R1648H	-33.6 ± 2.1	7.2	-73.0 ± 2.2$^{\#}$	5.4	10
hNav1.1 N1788K	-19.3 ± 2.3**	7.5*	-54.1 ± 2.2*	6.5$^{\#\#}$	11
hNav1.6 WT	-29.2 ± 1.2	6.2	-71.1 ± 1.8	6.4	18
hNav1.6 L1331V	-31.6 ± 1.9	8.4$^{\#\#}$	-78.2 ± 2.8	6.8	9
hNav1.6 N1768D	-24.8 ± 2.2	6.6	-58.5 ± 2.7$^{\#}$	7.6$^{\#\#}$	14

*, $p < 0.05$, **, $p < 0.01$, $^{\#}$, $p < 0.001$ and $^{\#\#}$, $p<0.0001$ as compared to the corresponding wildtype group with a one-way ANOVA with Dunnett *post hoc*.

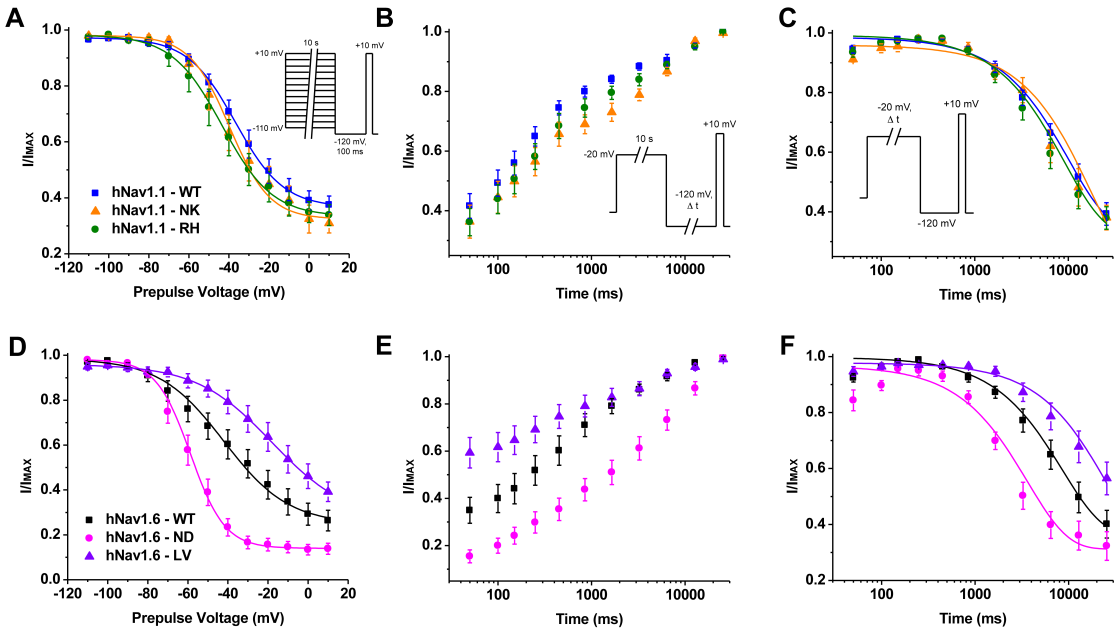

Figure 18. Steady-state, recovery and development of slow inactivation of wildtype and mutant channels in HEK293T cells. A, Steady-state slow inactivation curve for hNav1.1 wildtype (blue squares; *n* = 12), hNav1.1 N1788K (orange triangles; *n* = 9), and hNav1.1 R1648H (green circles; *n* = 12) fit with a Boltzmann function. Slow inactivation was examined with a 10 second conditioning pulse increasing incrementally from -110mV to +10mV followed by a step to -120mV for 100ms to recover channels from fast inactivation and a test pulse to +10mV to assess available channels. B, Normalized available current plotted versus recovery duration. Recovery from slow inactivation was measured by holding cells at -20mV for 10 seconds and subsequently hyperpolarizing to -120mV for increasing durations to recover channels and assessing channel availability with a final test pulse to +10mV. C, Development of slow inactivation curve with a single exponential function. To examine the development of slow inactivation cells were held at -20mV for increasing durations and then stepped to -120mV for 100ms to recover channels from fast inactivation after which a test pulse to +10mV was applied to assess channel availability. D, Steady-state slow inactivation curves for hNav1.6 wildtype (black squares; *n* = 12), hNav1.6 N1768D (magenta circles; *n* = 12), and hNav1.6 L1331V (purple triangles; *n* = 13). E, Recovery from slow inactivation. F, Development of slow inactivation.

Table 4. Summary of steady-state, recovery, and development of slow inactivation for wildtype and mutant channels.

	Slow Inactivation		Recovery	Development	
	$V_{1/2}$ (mV)	slope	τ (s)	τ (s)	*n*
hNav1.1 WT	-35.3 ± 3.0	10.8	0.43 ± 0.04	11.6 ± 2.7	12
hNav1.1 R1648H	-41.8 ± 3.9	10.8	0.51 ± 0.04	11.1 ± 3.8	12
hNav1.1 N1788K	-36.7 ± 4.5	11.2	1.48 ± 0.21##	14.1 ± 4.7	9
hNav1.6 WT	-38.8 ± 6.1	15.7	1.07 ± 0.19	12.5 ± 2.3	12
hNav1.6 L1331V	-17.6 ± 6.4*	15.6	1.84 ± 0.47	21.8 ± 3.5*	14
hNav1.6 N1768D	-59.0 ± 2.8*	7.1##	5.65 ± 2.06*	3.3 ± 0.32*	12

*, $p < 0.05$ and ##, $p<0.0001$ as compared to the corresponding wildtype group with a one-way ANOVA with Dunnett *post hoc*.

2. Epilepsy-associated mutations in Nav1.6 resulting in an epileptic encephalopathy increase peak resurgent current

Epilepsy-associated mutations in Nav1.6 are phenotypically distinct from those in Nav1.1 [199, 208]. Therefore we examined how epilepsy-associated mutations in Nav1.6 alter biophysical characteristics of the channel. We examined a leucine (L) to valine (V) mutation at position 1331 in hNav1.6, which is located in the S4-S5 linker in domain III, identified in a patient with an EIEE (Fig. 19A) [186]. This mutation is in a region of the channel important for coordinating the binding site for the intrinsic fast inactivation particle of the channel [209, 210]. Although this mutation has not yet been characterized, we predicted it would alter resurgent current generation based on its location. Additionally, we examined an asparagine to aspartic acid (D) mutation at position 1768 in hNav1.6, which is located at the end of the S6 segment of domain IV, identified in a patient with a severe epileptic encephalopathy (Fig. 19A) [211]. As mentioned previously, this mutation (hNav1.6 N1768D) occurs at the same position as the Dravet Syndrome-associated hNav1.1 N1788K mutation (Fig. 20A). Representative families of peak transient current traces from hNav1.6 wildtype and mutant channels can be seen in Figure 19B. We did not observe significant differences in peak current density or the $V_{1/2}$ of channel activation of mutant channels compared to wildtype hNav1.6 (Fig. 19C,D; Table 3). Peak current density was measured from hNav1.6 wildtype and mutant channels from HEK293T cells that had been cultured at 30°C overnight prior to obtaining patch clamp recordings. This procedure can boost channel expression at the cell

plasma membrane possibly by rescuing expression of mutant channels with folding or trafficking defects as has been reported by others [212-215]. While we do not know how specific disease mutations might alter functional channel density in patients, it is important to note that this methodological procedure does not effect the voltage-dependence of channel activation or inactivation [190]. The voltage dependence of steady-state inactivation is significantly ($p<0.001$; one-way ANOVA) depolarized for hNav1.6 N1768D (-58.5 ± 2.7mV; n = 14) compared to wildtype hNav1.6 (-71.1 ± 1.8mV; n = 18). Both mutations in hNav1.6 impaired fast inactivation as evidenced by incomplete inactivation in the steady-state inactivation curve (Fig. 19D, *inset*). We next examined persistent current and found that hNav1.6 N1768D produces a very large persistent current while hNav1.6 L1331V has similar persistent current amplitudes as wildtype (Fig. 19E). hNav1.6 mutant channels had opposing effects on slow inactivation (Fig. 18D-F; Table 4). hNav1.6 L1331V had a significantly ($p<0.05$; one-way ANOVA) more depolarized $V_{1/2}$ of slow inactivation and was slower to develop slow inactivation compared to wildtype hNav1.6. hNav1.6 N1768D had a significantly ($p<0.05$; one-way ANOVA) more hyperpolarized $V_{1/2}$ of slow inactivation, was slower to recover from slow inactivation and faster to develop slow inactivation (Fig. 18D-F). It is not clear how these effects on slow inactivation would impact excitability since the prolonged depolarizations that are needed to induce slow inactivation may not occur under normal physiological conditions and the temperature sensitivity of slow inactivation is unclear. However, slow inactivation could be a factor during seizure activity due to the sustained depolarization of some neurons during this hyperactivity. Our

findings on hNav1.6 N1768D mutant channels are consistent with previous reports and clearly demonstrate that this mutation results in gain-of-function [123]. In contrast, biophysical defects conferred by the hNav1.6 L1331V mutation are subtler but (at this point in the analysis) could be characterized as loss-of-function.

To further explore the biophysical consequences of the hNav1.6 epilepsy-associated mutations, we examined resurgent sodium current generation. Representative families of resurgent current traces generated by wildtype and mutant channels can be seen in Figure 19F. We found that both hNav1.6 L1331V and hNav1.6 N1768D have a greater propensity to generate resurgent sodium current compared to wildtype hNav1.6. The peak resurgent current amplitude generated by hNav1.6 L1331V and hNav1.6 N1768D is nearly tripled and doubled, respectively, compared to wildtype hNav1.6 (Fig. 19G). This finding clearly demonstrates that both mutations in hNav1.6 have gain-of-function effects on some channel properties which is in contrast to the mutations we examined in hNav1.1, suggesting that epilepsy-associated mutations in these two channel isoforms act by distinct mechanisms and consequently result in different phenotypes.

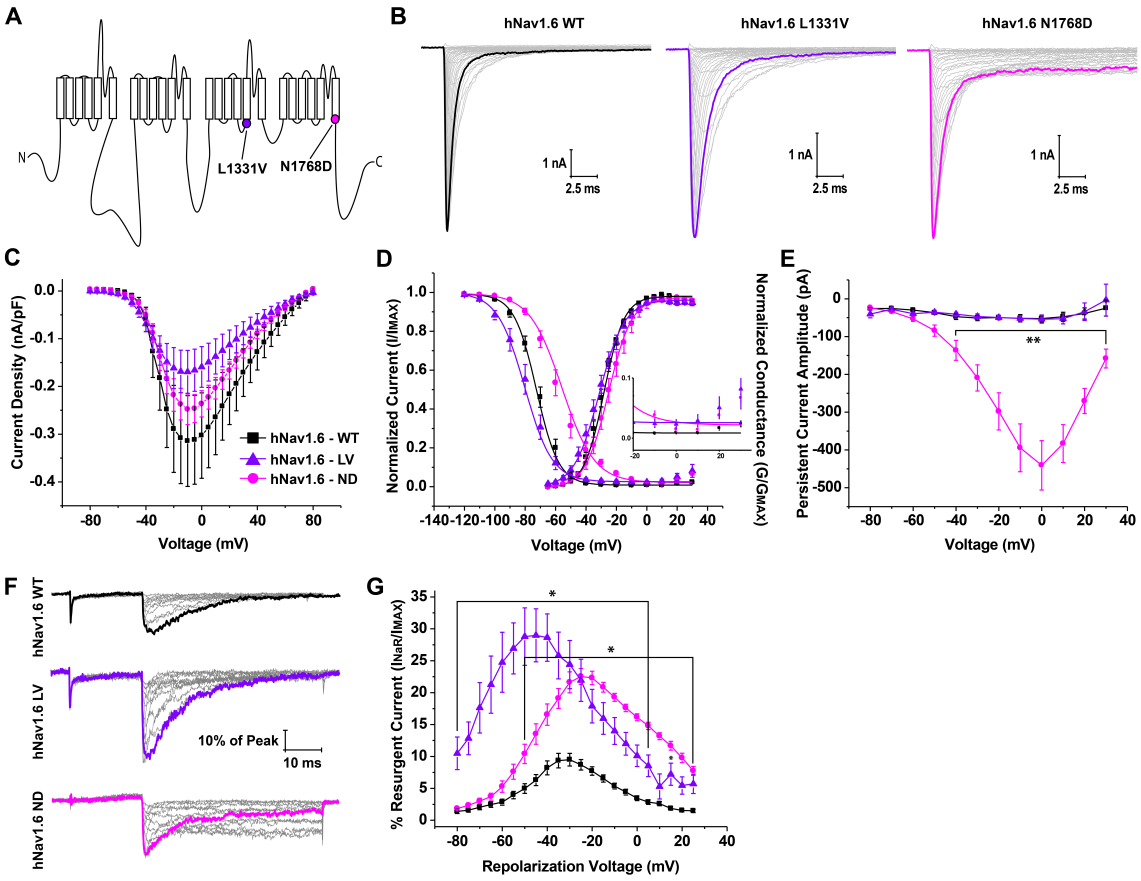

Figure 19. Biophysical characterization of hNav1.6 WT, L1331V and N1768D mutant channels. A, Linear schematic of the structure of the VGSC α- subunit depicting the locations of the hNav1.6 L1331V (purple circle) and N1768D (magenta circle) mutations. B, Representative family of current traces generated by HEK293T cells expressing hNav1.6 WT, L1331V and N1768D channels. Peak current traces are bolded. C, Plot of current density versus voltage. D, Steady-state inactivation and activation curves fit with a Boltzmann function. *Inset*, Magnification of the voltage-dependence of inactivation curve between -20mV to +30mV depicting incomplete inactivation of mutant channels. E, Peak persistent current amplitude plotted as a function of voltage. F, Representative family of resurgent current traces generated by hNav1.6 WT (top), L1331V (middle) and N1768D (bottom). Peak resurgent current traces are bolded. G, Percent resurgent current plotted as a function of the repolarization voltage for hNav1.6 WT (black squares; n = 20), L1331V (purple triangles; n = 11) and N1768D (magenta circles; n = 14). *, p<0.05; two-way ANOVA.

3. Alterations in peak resurgent and persistent current conferred by the mutation are independent of channel isoform

Nav1.6 N1768D was the first human epilepsy-associated mutation to be reported in the Nav1.6 isoform and coincidentally occurs at the same position as a previously identified Dravet Syndrome-associated mutation in Nav1.1 (Nav1.1 N1788K) (Fig. 20A) [123, 216]. This gave us a unique opportunity to ask whether disease mutations confer the same biophysical consequences to different channel isoforms. To address this we created the reciprocal mutations in the non-native channel isoform (hNav1.1 N1788D and hNav1.6 N1768K). We measured resurgent and persistent sodium current generation by these mutant channels since we observed dramatic changes in these properties with the epilepsy-associated mutant channels. It is noteworthy that these disease mutations result in oppositely charged residue substitutions. We found similar alterations in resurgent and persistent current for the reciprocal mutations in the non-native channel isoform, although the magnitudes of the changes varied. In hNav1.1 the N1788D mutation increases both resurgent and persistent current, similar to the epilepsy-associated hNav1.6 N1768D mutant (Fig. 20B,C). In hNav1.6 the N1768K mutation did not alter peak resurgent current or persistent current amplitude, similar to the epilepsy-associated hNav1.1 N1788K mutant (Fig. 20D,E). These data show that epilepsy-associated mutations cause similar alterations in channel properties independent of channel isoform and that different amino acid substitutions at the same position in the channel can cause significantly different effects on channel properties. This suggests

that distinct phenotypes likely arise from not only differences in the expression pattern and regulation of the channel isoform in which the mutation occurs but is also dependent on the amino acid residue itself.

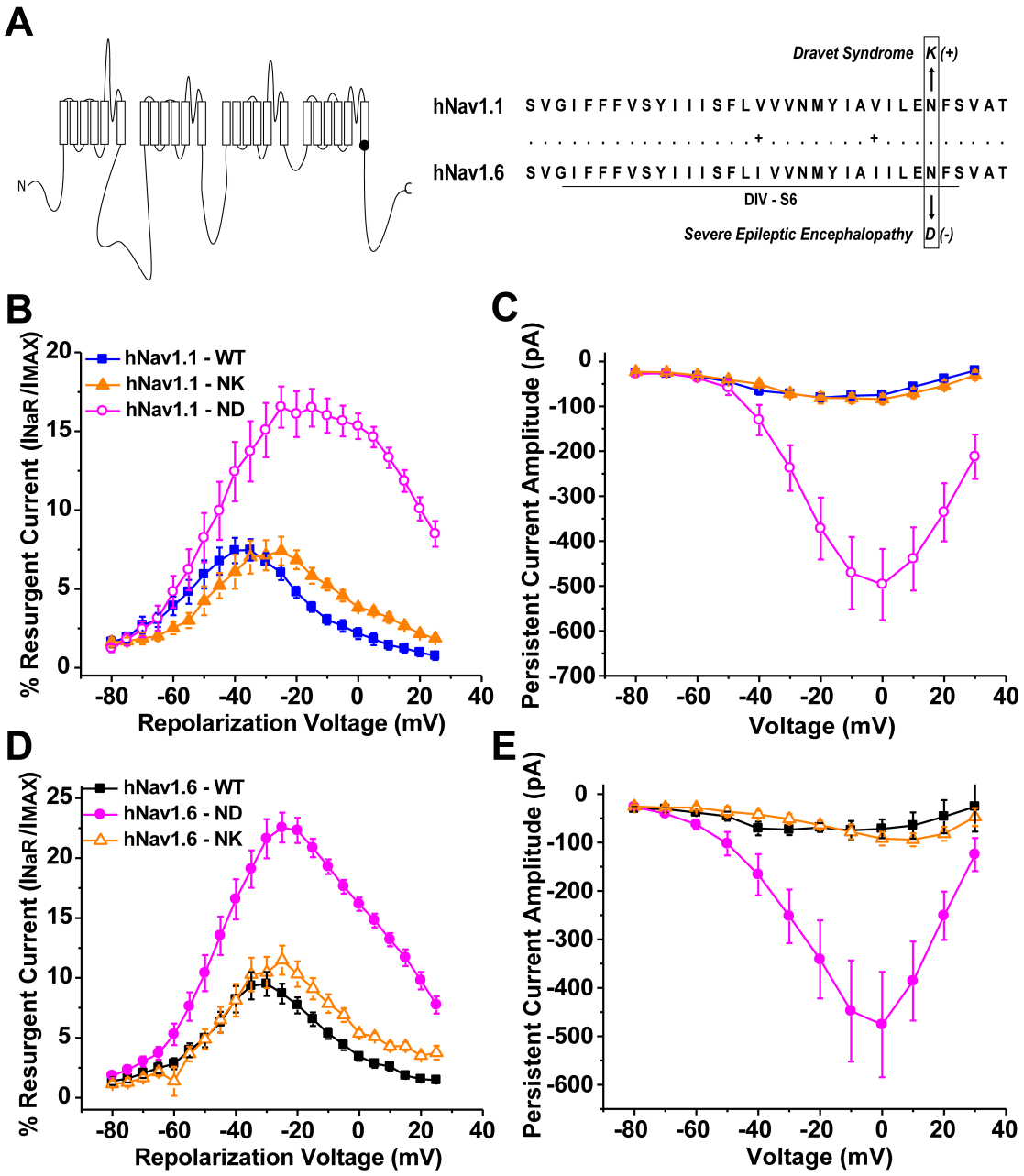

Figure 20. Resurgent and persistent current generation by reciprocal epilepsy-associated mutation in non-native channel isoform. A, Position of epilepsy-associated mutations in the linear schematic of the VGSC α- subunit and in the sequence alignment of hNav1.1 and hNav1.6. B and C, Percent resurgent current and peak persistent current amplitude generated by hNav1.1 WT (blue squares), hNav1.1 N1788K (orange triangles) and the reciprocal N1788D mutation in hNav1.1 (open, magenta circles). D and E, Percent resurgent current and peak persistent current amplitude generated by hNav1.6 WT (black squares), hNav1.6 N1768D (magenta circles) and the reciprocal N1768K mutation in hNav1.6 (open, orange triangles).

4. Cannabidiol selectively inhibits peak resurgent sodium current generated by wildtype Nav1.6

Targeting resurgent currents is a novel strategy for the treatment of epilepsy. However, there are currently no selective pharmacological inhibitors for brain isoforms of VGSCs. It has been shown that AEA and ajulemic acid can inhibit resurgent current generated by Nav1.7 and Nav1.5 [81, 139], respectively, but these isoforms are not present at significant levels in the brain. We therefore asked whether AEA could similarly inhibit resurgent current over peak transient current generated by hNav1.1 and hNav1.6. Additionally, we examined the effects of CBD due to its potential efficacy in the treatment of pediatric epilepsies [192] and similarity in structure to ajulemic acid. We found that neither 5μM AEA nor 1μM CBD had any significant effect on peak current density or peak resurgent current generated by hNav1.1 (Fig. 21A,B). Peak current density of hNav1.6 was significantly ($p<0.05$; unpaired t-test) inhibited by 5μM AEA, but peak resurgent current was not preferentially altered by 5μM AEA in our preparation (Fig. 21C). Remarkably, 1μM CBD significantly ($p<0.01$; unpaired test) inhibited the peak resurgent current generated by hNav1.6 (measured as a percentage of the peak transient current in each cell) while having no significant effect on peak current density (Fig. 21C,D). This finding identifies a novel target (i.e. resurgent sodium current) and mechanism underlying the anti-convulsant properties of CBD.

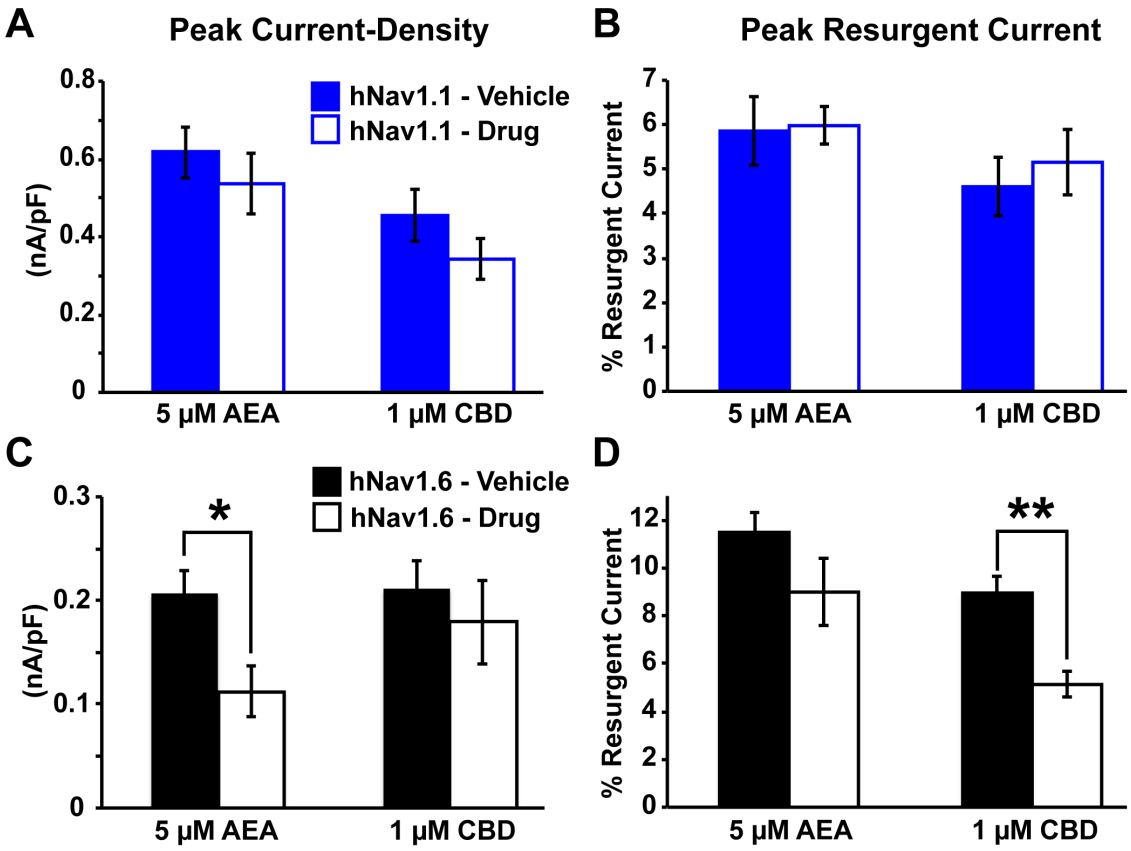

Figure 21. Effects of AEA and CBD on peak current density and resurgent current generated by WT hNav1.1 and hNav1.6 channels. A and B, Effects of 5μM AEA (n = 14) and 1μM CBD (n = 26 - 28) on peak current density and peak resurgent current generated by wildtype hNav1.1. C and D, Effects of 5μM AEA (n = 12 - 13) and 1μM CBD (n = 26 - 30) on peak current density and peak resurgent current generated by hNav1.6. *, p<0.05 and **, p<0.01; unpaired t-test.

5. Cannabidiol inhibits aberrant resurgent and persistent current generated by mutant Nav1.6 channels

One of the major biophysical defects we observed with epilepsy-associated mutations in hNav1.6 was increased resurgent current; we therefore asked if we could target this aberrant activity with CBD. We first examined the effects of 1μM CBD on hNav1.6 L1331V generated currents. CBD did not significantly inhibit peak current density at this concentration (Fig. 22A,B). However, peak resurgent current was significantly ($p<0.05$; two-way ANOVA) inhibited by CBD, similar to CBD effects on wildtype hNav1.6 (Fig. 22C,D). We also examined gating properties of hNav1.6 L1331V in the presence of CBD and found a slight but significant ($p<0.05$; unpaired t-test) depolarizing shift in channel activation (-28.6 ± 1.4mV; n =10) compared to hNav1.6 L1331V in the presence of vehicle (-33.8 ± 1.7mV; n =9) (Fig. 22E). Additionally, we measured channel recovery from inactivation at -80mV (Fig. 22F). To do this, we used a voltage command protocol in which we assessed the peak current by an initial depolarizing step to 0mV and allowed channels to recover from inactivation for increasing durations at -80mV before measuring channel availability with a test pulse to 0mV (Fig. 22F, *inset*). Unexpectedly, CBD significantly ($p<0.001$; unpaired t-test) slowed hNav1.6 L1331V (τ = 32.1 ± 2.5ms) recovery from inactivation compared to vehicle (τ = 16.8 ± 1.6ms), which was not observed with wildtype hNav1.6 (data not shown). We also examined persistent current and found no difference in the presence of CBD (Fig. 22G).

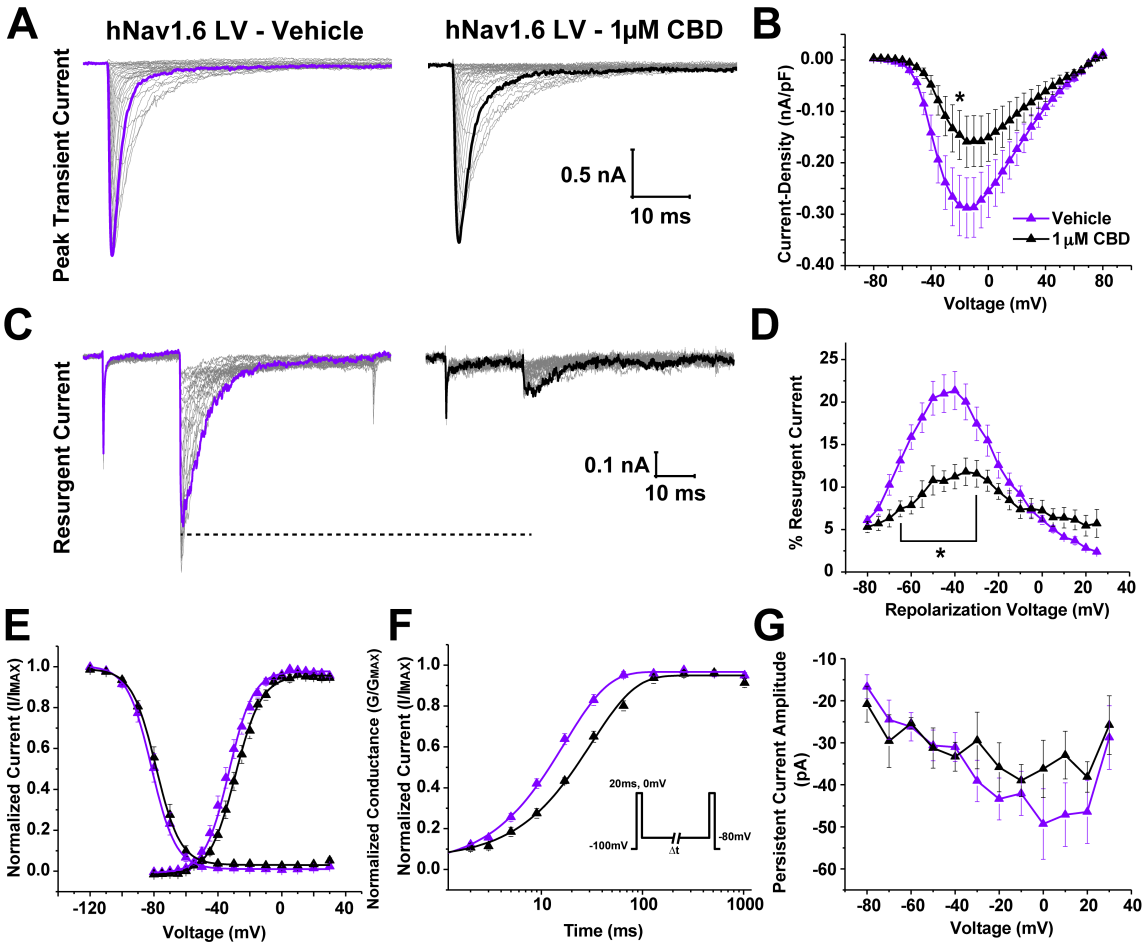

Figure 22. 1μM cannabidiol decreases resurgent current, hyperpolarizes the voltage-dependence of activation curve and slows recover of hNav1.6 L1331V channels. A, Representative family of current traces generated by hNav1.6 L1331V in presence of vehicle (left) and 1μM CBD (right) B, Current density curve showing no statistical difference in the peak current density between vehicle (purple triangles; *n* = 9) and CBD (black triangles; *n* = 10). C, Representative family of resurgent current traces generated by hNav1.6 L1331V in presence of vehicle (left) and 1μM CBD (right). Peak resurgent current traces are bolded. D, Percent resurgent current plotted against voltage. E, Steady-state activation and inactivation curves fit with a Boltzmann function. F, Normalized available current plotted against recovery duration and fit with an exponential function. Recovery from fast inactivation was measured by applying an initial depolarizing step to 0mV to assess the peak current and then repolarizing to -80mV for increasing durations followed by a final test pulse 0mV to measure channel availability (*inset*). G, Persistent current amplitude plotted versus voltage. *, p<0.05; two-way ANOVA.

We next examined CBD effects on hNav1.6 N1768D generated currents. Again, we found no significant difference in peak current density in the presence of 1μM CBD (Fig. 23A,B). CBD did significantly ($p<0.05$; two way ANOVA) inhibit peak resurgent current generated by the hNav1.6 N1768D mutant (Fig. 23C,D). Unlike with the hNav1.6 L1331V mutant, CBD did not alter the voltage dependence of activation of hNav1.6 N1768D channels (Fig. 23E). However, recovery from inactivation at -80mV was significantly ($p<0.05$; unpaired t-test) slowed in the presence of CBD ($\tau = 9.7 \pm 1.0$ms; $n = 10$) compared to vehicle ($\tau = 6.5 \pm 0.9$ms; $n = 9$) (Fig. 23F). Surprisingly, we found that CBD inhibited peak persistent current generated by the hNav1.6 N1768D mutant. The inhibition of persistent current occurs within the same voltage range as the inhibition of resurgent current and is likely contributing to the reduction in resurgent current. It is important to note that resurgent current is measured relative to the peak transient current in each cell. Thus while there is a slight, but non-significant, decrease in peak transient currents, the reported decrease in resurgent current is in addition to this effect of CBD. Overall, CBD alters multiple biophysical properties of Nav1.6 mutant channels in ways that are all consistent with decreasing channel activity.

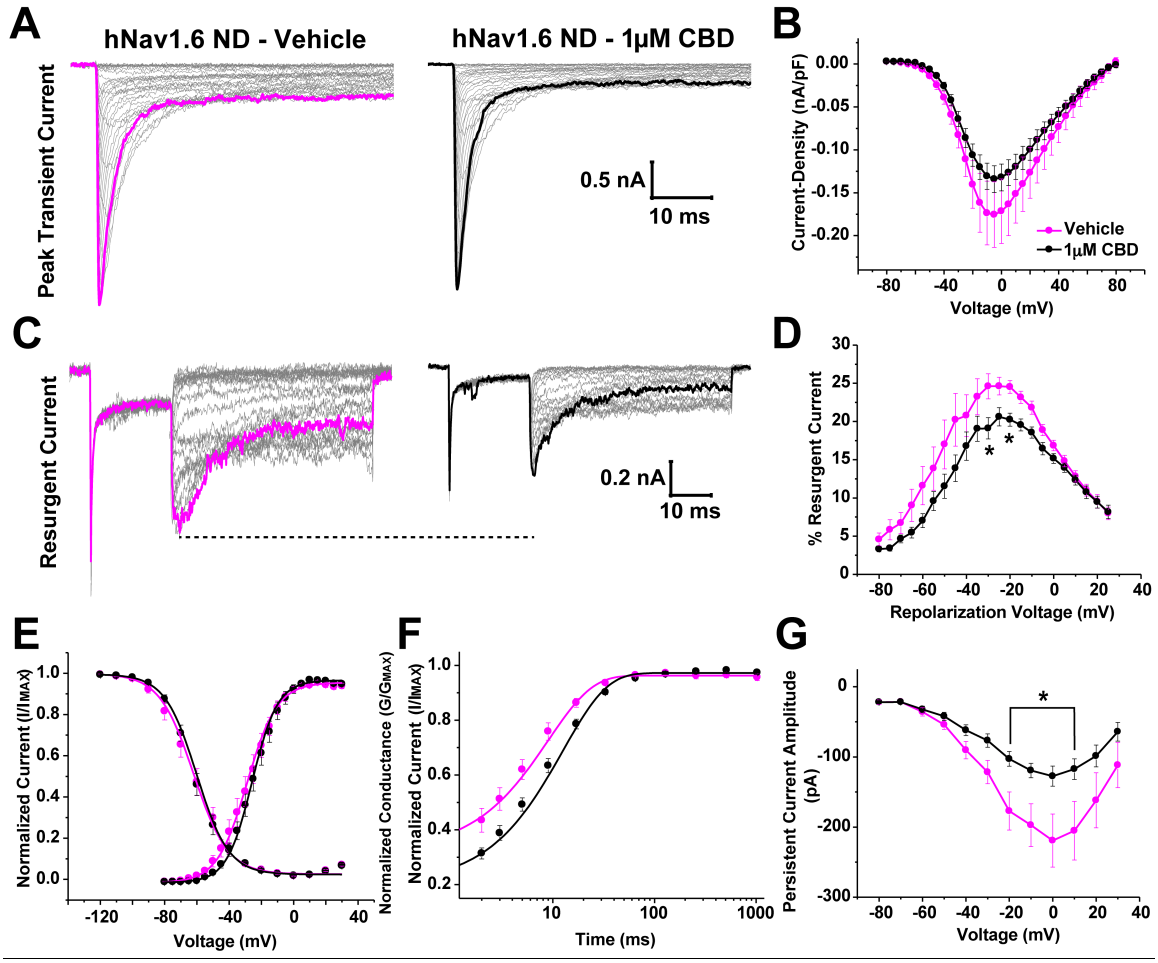

Figure 23. 1μM cannabidiol decreases resurgent and persistent current and slows recover of hNav1.6 N1768D channels. A, Representative family of current traces generated by hNav1.6 N1768D in the presence of vehicle (left) and CBD (right). B, Current density curves for hNav1.6 N1768D in the presence of vehicle (magenta circles; n = 20) and the presence of CBD (black circles; n = 19). C, Representative family of resurgent current traces generated by hNav1.6 N1768D in the presence of vehicle (left) and CBD (right). Peak resurgent current traces are bolded. D, Summary data showing the percent resurgent current versus the repolarization voltage. E, Steady-state activation and inactivation curves fit with a Boltzmann function. F, Normalized available current plotted versus recovery duration and fit with an exponential function. G, Persistent current amplitude plotted against voltage. *, $p<0.05$, two-way ANOVA.

6. Cannabidiol inhibits endogenous resurgent and persistent current and decrease excitability of striatal neurons

CBD inhibited Nav1.6 resurgent currents in HEK293T cells. However, these currents were elicited with the aid of the Navβ4 peptide, not full-length Navβ4. Therefore to further verify our findings, we examined the effects of CBD on endogenous sodium currents from striatal neurons. Striatal neurons have a very high expression of Navβ4 and generate resurgent sodium current [67]. This allowed us to determine if CBD can influence resurgent currents dependent on full-length Navβ4. As we observed in HEK293T cells expressing hNav1.6, 1μM CBD did not have a significant effect on peak transient current, estimated with a test pulse to +10mV from a holding potential of -80mV (Fig. 24A; Fig. 25A). We next examined resurgent currents using a standard protocol (Fig. 24B, *inset*). Representative resurgent current traces can be seen in Figure 24B. CBD significantly ($p<0.05$; two way ANOVA) decreased peak resurgent current in striatal neurons (Fig. 24C). Additionally, we found that the presence of 1μM CBD slightly but significantly ($p<0.05$; unpaired t-test) shifted the $V_{1/2}$ of steady-state inactivation to more hyperpolarizing potentials (-52.5 ± 1.14mV; $n = 23$) compared to vehicle control (-48.4 ± 1.1mV; $n = 24$) but did not alter steady-state activation or the rate of fast inactivation (Fig. 24D; Fig. 25B,C). However, we examined recovery from fast inactivation at -80mV and found that indeed CBD significantly ($p<0.05$; unpaired t-test) slows recovery ($\tau = 7.5 \pm 1.0$ms; $n = 22$) compared to vehicle control ($\tau = 4.4 \pm$

0.3ms; n = 24) (Fig. 24E). Moreover, persistent current was also significantly ($p<0.05$; two-way ANOVA) reduced by CBD (Fig. 24F).

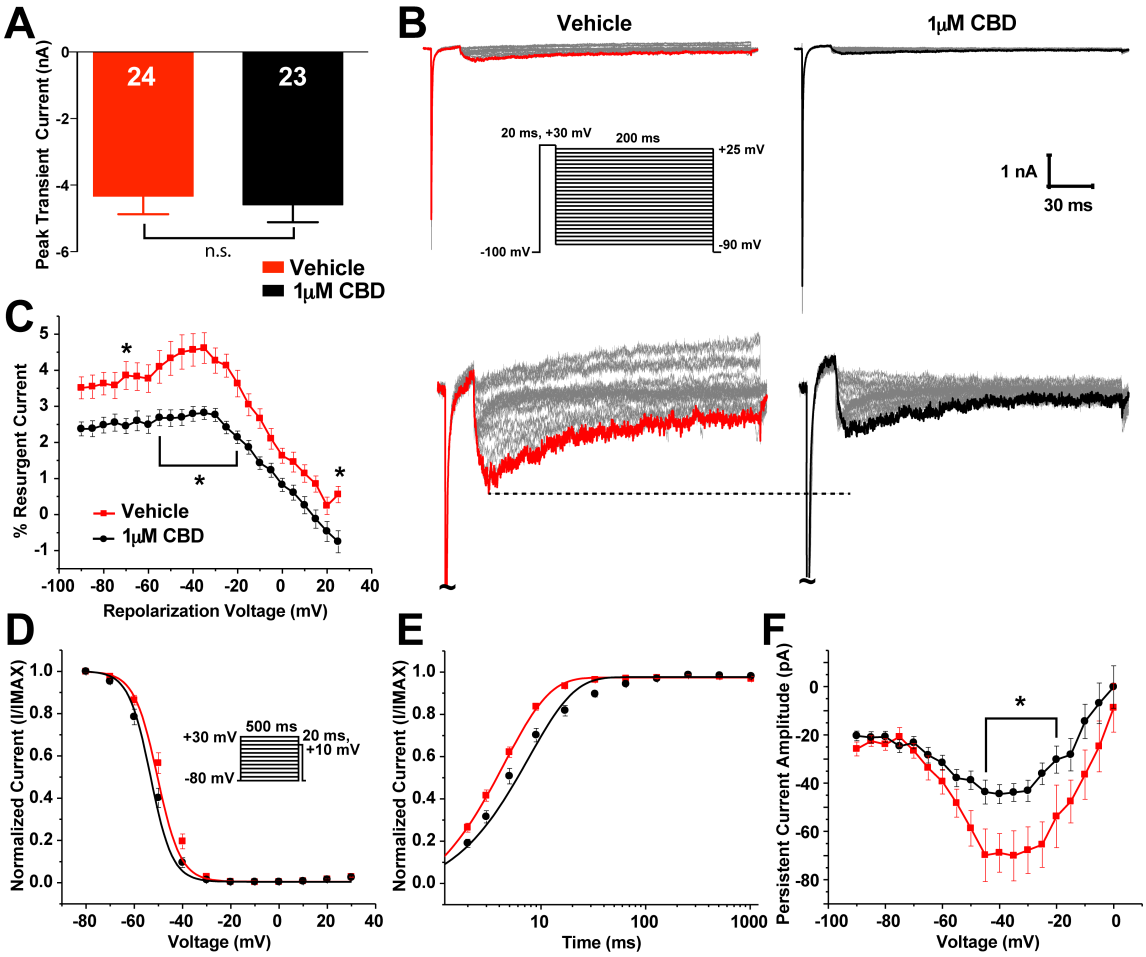

Figure 24. 1μM cannabidiol decreases resurgent and persistent current, hyperpolarized the voltage-dependence of inactivation curve, and slows recovery of endogenous sodium currents recorded from striatal neurons. A, Peak transient current for vehicle (red) and 1μM CBD (black). Peak transient current was measured with a step pulse from -80mV to +10mV from the steady-state inactivation protocol. B, Representative family of resurgent current traces from striatal neurons in the presence of vehicle (left) and 1μM CBD (right). Peak resurgent current traces are bolded and magnified below. To elicit resurgent current in striatal neurons an initial prepulse to +30mV for 20ms was applied and followed by repolarizing steps ranging from +25mV to -90mV for 200ms (*inset*). C, Percent resurgent current plotted versus the repolarization voltage. D, Steady-state inactivation curve fit with a Boltzmann function. Steady-state inactivation was measured using a prepulse ranging from -80mV to +30mV for 500ms followed by a test pulse to +10mV to measure channel availability (*inset*). E, Normalized available current plotted versus recovery duration and fit with an exponential function. F, Persistent current amplitude plotted as a function of voltage. *, $p<0.05$; two-way ANOVA; *n* values are depicted in bars.

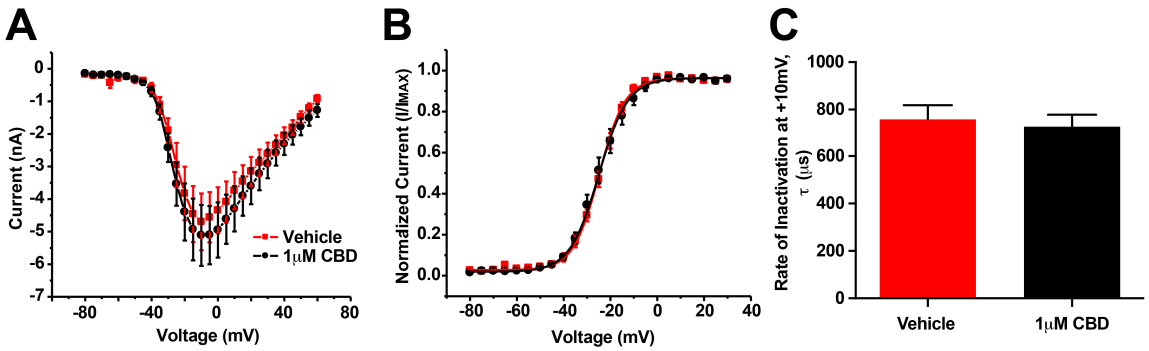

Figure 25. There is no difference in current-voltage, steady-state activation and rate of fast inactivation of sodium currents in striatal neurons with 1μM cannabidiol. A, Current-voltage curve for sodium currents in striatal neurons in the presence of vehicle (red squares; *n* = 10) or 1μM CBD (black cirlces; *n* = 14). Current-voltage curves were obtained by isolating somatic sodium current by applying a 4.5ms prepulse to -40mV followed by a short step to -55mV for 0.5ms before applying incremental steps from -80mV to +60mV for 50ms as has been previously described and validated [217]. Only cells with good voltage control over axial sodium currents were included for analysis of current-voltage relationship and steady-state activation. B, Steady-state activation curves fit with a Boltzmann function. C, Rate of fast inactivation measured by applying a single exponential fit to the decay phase of the peak macroscopic current measured from the steady-state inactivation protocol.

To further explore the implications of cannabidiol actions on excitability, we obtained current clamp recordings from striatal neurons. Striatal neurons were not spontaneously active and therefore evoked activity was measured. We observed no differences in the resting membrane potential or input resistance from striatal neurons in the presence of vehicle or cannabidiol (Fig. 26B,C). With a holding potential of −60mV, we found that the number of action potentials fired during a 200 ms stimulus with increasing intensity was significantly ($P < 0.05$; two-way ANOVA) reduced in the presence of cannabidiol (Fig. 26A and D). Peak action potential amplitude and current threshold for action potential firing from a holding potential of -60 mV was measured with a 1 ms stimulus increasing incrementally from 0 pA to 1 nA in 20 pA steps. Cannabidiol reduced ($P < 0.0001$; unpaired t-test) the peak action potential amplitude (20.9 mV ± 3.6; $n = 12$) compared to vehicle control (48.7 mV ± 2.8; $n = 14$) (Fig. 26E). Moreover, cannabidiol significantly ($P < 0.01$; unpaired t-test) increases the threshold current needed to elicit an action potential compared to vehicle (from 587.7 ± 48.2 pA to 776 ± 31 pA) (Fig. 26F). To determine if the effects on action potential number, amplitude and current threshold were due to the hyperpolarizing shift in the voltage-dependence of inactivation (Fig. 24D), we additionally examined the effects of cannabidiol on striatal neuron excitability with a holding potential of −80mV. We found that the number of action potentials fired with increasing stimulus intensity was still substantially reduced in the presence of cannabidiol with a holding potential of −80mV (Fig. 26A and G). We then measured peak action potential amplitude and current threshold from a holding potential of -80mV with a 1ms stimulus increasing

incrementally from 0 pA to 2 nA in 40 pA steps. Cannabidiol did not significantly (*n* = 33) change peak action potential amplitude or current threshold with this holding potential (Fig. 26H and I). Overall, our data shows that 1μM cannabidiol reduces excitability of striatal neurons.

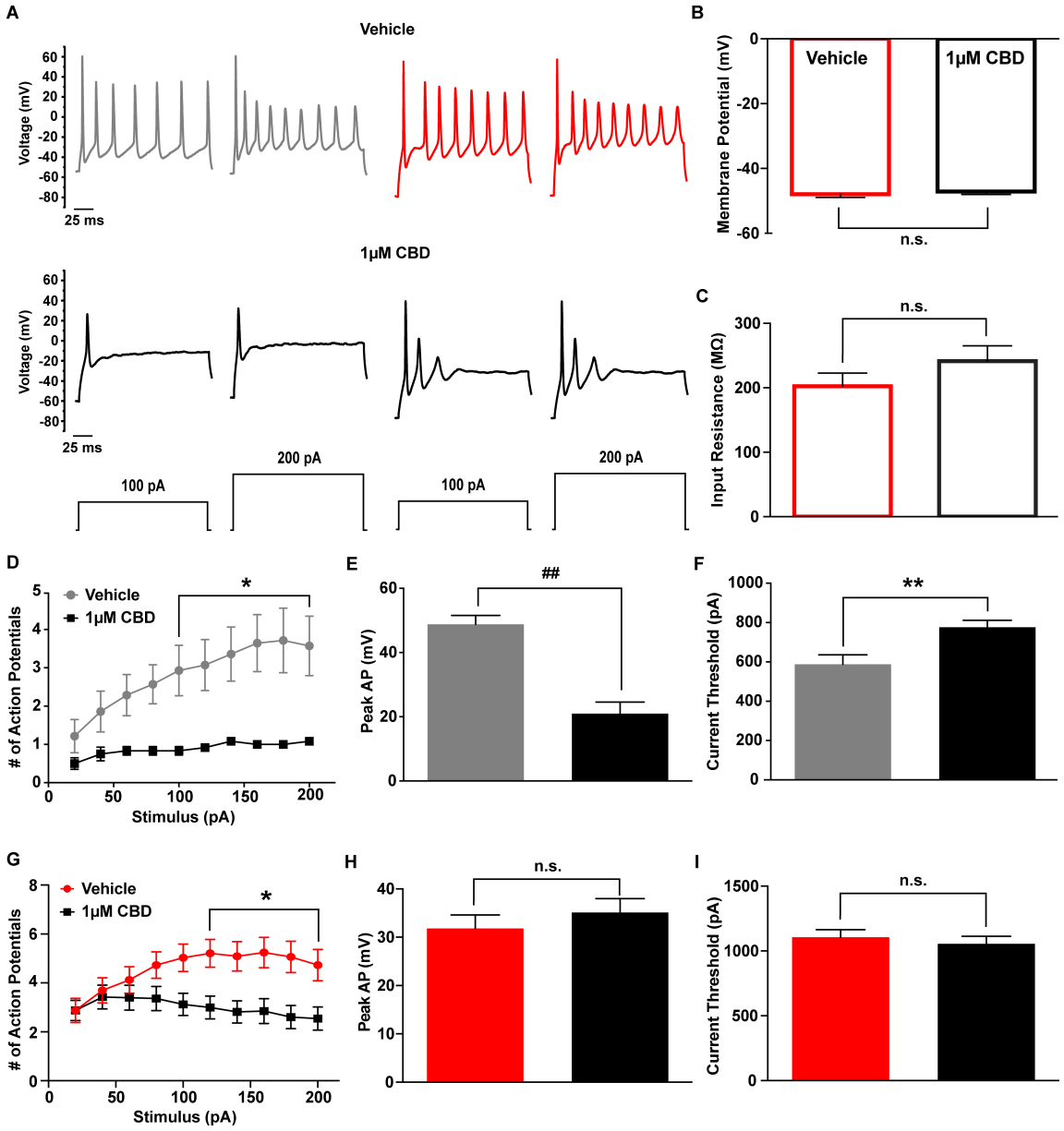

Figure 26. 1μM cannabidiol reduces excitability of striatal neurons. A, Representative traces of activity evoked with a 200ms stimulus of 100pA and 200pA for vehicle (top) and 1μM CBD (bottom) from a holding potential of -60mV (grey and black traces) and -80mV (red and black traces). B, Resting membrane potential of striatal neurons in the presence of vehicle (open, red) and 1μM CBD (open, black) from all recorded cells (n = 45 – 47). C, Input resistance calculated from the change in voltage with a 200ms, −200pA stimulus according to V = IR for vehicle (open, red) and 1μM CBD (open, black). D, Number of action potentials elicited by a 200ms stimulus of increasing intensity from 20pA to 200pA in 20pA steps from a holding potential of −60mV for vehicle (grey circles; n = 14) and CBD (black squares; n = 12). E, Action potential peak was measured at the current threshold with a holding potential of −60mV for vehicle (grey) and 1μM CBD (black). F, Current threshold

measured using a 1ms stimulus increasing incrementally from 0pA to 1nA in 20pA steps with a holding potential of −60mV. G, Number of action potentials elicited by a 200ms stimulus of increasing intensity from 20pA to 200pA in 20pA steps from a holding potential of −80mV for vehicle (red circles; n = 33) and CBD (black squares; n = 33). H, Action potential peak was measured at the current threshold with a holding potential of −80mV for vehicle (red) and 1μM CBD (black). I, Current threshold measured using a 1ms stimulus increasing incrementally from 0pA to 2nA in 40pA steps with a holding potential of −80mV. *, p<0.05, **, p<0.01 and ##, p<0.0001; unpaired t-test and two-way ANOVA.

D. Discussion

In this study, we determined whether epilepsy-associated mutations in Nav1.1 and Nav1.6 alter biophysical properties of these channels compared to the wildtype protein. Although several biophysical properties were altered by the disease mutations, we found differential effects on resurgent current generation, which suggests a divergence in the mechanism by which mutations in these two channel isoforms induce epileptogenesis and consequently result in different phenotypes. We found that mutations in Nav1.1 (R1648H and N1788K) that result in GEFS+ or Dravet Syndrome, did not alter peak resurgent current and caused loss-of-function effects on other biophysical properties. In contrast, mutations in Nav1.6 (L1331V and N1768D) that result in a severe EIEE, dramatically increased peak resurgent sodium current. These findings are consistent with the hypothesis that epilepsy-associated mutations in Nav1.1 are predominantly loss-of-function while mutations in Nav1.6 are primarily gain-of-function. Moreover, we found that CBD can preferentially inhibit Nav1.6 generated resurgent current over peak transient current. This led us to ask whether CBD could inhibit the aberrant activity generated by Nav1.6 mutant channels. We found that, indeed, 1μM of CBD can reduce mutant channel activity by: shifting the voltage-dependence of activation to more depolarizing potentials, slowing channel recovery from fast inactivation and inhibiting resurgent and persistent current. We further confirmed our findings using endogenous sodium currents from striatal neurons, again demonstrating that CBD

can inhibit endogenous resurgent and persistent current. Overall, CBD inhibits VGSC activity contributing to a decrease in neuronal excitability (Fig. 27).

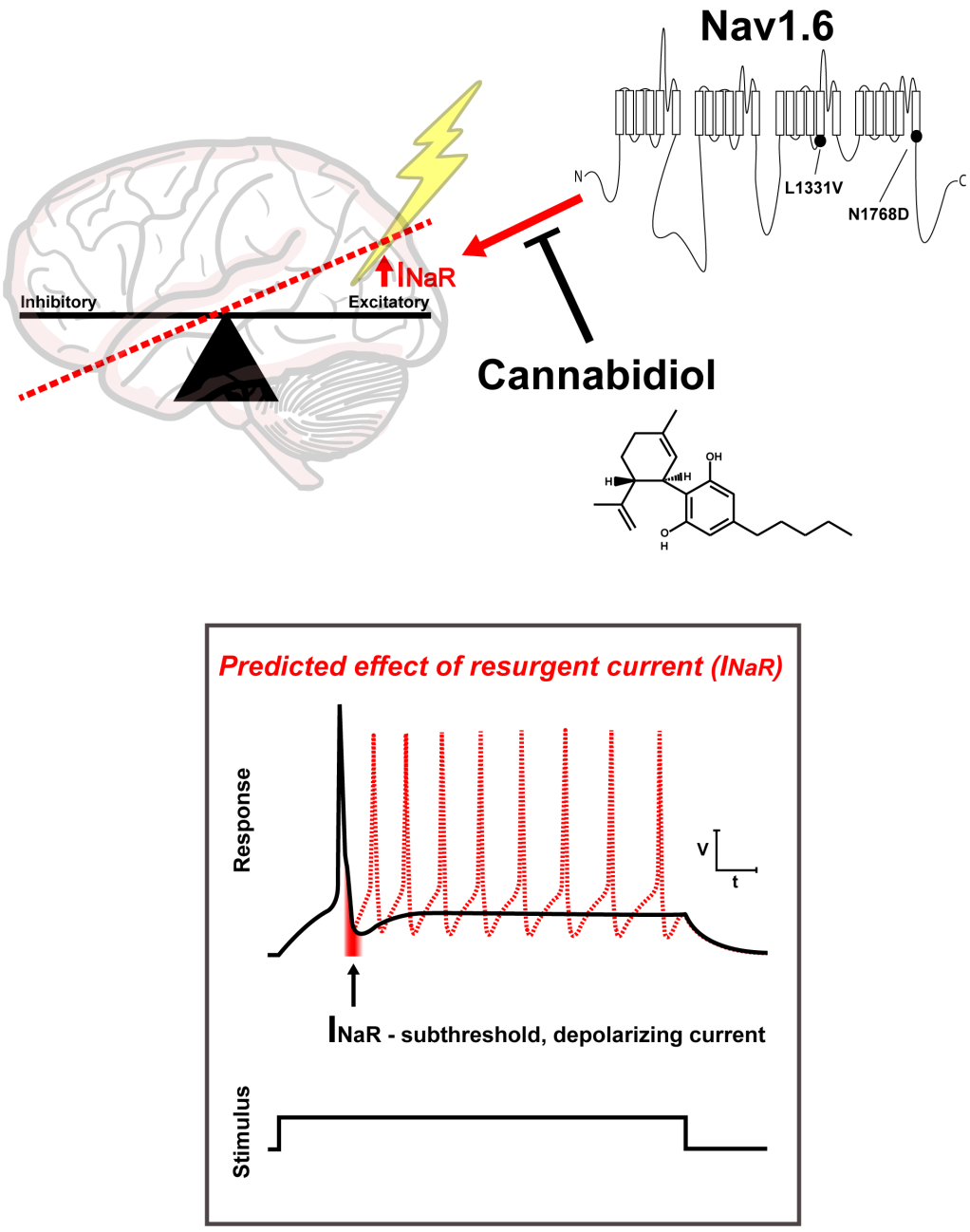

Figure 27. Schematic summarizing findings

In this study, we focused on Nav1.1 and Nav1.6 due to the phenotypic severity of epilepsy-associated mutations identified in these two channel isoforms. Nav1.1 and Nav1.6 only exhibit 75% sequence identity and have distinct expression patterns in the brain. Specifically, Nav1.1 is expressed in parvalbumin positive GABAergic neurons in somato-dendritic compartments as well as the proximal axon initial segment, while Nav1.6 is found ubiquitously but is highly concentrated in the distal axon initial segment [116, 145, 177]. The expression pattern of these two channel isoforms is critical to understanding the potential mechanisms by which mutations in these channels lead to pathological hyperexcitability. Our findings show that, despite having only 75% sequence identity, reciprocal disease mutations conferred similar biophysical defects to both channel isoforms; at least for this position, the specific amino acid substitution itself is critical to the biophysical consequences. Understanding the biophysical consequence of epilepsy-associated mutations can give us insight into the potential mechanism by which different phenotypes arise.

VGSCs are highly regulated proteins that can be modulated by many post-translational processes, and therefore the cellular background in which they are expressed can greatly influence the biophysical properties they exhibit. This caveat is a limitation of all studies of mutant channels in expression systems and is exemplified by the Nav1.1 R1648H mutant. While we replicated the impairment in inactivation and decreased current density, we did not observe an increase in persistent current or enhancement of slow inactivation as seen by some others [180,

201, 204, 205, 218, 219]. This could be due to the lack of co-expressing full-length auxiliary Navβ subunits in our study. Interestingly, enhanced persistent currents were not observed in interneurons from transgenic mice expressing the R1648H mutation [180, 204, 205, 219], but the possibility that Nav1.1 R1648H enhances persistent currents in specific neuronal populations cannot be ruled out. However, our study replicated all the biophysical defects previously characterized with the Nav1.6 N1768D mutant including: increased persistent current, incomplete inactivation, and a depolarizing shift in steady-state inactivation [211]. Heterologous expression systems and animal models are useful, but have limitations due to extensive modulation of sodium channels and therefore mutant channels may exhibit distinct biophysical properties in human neuronal subtypes.

Overall, our data suggests that mutations in Nav1.1 and Nav1.6 are acting by distinct mechanisms to induce epileptogenesis. Although the two Nav1.1 mutations that we characterized were selected from among hundreds of Nav1.1 mutations associated with epilepsy, most Nav1.1 mutations are believed to be loss-of-function. There will likely be exceptions to this paradigm. Several mutations in *Scn1a* have been identified in patients with migraine and some of these appear to be gain-of-function [220]. By contrast, far fewer *Scn8a* epilepsy mutations have been identified and characterized [208]. The two Nav1.6 mutations that we characterized, and an additional Nav1.6 I1327V mutant that we characterized (Fig. 28), had direct enhancing effects on resurgent currents. It is probable that not all gain-of-function mutations in Nav1.6 will enhance resurgent current activity. Indeed, we previously

found that painful Nav1.7 mutations could be divided into one of two groups [65]. Paroxysmal extreme pain disorder mutations impairing inactivation enhanced resurgent currents, while primary erythromelalgia mutations enhancing activation did not alter resurgent currents. Mutations in domains III and IV or the C-terminus of the channel Nav1.6 most likely impair inactivation and enhance resurgent currents, while mutations that enhance activation such as the Nav1.6 N984K mutant [187] may not directly enhance resurgent current. But alterations in both biophysical properties are still possible, as we found an enhancement of activation and increased resurgent current generation by the Nav1.6 I1330V mutant (Fig. 28). A few apparent loss-of-function mutations have also been reported in Nav1.6 [187, 190]. It is not entirely clear how these mutations lead to epilepsy, although since Nav1.6 is expressed in both excitatory and inhibitory neurons, there could be important reductions in inhibitory tone with loss-of-function Nav1.6 mutations. Interestingly, enhanced Nav1.6 resurgent currents have been observed in an animal model of induced temporal lobe epilepsy [194, 195]. This raises the intriguing possibility that Nav1.6 resurgent currents may be increased in epilepsy syndromes caused by brain injury and of other etiologies.

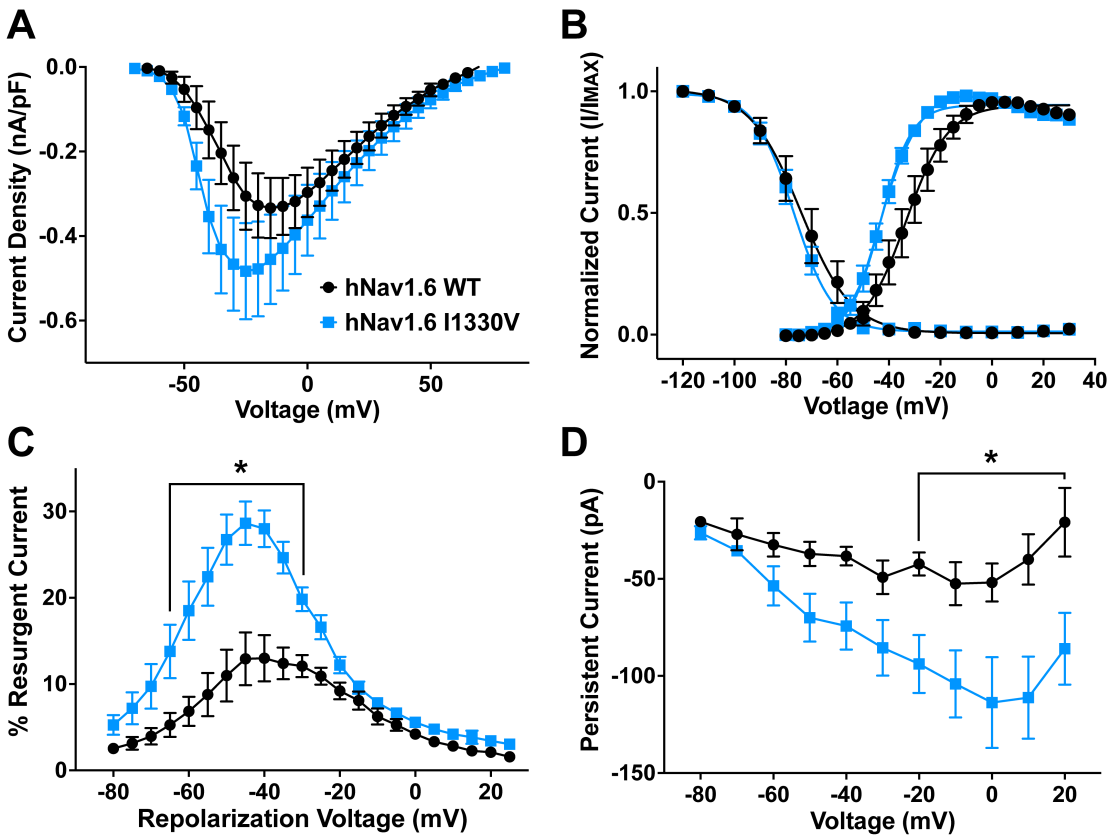

Figure 28. hNav1.6 I1330V mutant channels demonstrate a hyperpolarizing shift in the steady-state activation curve and generate larger resurgent and persistent current. A, Current density curve for hNav1.6 WT (black circles; *n* = 9) and hNav1.6 I1330V (light blue squares; *n* = 9). B, Voltage-dependence of activation and inactivation curves for hNav1.6 WT and hNav1.6 I1330V. C, Percent resurgent current plotted against repolarization voltage. D, Persistent current amplitude as a function of voltage. *, $p<0.05$ two-way ANOVA.

It is likely that the clinical phenotypes manifested by mutations in Nav1.1 and Nav1.6 will require tailored treatment strategies to achieve maximal seizure control in different patients. It has been observed that many VGSC blockers exacerbate seizure severity in patients with Dravet Syndrome while they may be efficacious in patients with mutations in Nav1.6 [186, 188, 221-223]. This can be expected due to the primary role of Nav1.1 in inhibitory neurons and the loss-of-function effects of Dravet Syndrome-associated mutations in Nav1.1. Further inhibition of inhibitory neuron excitability by non-selective VGSC blockers would not be expected to restore inhibitory-excitatory balance. In contrast mutations in Nav1.6 appear to be primarily gain-of-function and would lead to an overall increase in excitability of all neurons due to Nav1.6's ubiquitous expression; broadly inhibiting VGSC activity in this case could help dampen the overall increase in excitability. In this study, we found that CBD can inhibit VGSC activity, however CBD has shown some efficacy in the treatment of Dravet Syndrome as well as other epilepsy syndromes [192, 224, 225]. This may seem contradictory to our previous discussion, but we posit that CBD's efficacy lies in its specificity. At a concentration of 1μM, CBD appears to be specific for Nav1.6 over Nav1.1 generated currents. More specifically, CBD is selective for resurgent sodium current over peak transient currents generated by Nav1.6. Resurgent sodium currents are expressed in subpopulations of neuronal subtypes, many of which are in key circuits implicated in epilepsy syndromes such as striatal medium spiny neurons, perirhinal layer II pyramidal neurons, hippocampal dentate gyrus, ventral CA1 pyramidal neurons, globus pallidus, subthalamic nuclei, and medial entorhinal cortex [92]. Moreover,

these currents are thought to occur at the axon initial segment and therefore can directly influence action potential initiation [152]. In addition, there is the possibility that seizure activity itself can lead to increased Nav1.6 resurgent currents in excitatory neurons [194, 195]. Thus the selective expression of this atypical current may make it an ideal target to help rebalance inhibitory-excitatory tone and/or reduce pathological hyperexcitability even if the primary defect does not directly enhance Nav1.6 resurgent current activity.

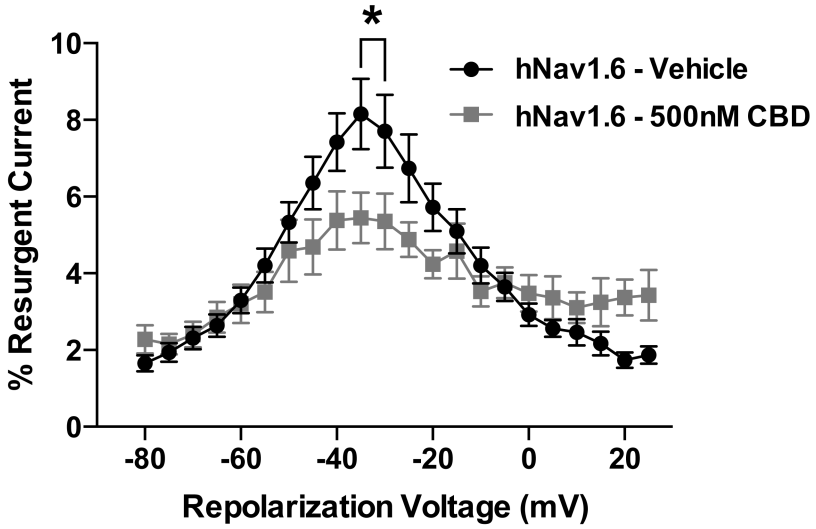

Figure 29. 500nM CBD decreases peak resurgent current generated by wildtype hNav1.6. Percent resurgent sodium current recorded in the presence of vehicle (black; *n* = 13) and 500nM CBD (grey; *n* = 12) plotted against the repolarization voltage. *, p<0.05; two-way ANOVA.

In this study, we used a low concentration (1μM) of CBD to mimic the concentrations achievable *in vivo* [226, 227]. We also tested a 500nM concentration of CBD and found a similar inhibition of peak resurgent current generated by wildtype Nav1.6 (Fig. 29). Hill *et al.* have found that high concentrations (10-30μM) of CBD can inhibit peak transient currents generated by other VGSC isoforms including: Nav1.1, Nav1.2, and Nav1.5, but the physiological significance of those findings are unclear. It still remains unclear as to how and where CBD is interacting with Nav1.6. Since CBD had no significant effect on Nav1.1, it is likely not acting on a conserved region in these two isoforms i.e. the local anesthetic site, which is consistent with findings by Foadi *et al.* with ajulemic acid on Nav1.5. One possibility is that CBD targets the domain IV voltage-sensor, which is critical for inactivation and can be differentially targeted by toxins and small molecules [140, 228]. We note that while we observed pronounced effects of CBD on resurgent currents in population studies, we did not observe significant effects on peak transient or resurgent current in perfusion experiments on cells already patch-clamped, presumably due to disruption of the cytoplasmic milleau. This could suggest a possible indirect mechanism of action. Physiologically, it is plausible that CBD is working indirectly on VGSCs. CBD has been shown to inhibit the degradation of AEA extracellularly, which we and others have found can inhibit Nav1.6 peak current density [196, 229]. In cultured striatal neurons CBD substantially reduced repetitive firing, which is consistent with the inhibition of resurgent and persistent currents. However, the signficant reduction in action potential amplitude from a holding potential of -60mV suggests additional actions. CBD induced a small but significant

negative shift in the voltage-dependence of steady-state inactivation of striatal sodium currents, which should reduce sodium channel availability and action potential amplitude. Indeed, when a more hyperpolarized membrane potential (-80mV) was used to measure excitability, the effect of cannabidiol on action potential amplitude and current threhsold were eliminated suggesting that the reduction was due to inactivation of VGSCs at -60mV by cannabidiol. The pronounced effect on excitability that we observed in cultured neurons may be reduced in CNS neurons *in vivo*, which tend to have more negative resting membrane potentials (-90 mV) compared to our in vitro preparation (-60 mV or -80mV) and larger overall sodium currents [67, 230]. Indeed, in the limited clinical reports that are available, CBD does not seem to be associated with major CNS depression [192, 224]. Importantly, a substantial decrease in action potentail number was still observed with the -80mV holding potential and this is consistent with the reduction in resurgent currents observed using a -80mV holding potential (Fig. 26). While our data leads us to predict that inhibition of resurgent currents by low concentrations of CBD could be important in acquired and inherited epilepsies, it is likely that the polypharmacological nature of CBD [231] also can contribute to its ability to reduce seizure activity.

In conclusion, our present findings further elucidate a potential mechanism by which epilepsy-associated mutations in Nav1.6 lead to pathological hyperexcitability, which is distinct from mutations in Nav1.1. In addition, we found that CBD can inhibit resurgent sodium current generated by wildtype and mutant

Nav1.6 channels. Overall, our findings suggest that CBD is mechanistically acting, in part, on VGSCs to decrease seizure activity and that resurgent sodium current may be a promising therapeutic target for the treatment of epilepsy syndromes.

IV. PREFERENTIAL PHARMACOLOGICAL INHIBITION OF NAV1.6, BUT NOT NAV1.1, ABOLISHES EPILEPTIFORM ACTIVITY INDUCED BY 4-AP IN MOUSE CORTICAL BRAIN SLICES

This chapter was adapted from a manuscript in preparation.

Reesha R. Patel, Xingjie Ping, Shaun R. Patel, Jeffrey L. Krajewski, Jeff S. McDermott, Xiaoming Jin, and Theodore R. Cummins

R. R. Patel designed experiments, conducted all electrophysiological experiments, analyzed and interpreted the data and drafted the manuscript.

A. Introduction

Voltage-gated sodium channels are critical for neuronal excitability as they are responsible for the initiation and propagation of action potentials. They are comprised of a large α subunit (Nav1.1 – Nav1.9) that can associate covalently or non-covalently with several auxiliary proteins including one or more β subunits (Navβ1 – Navβ4) [16]. Therefore, these channels function as an intricate channel complex that is highly regulated. Structurally, these channels consist of four homologous domains each with six transmembrane segments (S1-S6) wherein the S1-S4 segments make up the voltage-sensing modules while the S5-S6 segments make up the central pore of the channel. Conformational changes due to movement

of the voltage-sensing modules within the protein lead to state transitions of the channel. At hyperpolarized, resting membrane potentials, channels are primarily in a closed (non-conducting) state and upon membrane depolarization they transition to an open state, conducting an inward sodium current, and within milliseconds after opening they typically enter an inactivated state (non-conducting). The inward, depolarizing current generated by these channels underlies the rising phase of the action potential, making VGSCs essential for the electrical signals by which neurons transmit information.

There are four major VGSCs isoforms expressed in the central nervous system: Nav1.1, Nav1.2, Nav1.3, and Nav1.6 [16]. These brain isoforms of VGSCs have distinct cellular (i.e. neuronal populations) as well as subcellular (i.e. neuronal compartments) localization. Nav1.1 is expressed in the cell soma, dendrites, nodes of Ranvier and the axon initial segment [93-96]. Nav1.1 is predominantly expressed in parvalbumin and somatostatin positive GABAergic neurons [143, 144, 178, 232-234], although it has been observed in some excitatory neuronal populations [182]. Nav1.2 is highly expressed in the proximal axon initial segment, unmyelinated axons, and nerve terminals [88, 96, 101-104]. Specifically, Nav1.2 expression has been observed in the proximal axon initial segment of excitatory, pyramidal neurons [150, 235] and somatostatin positive, but not parvalbumin positive, GABAergic neurons [105]. While Nav1.3 mRNA has been detected during prenatal development, its expression diminishes during early postnatal days and is lost in the adult rodent brain [96, 106]. Nav1.6 is ubiquitously expressed in the brain. In

particular, Nav1.6 expression is dense in the axon initial segment and nodes of Ranvier of many neuronal populations [97, 101, 102, 114, 115]. Each isoforms function within these different regions is highly specialized as evidenced by disruption of their activity or expression leading to pathological conditions and/or premature lethality [143, 179, 236, 237].

It is not surprising given their critical role in excitability that alterations in VGSC activity has been implicated in epilepsy. The most convincing evidence for this is that certain inherited epilepsies occur in patients with mutations in VGSCs. Indeed, mutations have been identified in all brain isoforms of VGSCs and result in distinct epileptic syndromes [119, 124, 238, 239]. Much insight into the role of VSGSs in epilepsy has been provided from studying animal models of these genetic epilepsies. To date, the leading hypothesis for the mechanism underlying epileptic phenotypes due to Nav1.1 mutations is the decreased activity of inhibitory interneurons while little to no effect on excitatory neurons. Due to the prominent expression of Nav1.1 in inhibitory neurons, this would lead to an overall decrease in inhibitory tone [143, 145, 205, 234, 240]. Recently, the first epilepsy-associated mutation in Nav1.6 (N1768D) was identified and found to cause gain-of-function in heterologous expression systems – increasing both Nav1.6 activity and excitability of hippocampal neurons [123]. Heterozygous *Scn8a*$^{N1768D/+}$ knock-in mice exhibit seizures and sudden unexpected death in epilepsy demonstrating the causal role of this mutation [241]. These findings support the primary hypothesized mechanism by which mutations in Nav1.6 lead to epilepsy is through increased activity of

Nav1.6 and a consequent increase in overall neuronal excitability. Interestingly, seizure thresholds and premature lethality of Nav1.1 heterozygous mice, a model for SMEI, can be restored and rescued to wildtype levels by essentially eliminating a single Nav1.6 allele, suggesting that a reduction in Nav1.6 activity may decrease seizure generation [242]. Indeed, heterozygous Nav1.6 mice have increased thresholds to chemically and electrically induced seizures [242, 243]. Moreover, Nav1.6 channel expression and activity is increased in kindling models of epilepsy as well as genetic epilepsies such as those due to Celf4 deficiency [194, 244-246]. The findings presented in chapter II and III suggest that broadly inhibiting Nav1.1 activity could have adverse effects, while selectively inhibiting Nav1.6 may be more beneficial for the treatment of epilepsy syndromes.

The primary mechanism of action for commonly used AEDs such as phenytoin, carbamazepine, lamotrigine and others is to inhibit VGSC activity. These drugs bind to the pore of the channel with higher affinity for channels in an open or inactivated state, thus giving them with a use-dependence property [31]. Since the pore region of the channel is highly conserved among VGSC isoforms, classic AEDs are relatively nonselective. While classic AEDs can help control seizures in some patients, approximately 20 to 40% of epilepsy patients are refractory to treatment. Therefore, there is a need to develop novel AEDs. From animal model studies, it seems plausible that selectively targeting specific isoforms of VGSCs may be a more efficacious strategy for the treatment of epilepsy syndromes.

Here we focus on the contribution of Nav1.1, Nav1.2 and Nav1.6 to epileptic activity due to their distinct expression pattern and availability of selective small molecule inhibitors of these channel isoforms. We first determined the selectivity of the ICA-121431 (ICA compound) and LY-03049227 (LY compound) for Nav1.1, Nav1.2 and Nav1.6 using whole-cell patch clamp recordings in HEK293T cells. We then asked whether preferential inhibition of Nav1.1 or Nav1.6 by ICA and LY compounds, respectively, would have differential effects on epileptiform activity. To address this question we used a 4-aminopyradine (4-AP) model of epileptic activity [247, 248], and multielectrode array (MEA) recordings from mouse cortical brain slices. We found that preferential inhibition of Nav1.6 abolishes epileptiform activity, while inhibition of Nav1.1 did not. This led us to ask if inhibition of Nav1.1 alone could induce synchronized activity. We found that partial inhibition of Nav1.1 activity in mouse cortex can increase basal activity. Our findings suggest that selective targeting of VGSC isoforms may be a more efficacious treatment strategy for epileptic syndromes than current AEDs that broadly inhibit VGSCs.

B. Materials and methods

1. cDNA Constructs

Optimized human constructs for Nav1.1, Nav1.2 and Nav1.6 were designed in-house and purchased from Genscript (Piscataway, NJ). cDNA constructs for wildtype Nav1.1, Nav1.2 and Nav1.6 channels encode for amino acid sequences

corresponding to the accession numbers BAC21102.1, NP_001035232.1 and NP_055006.1 in the NCBI database, respectively.

2. Cell cultures and transfections

The use of HEK293T cells [153] was approved by the Institutional Biosafety Committee and followed the ethical guidelines for the National Institutes of Health for the use of human-derived cell lines. HEK293T cells were grown under standard tissue culture conditions (5% CO_2; 37°C) with DMEM supplemented with 10% fetal bovine serum. HEK293T cells were transiently transfected using the calcium phosphate precipitation method. Briefly, calcium phosphate-DNA mixture (4.5 μg channel construct and 0.5 μg EGFP) was added to cells in serum-free media for 4-5 hours after which it was replaced with normal media. 12-24 hours post-transfection, cells were split onto laminin-coated glass coverslips. Cells were identified by expression of EGFP using a fluorescent microscope and whole-cell patch clamp recordings were obtained 36-72 hours post-transfection.

3. Chemicals and solutions

ICA-121431 (ICA compound) and 4-aminopyridine (4-AP) was obtained from Sigma Aldrich Co. (St. Lousi, MO). LY-03049227 (LY compound) was a generous gift from Eli Lilly and Co. (Indianapolis, IN). ICA and LY compounds were dissolved in MPL to a stock concentration of 10mM and stored at 4°C. 4-AP was also dissolved in

MPL to a stock concentration of 100mM and stored at 4°C. All drugs were diluted to desired concentration in artificial cerebrospinal fluid (ACSF) or extracellular patch-clamp solution just prior to use.

4. Whole-cell patch clamp recordings

Whole-cell patch clamp recordings were obtained at room temperature (~23°C) using a HEKA EPC-10 amplifier and the Pulse program (v 8.80, HEKA Electronic, Germany) was used for data acquisition. Electrodes were fabricated from 1.7 mm capillary glass and fire-polished to a resistance of 0.9-1.3 MΩ using a Sutter P-97 puller (Sutter Instrument Company, Novato, CA). All voltage protocols were started 5 minutes after obtaining a gigaΩ seal and entering the whole-cell configuration, which controlled for time-dependent shifts in channel properties. Voltage errors were minimized to less than 5 mV using series resistance compensation and passive leak currents were cancelled by P/-5 subtraction. The bath solution contained in (mM): 140 NaCl, 1 $MgCl_2$, 3 KCl, 1 $CaCl_2$, and 10 Hepes, adjusted to a pH of 7.30 with NaOH. The pipette solution contained in (mM): 140 CsF, 10 NaCl, 1.1 EGTA, and 10 Hepes, adjusted to a pH of 7.30 with CsOH. Recordings were made in the presence of extracellular solution containing the drug. Each coverslip was recorded from for up to one and half hours before discarding.

5. Cortical slice preparation

Male and female C57BL/6 mice from postnatal day 11 to 16 were anesthetized with ketamine and decapitated. Brains were quickly removed and placed in chilled, oxygenated dissecting solution containing (in mM): 111 choline-Cl, 2.5 KCl, 1.25 NaH_2PO_4, 10 $MgSO_4$, 0.5 $CaCl_2$, 26 $NaHCO_3$, and 10 D-glucose (pH 7.4 and ~305mOsm). Brains were bisected along the sagittal plane, leaving the left and right hemispheres intact and coronal cortical slices were cut to a thickness of 300μM using a vibratome (Leica VT1200, Buffalo Grove, IL). After cutting, slices were incubated in oxygenated ACSF for at least 1 hour at room temperature before being used for recording. ACSF solution contained (in mM): 126 NaCl, 2.5 KCl, 1.25 NaH_2PO_4, 2 $MgSO_4$, 2 $CaCl_2$, 26 $NaHCO_3$ and 10 D-Glucose (pH 7.4 and ~315mOsms).

6. Multielectrode array recordings

MEA recordings were performed similarly to methods previously described [249]. Briefly, multielectrode array probes were coated with 0.1% polyethylenimine in boric solution for approximately three hours and washed with deionized water. Slices were placed by eye in a manner that neocortical layers I-V covered the array (Figure 31). Slices were maintained at 37°C and continuously perfused with oxygenated ACSF containing drugs. Experiments testing drug effects on 100μM 4-AP induced hyper-excitability were conducted as follows: one hour of baseline (100μM 4-AP only) recording followed by thirty minutes of treatment (100μM 4-AP and drug of interest) recording and lastly washout (100μM 4-AP only) to confirm slice viability. For experiments testing the effects of drugs on basal activity, a forty

minute recording of activity in the presence of normal ACSF or drug alone was followed by a 20 minute recording in the presence of 100μM 4-AP, to assure slice viability, was obtained. Activity was sampled from all sixty electrodes at a sampling rate of 1kHz and amplified using MC_Rack software from Multichannel Systems (Reutlingen, Germany). Data was stored for further offline analysis.

7. Data analysis

Whole-cell voltage clamp data are represented as the mean ± the standard error and *n* reflects the number of separate experimental cells. Concentration response curves were fit with the Hill logistic equation: y = 100/(1+10^((LogIC_{50}-x) * HillSlope))) to obtain IC50 values using Graphpad Prism (La Jolla, CA).

Analysis of multielectrode array data was done using an in-house generated MATLAB script. A twenty-minute window in the middle of each recording was used for analysis of activity. Data was filtered using a second order butterworth filter with a cutoff frequency of 15Hz to get rid of high frequency noise and isolate slow local field potentials (LFPs). The script returns peak values above or below a threshold set to at least six times the standard deviation of the noise (after filtering) measured for 20 seconds during which no LFPs occur for each recording. The top ten most active electrodes, as determined by the number of events, during the baseline recording from each slice were used for further analysis. Peak amplitude was calculated as the average of all peak values from a single electrode and

subsequently averaged across the top ten electrodes. Valley amplitudes were calculated in a similar manner. The duration of the LFPs was measured from the mean waveform from each electrode. Duration values were then averaged across the top ten electrodes. The mean waveform was obtained by plotting LFPs aligned by their peak values. Only LFPs of the most common type, which always included interictal events, were used for measurement of duration. MATLAB and Graphpad Prism (La Jolla, CA) were used to make graphs. Black data points represent the mean value from each slice, while the mean of all slices in the group are represented in red data points. The sample number, *n*, signifies the number of separate experimental slices. Statistical significance was determined using either a paired, when appropriate, or unpaired t-test.

C. Results

1. Preferential inhibition of Nav1.1 and Nav1.6 by ICA and LY compounds, respectively

Recently, it was discovered that small molecule, aryl sulfonamide, inhibitors can selectively target VGSC isoforms [140, 250]. In this study, we examined the effects of the ICA compound and a derivative of the previously described PF-04856262, the LY compound [140]. The selectively of these molecules has been attributed to specific extracellularly accessible amino acid residues of the voltage-sensing module of domain IV. Based on the conservation of these residues in the

different isoforms, we hypothesized that these compounds would differentially inhibit Nav1.1 and Nav1.6. Indeed, the ICA compound has previously been found to inhibit Nav1.3 and Nav1.1 (IC50 = ~10-20nM) greater than Nav1.2 (IC50 = ~250nM) and to an even greater degree than Nav1.6 (IC50 > 10μM) [140]. To test the selectively of these compounds on Nav1.1, Nav1.2, and Nav1.6 activity, we obtained whole-cell patch clamp recordings from transiently transfected HEK293T cells. We used a voltage command protocol in which we applied an initial conditioning pulse to -100mV or -70mV, to determine the maximum and inhibited current, respectively, for 8 seconds followed by a recovery pulse to -100mV for 100ms and a final test pulse to 0mV for 20ms (Figure 30A *inset)*. We generated concentration response curves for each compound and isoform to determine the apparent concentration at which fifty percent of activity was inhibited (IC50) (Figure 30). We found that the LY compound inhibits Nav1.6 (IC50 = 0.39μM) and Nav1.2 (IC50 = 0.44μM) greater than Nav1.1 (IC50 = 2.25μM) (Figure 30A). In contrast, the ICA compound is preferentially inhibits for Nav1.1 (IC50 = 0.07μM) over Nav1.2 (IC50 = 0.33μM) and Nav1.6 (IC50 = 2.24μM) (Figure 30B). In our preparation, these compounds showed less selectivity compared to previously reported IC50 values [140]. This can be explained in part by the use of a different voltage command protocol to measure sensitivity. In this study, we used an 8 second conditioning pulse to -70mV to mimic physiological resting membrane potentials and thus obtain a physiologically relevant measure of inhibition and relative selectivity. Regardless, the differential selectivity of these compounds gave us the opportunity to ask how different VGSC isoforms contribute to epileptic activity.

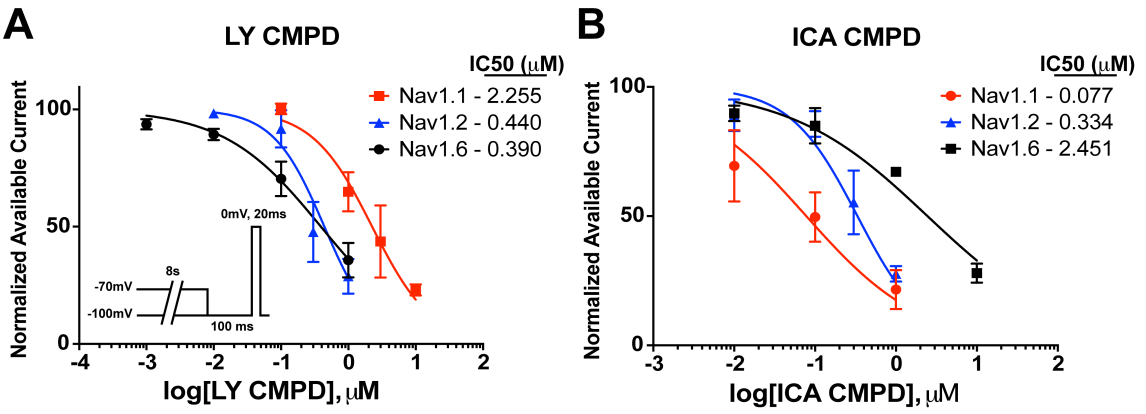

Figure 30. Concentration response curves for LY and ICA compounds A, Concentration response curves for Nav1.1 (red squares), Nav1.2 (blue triangles) and Nav1.6 (black circles) with the LY compound. B, Concentration response curves for Nav1.1 (red circles), Nav1.2 (blue triangles) and Nav1.6 (black squares) with the ICA compound. To assess current inhibition, a conditioning step to -70mV for 8s, allowing drug to bind the channel, followed by a recovery step to -100mV for 100ms and subsequently a final step to 0mV for 20ms was applied to measure available current (*inset*). The available current was normalized to the maximum current measured with a similar voltage protocol with a conditioning step to -100mV. Each data point represents an n = 2-8 of separate experimental cells.

2. Preferential inhibition of Nav1.6, but not Nav1.1, abolishes epileptiform activity

We used multielectrode array recordings from mouse cortex to study the effects of these small molecule inhibitors of VGSC isoforms on 4-AP induced epileptiform activity (Figure 31). We first examined the effects of continuous application of 100μM 4-AP for 1.5 hours on cortical activity to determine if activity changes over time. Representative traces of activity recorded during the first hour which is referred to as the baseline recording in the presence of 100μM 4-AP and the next thirty minutes which is referred to as the treatment recording in the presence of 100μM 4-AP can be seen in Figure 32A. We found that there was no significant change in the number of interictal LFP events between baseline and treatment recordings. Baseline activity induced by 4-AP was variable between slices; therefore we performed paired experiments and show the mean value from each slice (black data points) as well as the overall mean for each group (red data points) (Figure 32B-D, F). As seen in Figure 32E, the interictal like LFP events were biphasic with an upstroke to a peak followed by downstroke to a valley. The peak and valley amplitudes as well as the duration of the LFPs remained the same over time (Figure 32B-F). This allowed us to directly measure drug effects on 4-AP induced activity without having to compensate for run –up or –down effects of the model.

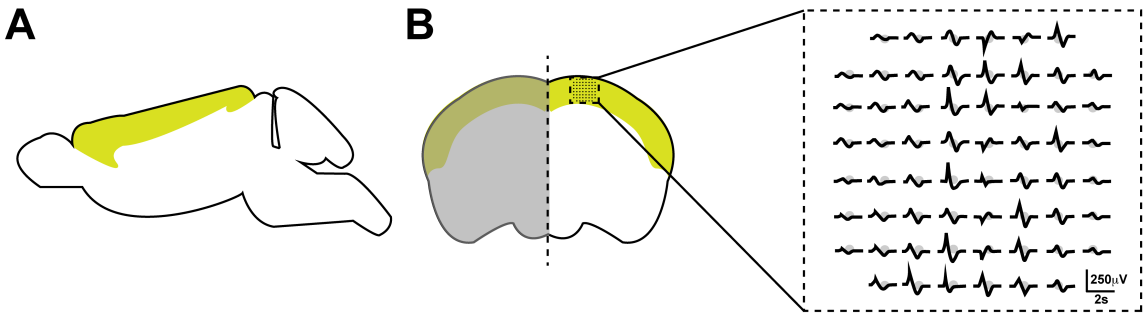

Figure 31. Multielectrode array recordings A, Sagittal view of mouse brain highlighting cortex region in green. B, Coronal brain slice depicting the approximate placement of the multielectrode array in the neocortical layers I-V. An illustration of the arrangement of the sixty electrodes, which were 30µM in diameter and height and spaced 200µM apart, overlaid with typical recorded activity, can be seen in the dotted box.

We next tested the effects of the 500nM LY compound on 4-AP induced epileptiform activity, which preferentially inhibits Nav1.6 and Nav1.2, by approximately fifty percent according to the apparent IC50 values we observed, while having little to no effect on Nav1.1 or Nav1.3 channel activity at this concentration. We recorded baseline activity for one hour with 100μM 4-AP to induce epileptiform activity and subsequently recorded the treatment condition consisting of 100μM 4-AP with 500nM LY compound for thirty minutes. We found that 500nM LY compound completely abolishes interictal LFPs (Figure 33A). We did not observe interictal LFPs in any recordings with the LY compound. The number of LFP events detected was significantly ($p<0.05$; paired t-test; $n = 5$) reduced in the presence of the LY compound (Figure 33B). Some slices still displayed activity, but of much smaller amplitude (Figure 33C, D). This activity did not exhibit the typical interictal LFP waveform (Figure 33E, F). To confirm slice viability and intact attachment of the slice to electrodes after treatment perfusion, we recorded a washout recording with only 100μM 4-AP that demonstrated activity could be recovered to some extent (Figure 33A *inset*). These data show that partial inhibition of Nav1.6 and Nav1.2 by the LY compound selectively abolishes epileptiform activity induced by 4-AP but does not completely inhibit slice activity.

We further investigated the effects of the 125nM ICA compound, which preferentially inhibits Nav1.1 and Nav1.3 while having little to no effect on Nav1.2 and Nav1.6 at this concentration, on 4-AP induced activity. Representative traces of baseline and treatment recordings can be seen in Figure 35A. We found no

siginficant effects of 125nM ICA compound on the number of interictal LFPs or peak or valley amplitudes of the LFPs (Figure 35B-D). Aligned LFPs from a single representative electrode during baseline and treatment recordings can be seen in Figure 35E. Interestingly, there was a slight but significant ($p<0.01$; paired t-test; $n = 5$) reduction in LFP duration in the presence of 125nM ICA compound. These data suggest that inhibition of Nav1.1 and Nav1.3 has minimal effects on 4-AP induced epileptiform activity.

To further dissern the effects of Nav1.2 inhibition on 4-AP induced hyper-excitability, we asked whether partial inhibition of Nav1.2 by the ICA compound would reduce activity. To address this, we additionally tested the effects of a higher concentration of the ICA compound (500nM) which would lead to inhibition Nav1.1, Nav1.3 and also Nav1.2 by approximatly fifty percent according to the apparent IC50 values we observed, while having little to no effect on Nav1.6. We obtained similar results to those obtained with 125nM ICA compound, with no significant difference in the number of interictal LFPs or peak and valley amplitues, but a signficant reduction in the duration of the LFPs (Figure 35). These data suggest that partial inhibition of Nav1.2 with the ICA cmpod does not overtly alter 4-AP induced hyper-excitability, and therefore the effects observed with the LY compound are likey due to inhibition of Nav1.6.

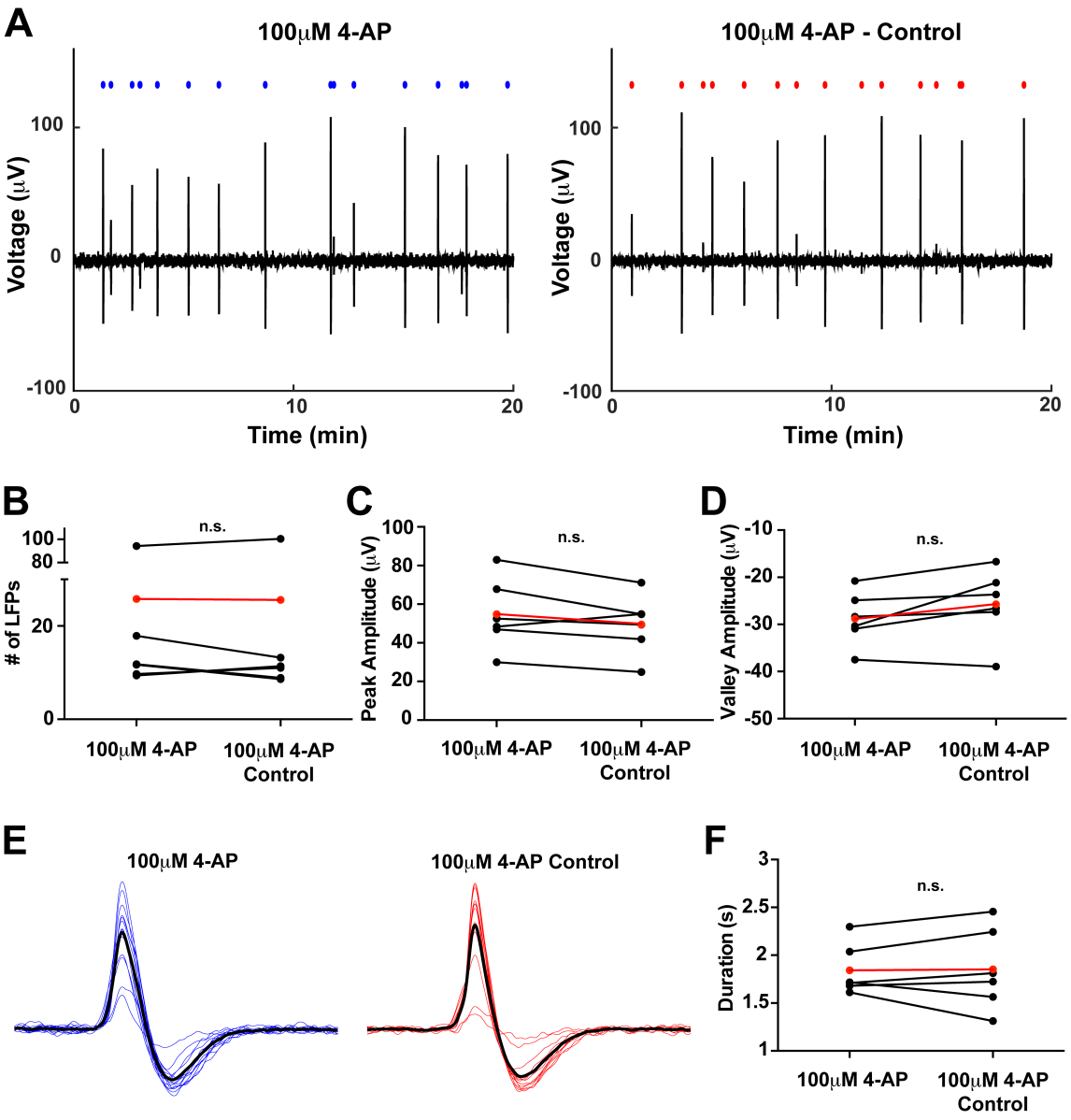

Figure 32. 100μM 4-AP induced hyper-excitability in mouse cortical brain slices does not change over time. A, Representative twenty minute traces of LFP activity from baseline recording (left) and corresponding treatment recording (right). The blue and red circles above traces depict the location of each LFP detected. B, Average number of LFPs detected from baseline and corresponding treatment recordings (n = 6). Data in red represent the mean across all slices. C and D, Average peak and valley amplitude calculated from baseline and treatment recordings. E, Alignment of all LFPs from a single electrode during baseline recording (blue) and treatment recording (red). The bolded black traces represent the mean LFP waveform from which the duration was measured. F, Average duration of LFPs recorded during baseline and corresponding treatment groups. n.s., not significant; paired t-test.

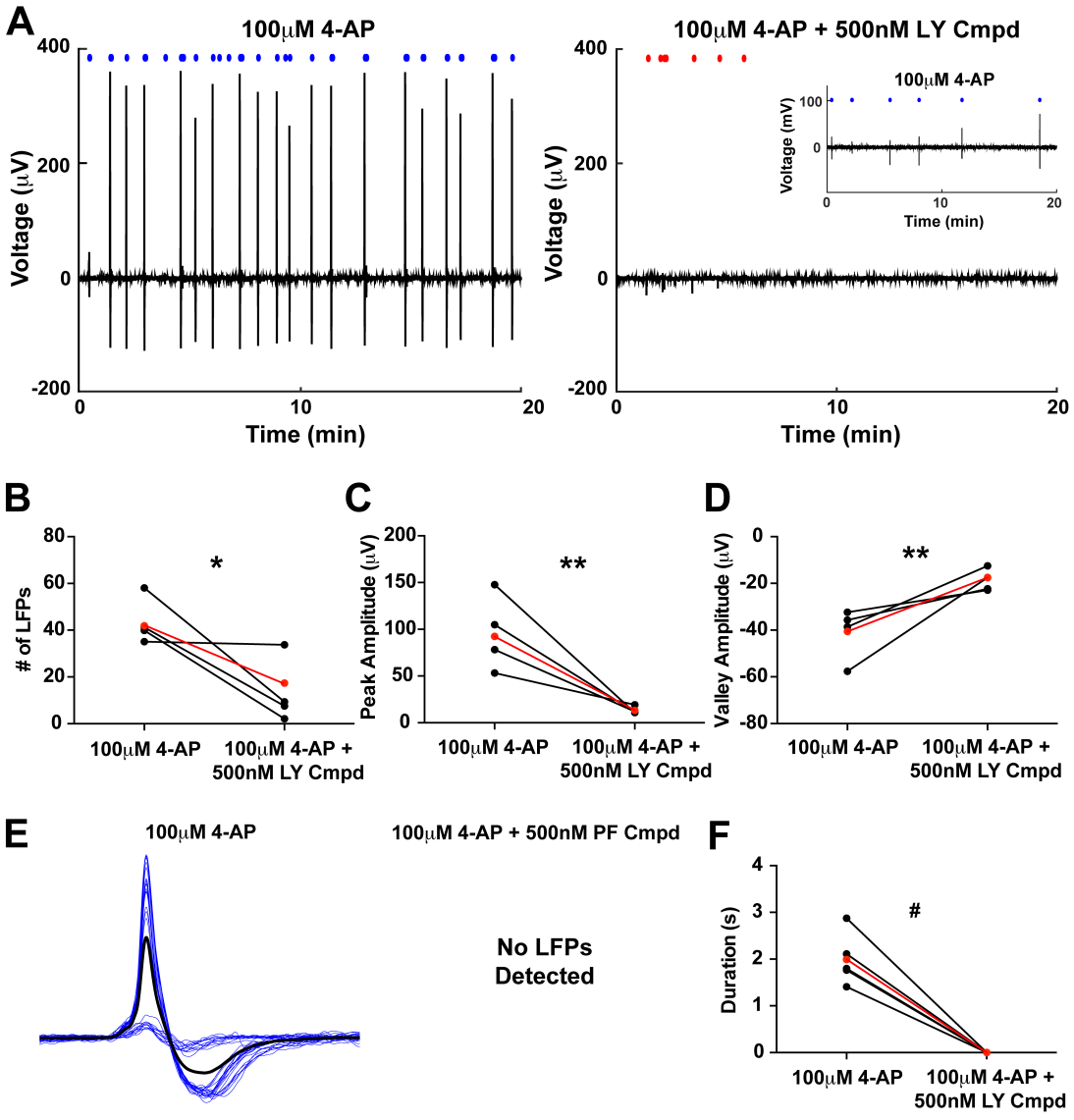

Figure 33. 500nM LY compound abolishes intericatal LFPs induced by 4-AP in mouse cortical brain slices. A, Representative twenty minute traces of LFP activity from baseline recording with 100μM 4-AP (left) and corresponding treatment recording with 100μM 4-AP and 500nM LY compound (right). Twenty minute trace of corresponding washout recording with 100μM 4-AP only (*inset*). The blue and red circles above traces depict the location of each LFP detected. B, Average number of LFPs detected from baseline and corresponding treatment recordings (n = 5). Data in red represent the mean across all slices. C and D, Average peak and valley amplitude calculated from baseline and treatment recordings. E, Alignment of all LFPs from a single electrode during baseline recording (blue). No interictal LFPs were detected during treatment recording. The bolded black trace represents the mean LFP waveform from which the duration was measured. F, Average duration of LFPs recorded during baseline and corresponding treatment groups. *p<0.05, **p<0.01, #p<0.001; paired t-test.

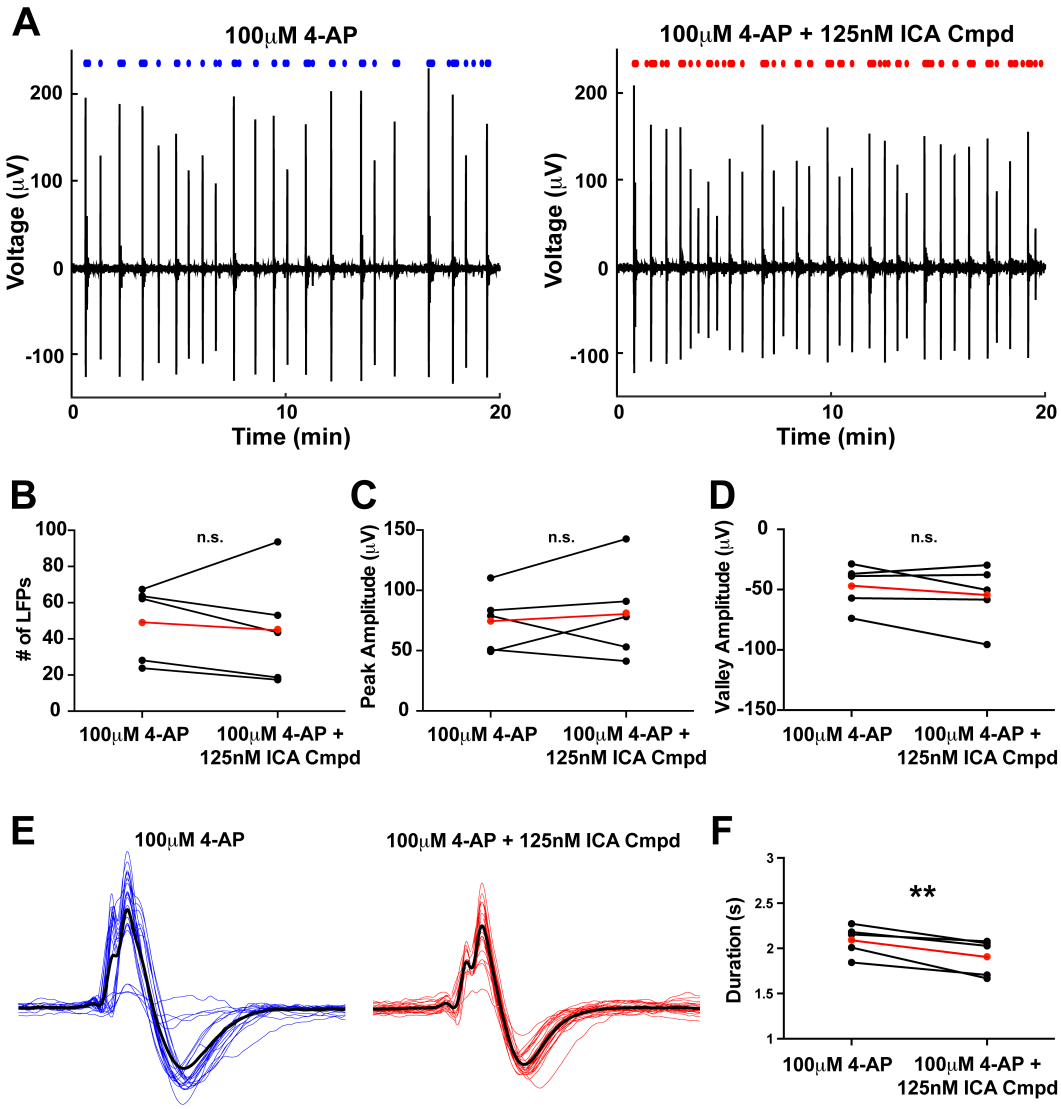

Figure 34. 125nM ICA compound decreases interictal LFP duration but does not effect the number or amplitude of interictal LFPs induced by 4-AP in mouse cortical brain slices. A, Representative twenty minute traces of LFP activity from baseline recording with 100μM 4-AP (left) and corresponding treatment recording with 100μM 4-AP and 125nM ICA compound (right). The blue and red circles above traces depict the location of each LFP detected. B, Average number of LFPs detected from baseline and corresponding treatment recordings (n = 5). Data in red represent the mean across all slices. C and D, Average peak and valley amplitude calculated from baseline and treatment recordings. E, Alignment of all LFPs from a single electrode during baseline recording (blue) and treatment recording (red). The bolded black traces represent the mean LFP waveform from which the duration was measured. F, Average duration of LFPs recorded during baseline and corresponding treatment groups. n.s., not significant, **p<0.01; paired t-test.

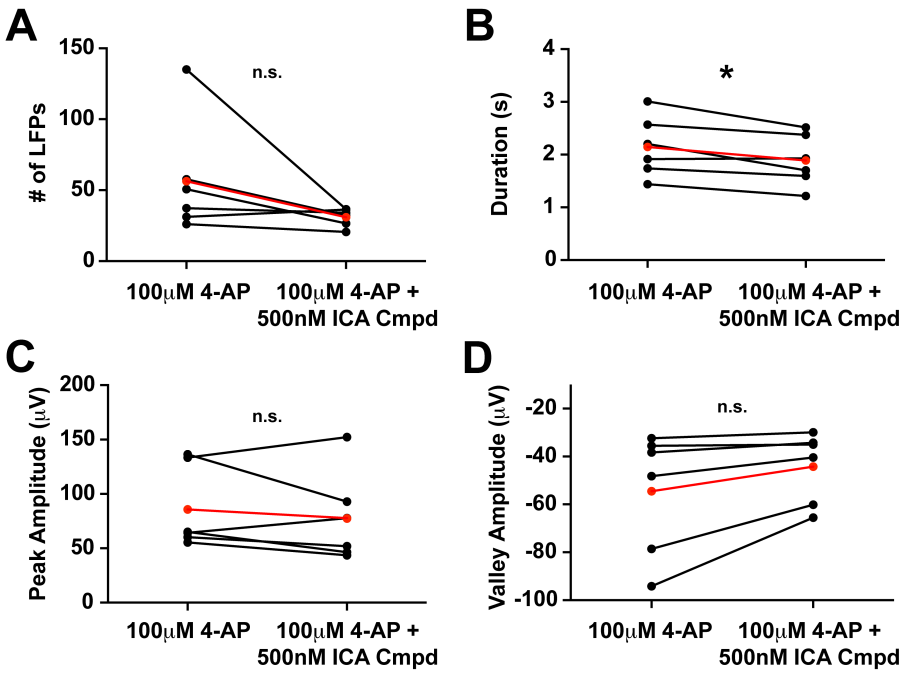

Figure 35. 500nM ICA compound inhibits the duration of interictal LFPs but has no effect on the number or amplitude of interictal LFPs induced by 4-AP in mouse cortical brain slices. A, Number of LFPs detected during baseline (100μM 4-AP) and corresponding treatment (100μM 4-AP + 500nM ICA compound) recordings (n = 6). B, Average duration of LFPs recorded during baseline and treatment recordings. C and D, Average peak and valley amplitudes for LFPs recording during baseline and treatment conditions. n.s., not significant, *, $p<0.05$; paired t-test.

3. Partial inhibition of Nav1.1 increases basal activity

The prominent expression of Nav1.1 in GABAergic neurons [143-145] led us to ask whether partial inhibition of Nav1.1 is sufficient to induce synchronized activity. To address this question, we recorded basal activity in the presence of normal ACSF or 300nM ICA compound and subsequently perfused 100uM 4-AP at the end of each recording to confirm slice viability (Figure 36A). While statistical significance was not reached, we found a trend towards an increase in the number of LFPs in the presence of 300nM ICA compound. Moreover, the LFPs recorded in the presence of 300nM ICA compound were significantly larger in magnitude (green bars; $n = 5$) ($p<0.05$; unpaired t-test), both peak and valley amplitudes, compared to LFPs recorded in the presence of normal ACSF (black bars; $n = 3$)(Figure 36B-D). This data suggests that partial inhibition of Nav1.1 can increase basal synchronized activity.

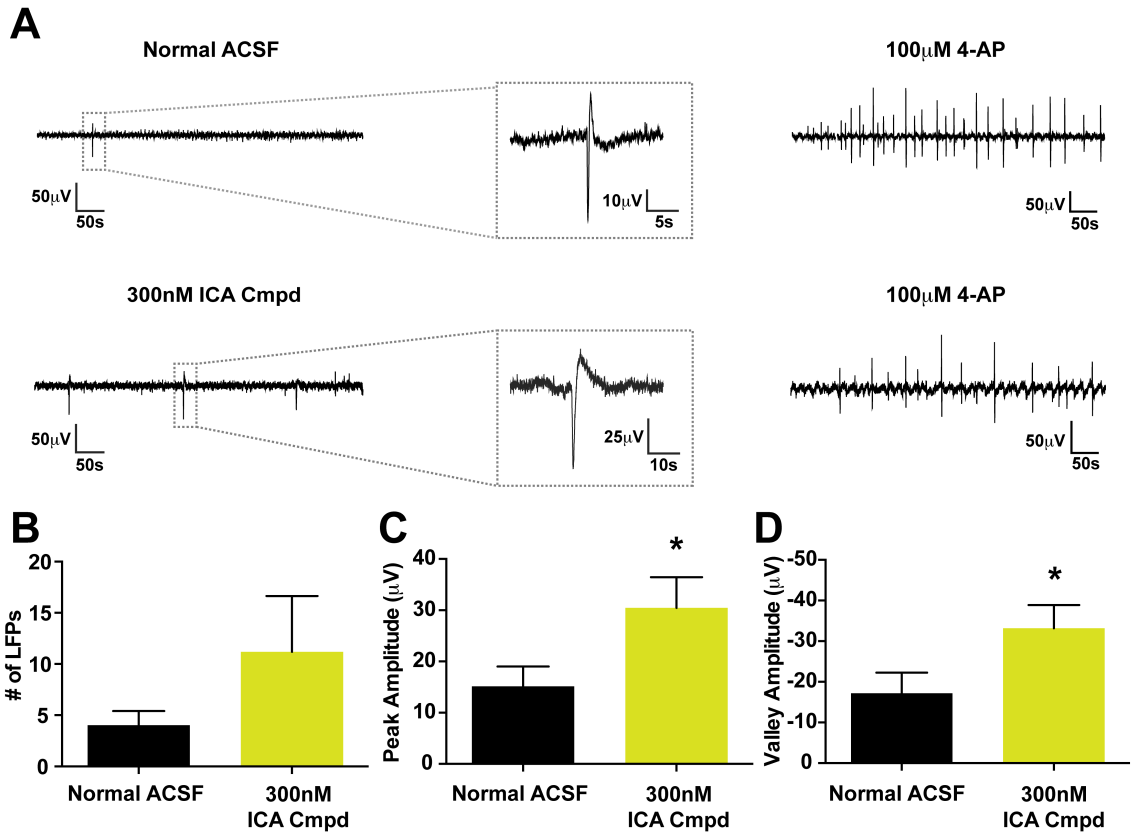

Figure 36. 300nM of the ICA compound alone increases the peak and valley amplitude of basal activity in mouse cortical brain slices A, Representative twenty minute traces of basal activity from recordings in the presence of normal ACSF (top) and ACSF containing 300nM ICA compound (bottom). B, Average number of events detected from normal ACSF (n = 3; black bars) and ACSF containing 300nM ICA compound (n = 5; green bars). C and D, Average peak and valley amplitude calculated for each condition. *p<0.05; unpaired t-test.

D. Discussion

In this study, we examined the contribution of VGSC isoforms to epileptiform activity in order to further our understanding of the roles of specific isoforms in the brain. We tested the selectivity of newly discovered small molecule inhibitors, ICA and LY compounds, against Nav1.1, Nav1.2 and Nav1.6 activity in HEK293T cells. We found that the ICA and LY compounds preferentially inhibits Nav1.1 and Nav1.6, respectively, which allowed us to parse out the roles of each isoform. To address our main question of how specific VGSCs isoforms contribute to epileptiform activity, we observed the effects of the ICA and LY compounds on 4-AP induced hyper-excitability, an established *in vitro* model of epilepsy [247, 248], with MEA recordings from mouse cortical brain slices. Interestingly, we found that brain isoforms of VGSCs play distinct roles during epileptiform activity. Inhibiting approximately half of Nav1.6 and Nav1.2 activity with 500nM of the LY compound completely abolished interictal LFPs induced by 4-AP, but preserved slice activity. In contrast, inhibiting Nav1.1, Nav1.2 and Nav1.3 with 500nM of the ICA compound had minimal effect on 4-AP induced hyper-excitability. These findings are consistent with our current understanding of the localization of these channels in the brain. This led us to ask whether partial inhibition of Nav1.1 could alter basal slice activity due to the prominent expression of Nav1.1 in inhibitory neurons. Indeed, we found that inhibition of Nav1.1 with 300nM ICA compound increased the peak and valley amplitudes of basal LFPs with a trend toward an increase in the overall number of basal LFPs compared to normal ACSF in the absence of 4-AP. Overall, our findings

clearly demonstrate that brain isoforms of VGSCs have distinct roles in epileptiform activity and suggest that selectively targeting Nav1.6 activity may be a more efficacious treatment strategy for epileptic syndromes.

It has been demonstrated that *Scn1a*$^{+/-}$ heterozygous mice display spontaneous seizures mimicking a SMEI phenotype [143, 145]. However, it is still unclear if these seizures arise because of the direct loss of Nav1.1 or due to other compensatory mechanisms that often occur in genetic models. While some studies have found decreased somatic sodium currents of GABAergic neurons in *Scn1a*$^{+/-}$ heterozygous mice [145], others report no change in somatic sodium currents but still find an impairment in excitability of GABAergic neurons [234, 251]. In this study, we asked how inhibition of Nav1.1 influences epileptiform activity induced by 4-AP and whether inhibition of Nav1.1 is sufficient to induce synchronized activity. We did not observe any significant effects of inhibition of Nav1.1 on epileptiform activity induced by 4-AP except for a slight decrease in the duration of the LFPs. We hypothesized that inhibition of Nav1.1 might in fact increase epileptiform activity, however we did not observe this in our preparation. We did find that inhibition of Nav1.1 with the ICA compound, in the absence of 4-AP, increased basal synchronized activity. It is possible that an increase in basal synchronized activity could create a circuit more susceptible to seizure generation upon a secondary insult. Indeed, a hallmark of SMEI due to *Scn1a* mutations is the initial development of febrile seizures, which later progress into other seizure types [252].

As mentioned previously, Nav1.1 is prominently expressed in inhibitory GABAergic neurons, specifically those that express somatostatin or parvalbumim [143-145, 233, 234]. Parvalbumin positive GABAergic neurons consist of two major subtypes, basket cells and chandelier cells, that provide strong synaptic inhibition to the proximal dendrites/soma and axon initial segment, respectively, of pyramidal neurons – placing them in a critical position for regulating circuit excitability [253]. Impaired excitability of parvalbumin positive neurons has been associated with epilepsy and a number of other neurological disorders [254], possibly due to their importance in the generation of gamma oscillations [136, 255]. Therefore, avoiding inhibition of Nav1.1 will likely have therapeutic benefits. However, while hyper-synchronous activity underlying seizures is commonly attributed to either an increase in synchronized excitatory neuronal activity or a decrease in inhibition, there is increasing evidence that synchronized activity of GABAergic neurons can underlie epileptiform activity [256-260]. Specifically, the synchronized activity of somatostatin positive GABAergic neurons, which express Nav1.1 or Nav1.2 and 1.6, have been shown to contribute to the generation of epileptiform activity with 4-AP application [261]. In fact, optogenetic activation of somatostatin and parvalbumin positive GABAergic neurons in the presence of 4-AP produces ictal-like events similar to those occurring spontaneously [262]. In most of our recordings, we observed only interictal events possibly due to the location of recordings, species or age of animals used. This is not surprising as only 6% of slices obtained from rat neocortex produced ictal-like events with 4-AP [263]. Indeed, in one recording we observed ictal-like events that were approximately 15 seconds in length (Fig. 37A).

Interestingly, 500nM ICA cmpd, presumably inhibiting Nav1.1, Nav1.2 and Nav1.3, inhibited the low voltage, high frequency phase of the ictal-like event (Fig. 37B). While we have a limited sample number, our data is in accordance with inhibitory activity underlying some types of synchronized activity induced by 4-AP. Overall, inhibition of Nav1.1, Nav1.2 and Nav1.3 with the ICA compound had no significant effect on the most commonly observed epileptiform activity, with the exception of a decrease in LFP duration, supporting the idea that perhaps Nav1.1 is not a good target for the treatment of epilepsy syndromes.

Nav1.2 activity is inhibited by approximately fifty percent at a concentration of 500nM with both the ICA and LY compounds. Since we observed starkly different effects of these two compounds on 4-AP induced hyper-excitability at this concentration, we were compelled to conclude that Nav1.2 does not play an overt role in epileptiform activity in this model. However, Nav1.2 has been implicated in epilepsy as evidenced by genetic mutations in Nav1.2 that result in epileptic syndromes [239]. Interestingly, the epilepsy-associated missense mutations in Nav1.2 have been reported to cause both gain- and loss- of function effects on channel properties when expressed in heterologous expression systems [264-266]. While this may seem paradoxical, it is not entirely surprising due to the dense expression of Nav1.2 in the proximal axon initial segment of both excitatory, pyramidal neurons as well as somatostatin positive GABAergic, inhibitory neurons. Alternatively, it is possible that the effects of inhibiting Nav1.2 are masked by concurrently inhibiting either Nav1.1 with the ICA compound or Nav1.6 with the LY

compound. In the case of the ICA compound, inhibiting Nav1.1 and Nav1.2 activity, would result in decreased excitability of both parvalbumin and somatostatin positive GABAergic neurons, which comprise the majority of GABAergic neurons in the cortex [253, 267]. Therefore, a decrease in excitatory neuron excitability due to partial inhibition of Nav1.2 in pyramidal neurons would not be predicted to restore inhibitory-excitatory balance. Indeed, global inhibition of Nav1.2 results in a decreased threshold for recurrent network activity suggesting that the effects of Nav1.2 inhibition in somatostatin positive GABAergic neurons outweigh the effects of Nav1.2 inhibition in pyramidal neurons [233].

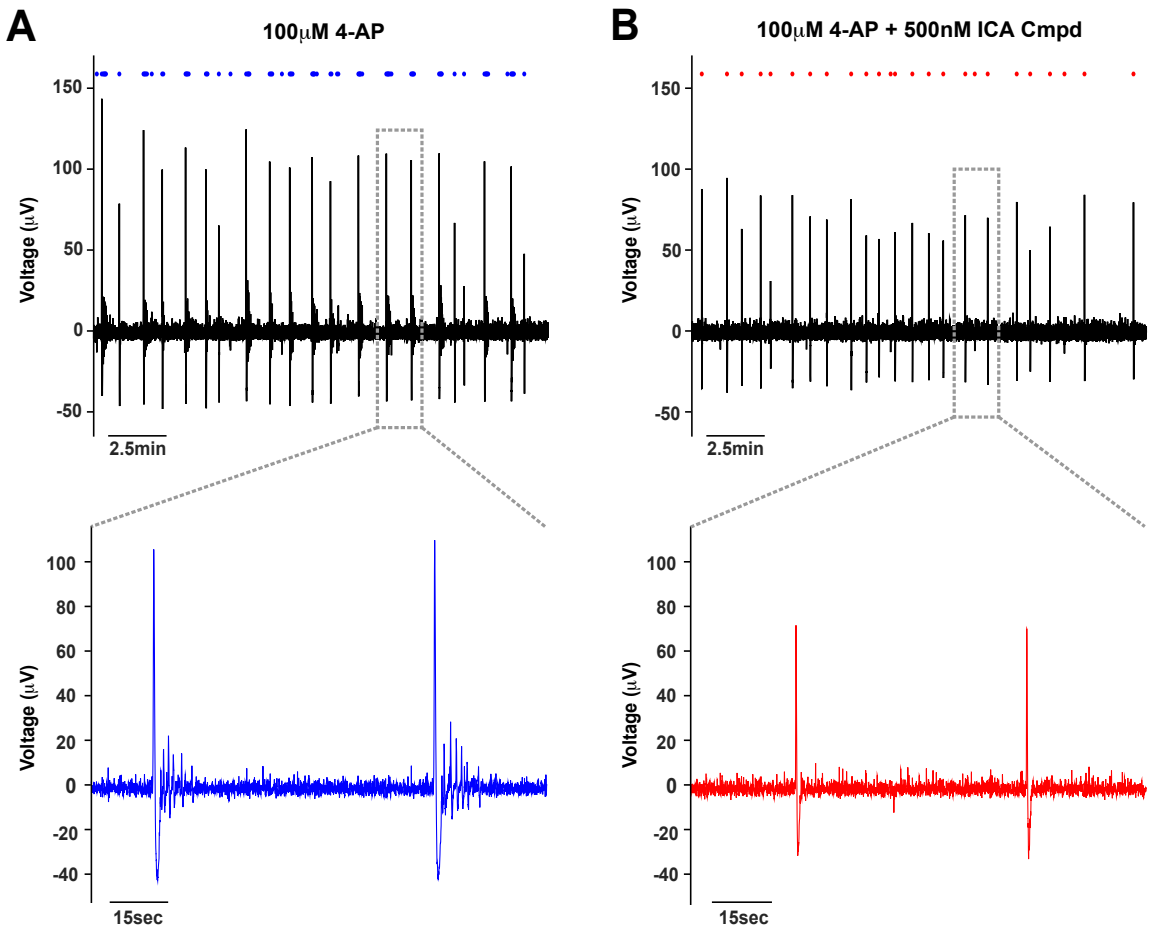

Figure 37. An example of 4-AP induced ictal-like events in mouse cortical brain slices. Twenty minute traces of epileptiform activity induced by 100μM 4-AP (A) and 100μM plus 500nM ICA compound (B). Below is a magnification of boxed area depicting ictal-like events (blue trace) and interitcal events (red trace).

Overall, our findings suggest that selective inhibition of Nav1.6 may be a better treatment strategy for epileptic syndromes. We found that partially inhibiting Nav1.6 activity pharmacologically can abolish interictal LFPs in a 4-AP model of epilepsy, while preserving some slice activity. Selective targeting of this isoform, rather than broadly inhibiting all VGSC isoforms as many current AEDs do, may reduce unwanted side effects. While genetic studies support the idea that partial loss of Nav1.6 reduces seizure generation, they also demonstrate the potential adverse consequences that have been associated with loss of Nav1.6 activity including: absence seizures, motor defects and cognitive defects [268-271]. However, these genetic studies result in global loss of one allele of Nav1.6 and possibly compensatory changes that could further fuel these adverse effects, whereas pharmacological inhibition of Nav1.6 can supposedly be titrated to achieve a balance wherein the benefits of seizure control could outweigh the consequences of unwanted side effects. Moreover, the compounds used in this study demonstrate a use-dependence property that is a greater degree of inhibition with repetitive stimulation, similar to current AEDs that broadly target voltage-gated sodium channels [140], which allows for the selective targeting of hyper-excitable neurons, further reducing unnecessary inhibition of activity.

In the previous chapters, it was demonstrated that Nav1.6 has a greater propensity to generate resurgent current (Chapter II) and that epilepsy-associated mutations in Nav1.6 enhance resurgent current generation (Chapter III), suggesting that the selective inhibition of Nav1.6 may have greater advantages in some types of

inherited and even acquired epileptic syndromes. Cannabidiol is one potential compound that was found to selectively inhibit resurgent and persistent current generated by Nav1.6, but not Nav1.1 (Chapter III). Indeed, cannabidiol has recently been shown to be efficacious in the treatment of intractable pediatric epilepsies [192]. We performed pilot experiments examining the effects of 1μM CBD on 4-AP induced epileptiform activity, but did not find any major effect. However, Jones *et al.* found a significant reduction in LFP frequency induced by 4-AP with CBD at concentrations ranging from (0.01 – 100μM) using hippocampal slices [272]. Overall, selective inhibition of Nav1.6, potentially underlying the efficacy of cannabidiol, may provide a more efficacious treatment strategy for many epileptic syndromes.

V. CONCLUSIONS

A. Summary of findings

1. Human Nav1.6 channels generate larger resurgent currents than human Nav1.1 channels, but the Navβ4 peptide does not protect either isoform from use-dependent reduction

Voltage-gated sodium channels are responsible for the initiation and propagation of APs. Two brain isoforms, Nav1.1 and Nav1.6, have very distinct cellular expression and subcellular localization. Specifically, Nav1.1 is predominantly expressed in the soma and proximal axon initial segment of fast-spiking GABAergic neurons [143-145], while Nav1.6 is found at the distal axon initial segment and nodes of Ranvier of both fast-spiking GABAergic and excitatory neurons [116, 144, 145]. Interestingly, an auxiliary voltage-gated sodium channel subunit, Navβ4, is also enriched in the axon initial segment of fast-spiking GABAergic neurons [138]. The C-terminal tail of Navβ4 is thought to mediate resurgent sodium current, an atypical current that occurs immediately following the action potential and is predicted to enhance excitability [68, 70, 273, 274]. To better understand the contribution of Nav1.1, Nav1.6 and Navβ4 to high frequency firing, we compared the properties of these two channel isoforms in the presence and absence of a peptide corresponding to part of the C-terminal tail of Navβ4. We used whole-cell patch clamp recordings to examine the biophysical properties of these

two channel isoforms in HEK293T cells and found several differences between human Nav1.1 and Nav1.6 currents. Nav1.1 channels exhibited slower closed-state inactivation but faster open-state inactivation than Nav1.6 channels. We also observed a greater propensity of Nav1.6 to generate resurgent currents, most likely due to its slower kinetics of open-state inactivation, compared to Nav1.1. These two isoforms also showed differential responses to slow and fast AP waveforms, which were altered by the Navβ4 peptide. Although the Navβ4 peptide substantially increased the rate of recovery from apparent inactivation, Navβ4 peptide did not protect either channel isoform from undergoing use-dependent reduction with 10 Hz step-pulse stimulation or trains of slow or fast AP waveforms. Overall, these two channels have distinct biophysical properties that are predicted to differentially contribute to regulating neuronal excitability.

2. Aberrant epilepsy-associated mutant Nav1.6 voltage-gated sodium channel activity can be targeted with cannabidiol

Mutations in brain isoforms of VGSCs have been identified in patients with distinct epileptic phenotypes. Clinically, these patients often do not respond well to classic AEDs and many remain refractory to treatment. Exogenous as well as endogenous cannabinoids have been shown to target VGSCs and cannabidiol has recently received attention for its potential efficacy in the treatment of childhood epilepsies [81, 139, 196, 197]. In this study, we further investigated the ability of cannabinoids to modulate sodium currents from wildtype and epilepsy-associated

mutant VGSCs. We first determined the biophysical consequences of epilepsy-associated missense mutations in both Nav1.1 (R1648H and N1788K) and Nav1.6 (N1768D and L1331V) by obtaining whole-cell patch clamp recordings in HEK293T cells with 200μM Navβ4 peptide in the pipette solution to induce resurgent sodium currents. Resurgent sodium currents have been implicated in multiple disorders of excitability [64, 80, 195, 275]. We found that three mutations in Nav1.6 dramatically increased resurgent currents while mutations in Nav1.1 did not. We then examined the effects of anandamide and cannabidiol on peak transient and resurgent currents from wildtype and mutant channels. Interestingly, we found that cannabidiol can preferentially target resurgent sodium currents over peak transient currents generated by wildtype Nav1.6 as well as the aberrant resurgent and persistent current generated by Nav1.6 mutant channels. To further validate our findings, we examined the effects of cannabidiol on endogenous sodium currents from striatal neurons, and similarly we found an inhibition of resurgent and persistent current by cannabidiol. Moreover, current clamp recordings show that cannabidiol increases the reduces overall action potential firing of striatal neurons. These findings suggest that cannabidiol could be exerting its anticonvulsant effects, at least in part, through its actions on VGSCs, and resurgent current may be a promising therapeutic target for the treatment of epilepsy syndromes.

3. Preferential pharmacological inhibition of Nav1.6, but not Nav1.1, abolishes epileptiform activity induced by 4-aminopyridine in mouse cortical brain slices

Brain isoforms of VGSCs have distinct cellular and subcellular expression patterns as well as functional roles that are critical for normal physiology as aberrations in their expression and/or activity can lead to pathophysiological conditions. In this study, we asked how inhibition of select isoforms of VGSCs alters epileptic activity to further parse out the roles of VGSCs in the brain. We first determined the relative selectivity of recently discovered small molecule, aryl sulfonamide, inhibitors (ICA-121431 and LY-03049227) [140] against Nav1.1, Nav1.2, and Nav1.6 activity using whole-cell patch clamp recordings obtained from HEK293T cells. To test the effects of these inhibitors on epileptic activity, we obtained MEA recordings from mouse cortical brain slices in the presence of 4-AP to induce epileptiform activity. We found that the ICA-121431 and LY-03049227 compounds are relatively selective for Nav1.1 and Nav1.6, respectively. From the MEA recordings, we found that 500nM of the LY-03049227 compound, a concentration that partially inhibits Nav1.6 and Nav1.2, completely abolishes interictal LFPs induced by 4-AP, whereas in contrast 500nM of the ICA-121431 compound, a concentration that produces inhibition of Nav1.1, Nav1.2, and Nav1.3, had minimal effect on epileptic activity induced by 4-AP. Due to the prominent expression of Nav1.1 in inhibitory neurons [143, 145], we asked whether preferential inhibition of Nav1.1 over Nav1.6 alters baseline brain slice activity. We found that, indeed, inhibition with 300nM of the ICA-121431 compound increased basal activity in the absence of 4-AP. These findings expand our current understanding of the roles of VGSC isoforms in the brain and suggest that selective

targeting of Nav1.6 may be a more efficacious treatment strategy for epileptic syndromes.

B. Benefits and limitations of experimental design

A. Use of HEK293T cell line as a model system to study VGSCs

Many of the experiments conducted for this dissertation involved the use of HEK293T cells to study VGSC activity. While this is a common practice in the field, it is important to recognize the benefits and limitations of this model system especially in regards to data interpretation and extrapolation to higher model systems. For the study of ion channels, specifically VGSCs in this case, HEK293T cells are advantageous in that they provide a reduced system in which the current of interest can easily be isolated due to the lack of significant endogenous expression of VGSCs. This allowed for the study of human channel clones, which have differences in their amino acid sequences compared to other species and of specific VGSC isoforms. Moreover, their relatively small and simple cell morphology allows for excellent voltage control over the entire cell, reducing voltage-clamp error, and allowing for the precise measurement of sodium currents. However, VGSCs function as a channel complex wherein many auxiliary proteins can associate and modulate channel activity. Therefore, the cellular background in which these channels are studied can potentially greatly influence their biophysical properties. HEK293T are derived from human embryonic kidney cells, although they express some neuronal

specific proteins [276], they lack a complete neuronal background. A caveat that is particularly important to point out for this dissertation is that the full length Navβ4 does not produce resurgent currents in HEK293T cells. It is unclear why this is but it may be due in part to cellular background as phosphorylation of channels has been demonstrated to be necessary for the generation of resurgent sodium currents in cerebellar Purkinje neurons [72]. For this reason a peptide corresponding to part of the C-terminal tail of Navβ4, that can induce resurgent sodium currents, was used. It is possible that the peptide does not mimic all the properties of the full length Navβ4 – a significant difference is the diffuse nature of the peptide compared to close proximity of the full length Navβ4 to the channel. Despite these disadvantages, the use of HEK293T cells as a model system was appropriate and very useful to address the questions posed in this dissertation. Reassuringly, findings in HEK293T cells with Nav1.6 and Navβ4 on use-dependent reduction (Fig. 14,15) were reproduced in DRG neurons with co-transfection of Nav1.6 and full-length Navβ4. Moreover, the effects of cannabidiol on Nav1.6 wildtype currents in HEK293T cells were reproduced in striatal neurons with endogenous sodium currents. Therefore, the findings cannot simply be attributed to an artifact of using the peptide rather than the full form of the Navβ4 subunit or due to lack of a neuronal background, further demonstrating the appropriate use of this simplified model system to study VGSC currents.

Another common practice in ion channel research that is important to recognize when extrapolating results to physiological implications is the

temperature at which recordings are obtained. All recordings in HEK293T cells were obtained at room temperature (~23°C). Temperature can greatly influence physiological processes. It is well recognized that ion channels are temperature sensitive and gating properties of both sodium and potassium channels are faster at higher temperatures [277]. Indeed, there are several temperature-associated pathologies linked to mutations in VGSCs and studies have revealed alterations in gating properties of mutant channels at increased temperatures (~32-40°C) [278-281]. However, recording at higher temperatures can increase potential voltage-clamp errors due to the significantly increased speed of gating transitions and difficulties with fully compensating for series resistance errors; this can be especially problematic with VGSCs due to their fast kinetics. Therefore, room temperature recordings were used for the purposes of addressing the aims of this dissertation.

B. Use of cultured striatal neurons as a model system to study sodium currents and excitability

Cultured striatal neurons were used to further validate the findings in HEK293T cells. The use of striatal neurons as a model system was specifically advantageous for addressing the questions posed in this dissertation due to their expression of endogenous resurgent sodium currents that are presumably mediated by Navβ4 [67]. Additionally, striatal neurons could be used for both examining VGSC currents as well as neuronal excitability – allowing for extrapolation of findings on

sodium currents to implications on neuronal excitability. However, because of the complex arborization of dendritic and axonal processes of cultured neurons, it can be difficult to maintain good voltage control over the entire neuron adding some voltage-clamp error associated artifacts to sodium current recordings. Moreover, most cultured neurons, especially CNS neurons, are relatively immature and may lack the full compliment of ion channels and consequently activity compared to adult neurons. The striatum contains many different cell types [282], therefore the cultured striatal neurons are heterogeneous, which can additionally add variability to the results. While the cultured striatal neurons are very useful, they still may not entirely reflect the activity of striatal neurons *in vivo*. For example, the resting membrane potential of striatal neurons *in vivo* are substantially more hyperpolarized (~90mV) compared to data in cultured striatal neurons (~50mV) [67, 230]. Indeed, in an intact circuit, striatal neurons *in vivo*, receive glutamatergic and dopaminergic inputs from other brain structures that can substantially modulate activity both acutely and long-term [230]. Therefore, the findings from cultured striatal neurons and their implications should be cautiously interpreted.

C. MEA recordings obtained from mouse cortical brain slices

To pharmacologically study epileptiform activity, multielectrode array recordings were used. MEAs are advantageous in that neuronal activity can be measured from multiple sites within a brain slice simultaneously. Since epileptiform activity is thought to be the result of synchronized activity of many neurons, it is

important to study this type of activity in a model in which local circuitry is intact. Therefore, acute coronal, cortical brain slices were used to examine how selective inhibition of VGSC isoforms alters epileptiform activity. Coronal, cortical brain slices are advantageous in that the columnar circuitry of the cerebral cortex (layers I-IV) remains intact along with some long-range projects from sub-cortical areas. Seizures can occur anywhere in the brain but the most common types of partial (i.e. focal) seizures are localized to the temporal and frontal lobes according to the Epilepsy Foundation [283]. Indeed, the cerebral cortex is the origin site of seizures associated with several acquired epilepsy syndromes [284]. Therefore, the cortical slices provide a relevant model system in which to study epileptiform activity.

The 4-AP model of epilepsy is well established and has been validated using current anti-epileptic drugs *in vitro* [248, 285, 286]. 4-AP is a potassium channel blocker that can induce spontaneous synchronized interictal and ictal-like activity in brain slices. Indeed, 4-AP can cause seizures *in vivo* [287]. It is important to recognize that this is a model for symptomatic epileptiform activity as washout of 4-AP abolishes epileptiform activity [288]. Mechanistically, 4-AP block of voltage-gated potassium channels presumably results in broadening of the AP, which consequently leads to increased calcium entry at the axon terminal and increased neurotransmitter release. Other mechanisms have also been proposed to underlie 4-AP induced interictal and ictal-like events [285]. Regardless, the model is likely to have limitations as still other mechanisms, not reflected in this model, may occur during epileptic activity *in vivo* in different syndromes and patients.

An important caveat of MEA recordings is that the recorded signals are generated from neurons near the surface of the slice directly adjacent to the electrodes. This region of the slice may be more damaged compared to the interior of the slice, although damage is reduced when slices are cut with a vibratome, and therefore may not function the same as healthy/undamaged neurons would. Another important consideration is that the signals being measured are complex. Although LFPs are thought to primarily reflect synchronized synaptic activity, LFPs are ultimately the superimposition of many other signals including: AP signals, calcium spikes and current movement through gap junctions [289]. Therefore, interpreting and understanding the molecular mechanism underlying alterations in LFP signals can be difficult. However, the paired nature of our experiments and the use of selective inhibitors along with our current understanding of cortical circuitry and localization of VGSCs allowed us to draw some conclusions regarding the roles of select isoforms in epileptiform activity.

C. Implications of findings towards disease and therapy

Brain isoforms of VGSCs have distinct expression and cellular localization patterns as described in Chapter I. Their functional roles within these specialized regions are not well understood. However, it is clear that disruption of their expression or activity can have pathophysiological consequences. The localization of specific isoforms in particular regions within a neuron such as the dendrites, axon initial segment, axon, or nerve terminals influences the integration and

amplification of synaptic signals, action potential initiation, backpropagation of action potentials into the dendrite, and neurotransmitter release. For example, it can be theorized that VGSC isoforms that generate large persistent current (i.e. Nav1.6) if expressed in the dendrites can amplify synaptic potentials leading to an increased dendritic summation of excitatory input, if expressed in the axon initial segment may lead to increased action potential generation in response to a single event, or if expressed in the nerve terminal may lead to longer duration action potential waveform and consequently more neurotransmitter release. The unique biophysical properties of each isoform are therefore crucial for maintaining physiological neuronal activity. Understanding the role of each isoform in different neuronal populations will help to identify potential mechanisms underlying pathophysiologies associated with disruption of VGSCs.

Genetic epilepsies due to mutations in brain isoforms of VGSCs arise from different mechanisms as a result of both the biophysical consequences conferred by the mutation and the neuronal expression of the channel isoform in which the mutation occurs (i.e. inhibitory versus excitatory). The Nav1.1 epilepsy-associated mutations studied here were found to be loss-of-function (Fig. 17, 18; Table 3, 4), consistent with the prominent hypothesis by which mutations in Nav1.1 cause epilepsy. That is, a decrease in Nav1.1 activity leading to an overall decrease in inhibitory tone due to the primary expression of Nav1.1 in GABAergic neurons. In contrast, Nav1.6 epilepsy-associated mutations were found to be gain-of-function (Fig. 18, 19, 28; Table 3, 4) in accordance with the major hypothesis of the

mechanism underlying epilepsy-associated mutations in Nav1.6. Due to the ubiquitous expression of Nav1.6, an increase in Nav1.6 activity is thought to lead to an overall increase in neuronal excitability. One novel, potential mechanism, identified in this work, by which Nav1.6 mutations could induce epileptogenesis is through increased generation of resurgent current, atypical currents predicted to enhance neuronal excitability, which was not observed with mutations in Nav1.1. Interestingly, of the epilepsy-associated mutations in Nav1.2 that have been characterized both gain- and loss-of-function effects have been observed. While not a major focus of this dissertation, we also observed mixed effects on resurgent current generation by epilepsy-associated mutations in Nav1.2 (Fig. 38). While seemingly paradoxical, it is consistent with the dense expression of Nav1.2 in the proximal axon initial segment of both somatostatin GABAergic neurons and excitatory pyramidal neurons [150, 233]. These findings further demonstrate the need for treatment strategies tailored to phenotype and genetic cause.

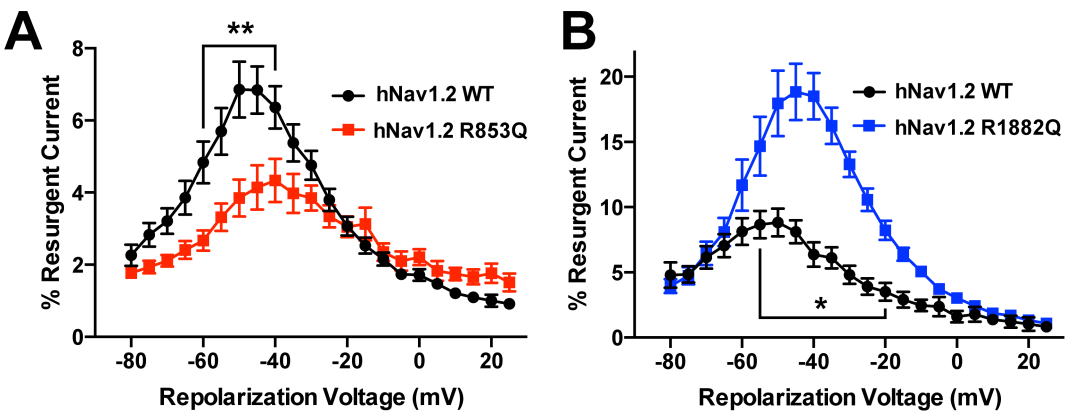

Figure 38. Epilepsy-associated mutations in hNav1.2 can increase or decrease resurgent current generation. A, hNav1.2 WT (black; *n* = 11) and hNav1.2 R853Q (red; *n* = 11) B, hNav1.2 WT (black; *n* = 9) and hNav1.2 R1882Q (blue; *n* = 11). *, p<0.05, **, p<0.01; two-way ANOVA.

Current AEDs are effective in controlling seizures in some patients, but 30% of patients are refractory to treatment. In particular, patients with intractable pediatric epilepsy syndromes do not respond well to AEDs. Indeed, in the case of SMEI, AEDs that broadly inhibit VGSC activity are contraindicated. Cannabidiol, marketed as Epidolex by GW pharmaceuticals, has recently passed phase III clinical trials for its use for intractable pediatric epilepsies [192]. Accordingly, cannabidiol reduced resurgent and persistent current produced by wildtype and mutant channels and decreased excitability of striatal neurons identifying a mechanism by which cannabidiol could be exerting its anti-epileptics actions. Importantly, cannabidiol's effects were specific to Nav1.6 as no affect on Nav1.1 generated currents were observed. Due to the ubiquitous expression of Nav1.6 and its upregulated activity in epileptic models, cannabidiol may be efficacious for the treatment of many epileptic syndromes. Indeed, preferentially inhibiting Nav1.1 versus Nav1.6 during epileptiform activity induced by 4-AP results in starkly different effects. Partial pharmacological inhibition of Nav1.6, but not Nav1.1, completely abolishes epileptiform activity suggesting that 1) these isoforms have very different functional roles in maintaining pathological activity, 2) Nav1.1 is likely not a good target and it may be beneficial to avoid inhibition of Nav1.1 and 3) selectively inhibiting Nav1.6 generated currents may be a better strategy for treatment of epileptic syndromes. Intriguingly, while Nav1.3 expression is negligible in the adult rodent brain, Nav1.3 activity is also upregulated in many animal models and human epilepsies [108, 145, 290, 291] suggesting a potential role of Nav1.3 activity in the development and/or maintenance of epileptic activity. Therefore,

Nav1.3 may be a good target for the treatment of some epilepsy syndromes. However, in an animal model of SMEI (*Scn1a*$^{+/-}$) up-regulated expression of Nav1.3 specifically occurred in a subpopulation of GABAergic neurons in the hippocampus [145]. This upregulated expression might compensate in part to the loss of Nav1.1 channel activity. In this case, targeting Nav1.3 activity may be deleterious. Overall, these findings add to our current understanding of the mechanisms underlying epilepsy syndromes associated with mutations in VGSC isoforms, their role in maintaining epileptiform activity and their potential to be targeted for treatment of epilepsy syndromes.

D. Future Directions

While the findings presented in this dissertation expand our current understanding of brain isoforms of VGSCs, they need further experimental validation and also raise additional questions. In regards to the mechanism underlying epilepsy-associated mutations in Nav1.1 and Nav1.6, a logical extension would be to confirm loss- and gain-of-function by examining the effects of these mutant channels on neuronal excitability. Moreover, it would be interesting to study these mutant channels in different neuronal populations including: paravalbumin positive GABAergic neurons, somatostatin positive GABAergic neurons, and pyramidal neurons. It is possible that the biophysical consequences of epilepsy-associated mutations may differ depending on cellular background as has been demonstrated with wildtype channels [292]. Trafficking and expression level, which

are highly regulated in neurons, of a particular isoform in a specific neuronal population will also influence the consequences of mutant channels on the electrical properties of the neuron and may help identify unknown mechanisms.

To further validate Nav1.6 and/or resurgent currents as an efficacious target for the treatment of epileptic syndromes, the effects of the compounds examined in this dissertation (CBD, ICA and LY compounds) should be tested in other epilepsy models. Specifically, MEA recordings from brain slices obtained from *Scn1a* heterozygous mice, a model of SMEI, and recently generated *Scn8a*$^{+/N168D}$ knock-in mice [241] would be useful. It is unknown whether these slices would be spontaneously active. Increasing slice temperature may induce epileptiform activity in slices obtained from *Scn1a* heterozygous mice as these mice are susceptible to hyperthermia-induced seizures [178]. Additionally, the theorized effects of the ICA and LY compounds on specific neuronal populations, due to the expression of select VGSC isoforms, should be confirmed in cortical slices using transgenic mice with labeled neuronal populations. Ultimately, the effects of viral mediated shRNA knockdown of Navβ4 in the hippocampus [293], thalamus [294] or entorhinal cortex [194, 195], regions strongly implicated in epilepsy and containing neurons known to express resurgent currents [90], on seizure thresholds or on seizure activity induced prior to knockdown could potentially provide strong evidence for the involvement of resurgent currents in epilepsy.

APPENDIX A

NATURE PUBLISHING GROUP LICENSE TERMS AND CONDITIONS

Mar 22, 2016

This is a License Agreement between Reesha R Patel ("You") and Nature Publishing Group ("Nature Publishing Group") provided by Copyright Clearance Center ("CCC"). The license consists of your order details, the terms and conditions provided by Nature Publishing Group, and the payment terms and conditions.

All payments must be made in full to CCC. For payment instructions, please see information listed at the bottom of this form.

License Number	3834281148429
License date	Mar 22, 2016
Licensed content publisher	Nature Publishing Group
Licensed content publication	Nature
Licensed content title	The crystal structure of a voltage-gated sodium channel
Licensed content author	Jian Payandeh, Todd Scheuer, Ning Zheng, William A. Catterall
Licensed content date	Jul 10, 2011
Volume number	475
Issue number	7356
Type of Use	reuse in a dissertation / thesis
Requestor type	academic/educational
Format	print and electronic
Portion	figures/tables/illustrations
Number of figures/tables/illustrations	1
High-res required	no
Figures	Panel A of Figure 1
Author of this NPG article	no
Your reference number	None
Title of your thesis / dissertation	Nav1.1 and Nav1.6: Electrophysiological properties, epilepsy-associated mutations and therapeutic targets
Expected completion date	May 2016
Estimated size (number of pages)	150

VI. REFERENCES

1. French, J.A., *Refractory epilepsy: clinical overview.* Epilepsia, 2007. 48 Suppl 1: p. 3-7.
2. Hodgkin, A.L. and A.F. Huxley, *Resting and action potentials in single nerve fibres.* J Physiol, 1945. 104(2): p. 176-95.
3. Hodgkin, A.L. and B. Katz, *The effect of sodium ions on the electrical activity of giant axon of the squid.* J Physiol, 1949. 108(1): p. 37-77.
4. Hodgkin, A.L. and A.F. Huxley, *Currents carried by sodium and potassium ions through the membrane of the giant axon of Loligo.* J Physiol, 1952. 116(4): p. 449-72.
5. Hodgkin, A.L. and A.F. Huxley, *The components of membrane conductance in the giant axon of Loligo.* J Physiol, 1952. 116(4): p. 473-96.
6. Hodgkin, A.L. and A.F. Huxley, *The dual effect of membrane potential on sodium conductance in the giant axon of Loligo.* J Physiol, 1952. 116(4): p. 497-506.
7. Hodgkin, A.L. and A.F. Huxley, *A quantitative description of membrane current and its application to conduction and excitation in nerve.* J Physiol, 1952. 117(4): p. 500-44.
8. Chandler, W.K. and H. Meves, *Voltage clamp experiments on internally perfused giant axons.* J Physiol, 1965. 180(4): p. 788-820.
9. Hodgkin, A.L., A.F. Huxley, and B. Katz, *Measurement of current-voltage relations in the membrane of the giant axon of Loligo.* J Physiol, 1952. 116(4): p. 424-48.

10. Nakamura, Y., S. Nakajima, and H. Grundfest, *The action of tetrodotoxin on electrogenic components of squid giant axons.* J Gen Physiol, 1965. 48(6): p. 975-96.

11. Rojas, E. and C. Armstrong, *Sodium conductance activation without inactivation in pronase-perfused axons.* Nat New Biol, 1971. 229(6): p. 177-8.

12. Narahashi, T., J.W. Moore, and W.R. Scott, *Tetrodotoxin Blockage of Sodium Conductance Increase in Lobster Giant Axons.* J Gen Physiol, 1964. 47: p. 965-74.

13. Takata, M., et al., *Blockage of sodium conductance increase in lobster giant axon by tarichatoxin (tetrodotoxin).* J Gen Physiol, 1966. 49(5): p. 977-88.

14. Neher, E., B. Sakmann, and J.H. Steinbach, *The extracellular patch clamp: a method for resolving currents through individual open channels in biological membranes.* Pflugers Arch, 1978. 375(2): p. 219-28.

15. Hamill, O.P., et al., *Improved patch-clamp techniques for high-resolution current recording from cells and cell-free membrane patches.* Pflugers Arch, 1981. 391(2): p. 85-100.

16. Catterall, W.A., *Voltage-gated sodium channels at 60: structure, function and pathophysiology.* Journal of Physiology-London, 2012. 590(11): p. 2577-2589.

17. Agnew, W.S., et al., *Identification of a large molecular weight peptide associated with a tetrodotoxin binding protein from the electroplax of Electrophorus electricus.* Biochem Biophys Res Commun, 1980. 92(3): p. 860-6.

18. Catterall, W.A. and D.A. Beneski, *Interaction of polypeptide neurotoxins with a receptor site associated with voltage-sensitive sodium channels.* J Supramol Struct, 1980. 14(3): p. 295-303.

19. Noda, M., et al., *Primary structure of Electrophorus electricus sodium channel deduced from cDNA sequence.* Nature, 1984. 312(5990): p. 121-7.

20. Noda, M., et al., *Existence of distinct sodium channel messenger RNAs in rat brain.* Nature, 1986. 320(6058): p. 188-92.

21. Goldin, A.L., et al., *Messenger RNA coding for only the alpha subunit of the rat brain Na channel is sufficient for expression of functional channels in Xenopus oocytes.* Proc Natl Acad Sci U S A, 1986. 83(19): p. 7503-7.

22. Payandeh, J., et al., *The crystal structure of a voltage-gated sodium channel.* Nature, 2011. 475(7356): p. 353-8.

23. Payandeh, J., et al., *Crystal structure of a voltage-gated sodium channel in two potentially inactivated states.* Nature, 2012. 486(7401): p. 135-9.

24. Hodgkin, A.L. and A.F. Huxley, *A quantitative description of membrane current and its application to conduction and excitation in nerve. 1952.* Bull Math Biol, 1990. 52(1-2): p. 25-71; discussion 5-23.

25. Stuhmer, W., et al., *Structural parts involved in activation and inactivation of the sodium channel.* Nature, 1989. 339(6226): p. 597-603.

26. Kontis, K.J., A. Rounaghi, and A.L. Goldin, *Sodium channel activation gating is affected by substitutions of voltage sensor positive charges in all four domains.* J Gen Physiol, 1997. 110(4): p. 391-401.

27. Yarov-Yarovoy, V., D. Baker, and W.A. Catterall, *Voltage sensor conformations in the open and closed states in ROSETTA structural models of K(+) channels.* Proc Natl Acad Sci U S A, 2006. 103(19): p. 7292-7.

28. Guy, H.R. and P. Seetharamulu, *Molecular model of the action potential sodium channel.* Proc Natl Acad Sci U S A, 1986. 83(2): p. 508-12.

29. Catterall, W.A., *Molecular properties of voltage-sensitive sodium channels.* Annu Rev Biochem, 1986. 55: p. 953-85.

30. Tombola, F., M.M. Pathak, and E.Y. Isacoff, *How does voltage open an ion channel?* Annu Rev Cell Dev Biol, 2006. 22: p. 23-52.

31. Hille, B., *Ion Channels of Excitable Membranes*. 3rd ed. 2001, Sunderland, MA: Sinauer.

32. Armstrong, C.M., *Sodium channels and gating currents.* Physiol Rev, 1981. 61(3): p. 644-83.

33. Vassilev, P.M., T. Scheuer, and W.A. Catterall, *Identification of an intracellular peptide segment involved in sodium channel inactivation.* Science, 1988. 241(4873): p. 1658-61.

34. Vassilev, P., T. Scheuer, and W.A. Catterall, *Inhibition of inactivation of single sodium channels by a site-directed antibody.* Proc Natl Acad Sci U S A, 1989. 86(20): p. 8147-51.

35. West, J.W., et al., *A cluster of hydrophobic amino acid residues required for fast Na(+)-channel inactivation.* Proc Natl Acad Sci U S A, 1992. 89(22): p. 10910-4.

36. Eaholtz, G., T. Scheuer, and W.A. Catterall, *Restoration of inactivation and block of open sodium channels by an inactivation gate peptide.* Neuron, 1994. 12(5): p. 1041-8.

37. Lerche, H., et al., *Role in fast inactivation of the IV/S4-S5 loop of the human muscle Na+ channel probed by cysteine mutagenesis.* J Physiol, 1997. 505 (Pt 2): p. 345-52.

38. Smith, M.R. and A.L. Goldin, *Interaction between the sodium channel inactivation linker and domain III S4-S5.* Biophys J, 1997. 73(4): p. 1885-95.

39. Motoike, H.K., et al., *The Na+ channel inactivation gate is a molecular complex: a novel role of the COOH-terminal domain.* J Gen Physiol, 2004. 123(2): p. 155-65.

40. Nguyen, H.M. and A.L. Goldin, *Sodium channel carboxyl-terminal residue regulates fast inactivation.* J Biol Chem, 2010. 285(12): p. 9077-89.

41. Yang, Y.C. and C.C. Kuo, *The position of the fourth segment of domain 4 determines status of the inactivation gate in Na+ channels.* J Neurosci, 2003. 23(12): p. 4922-30.

42. Capes, D.L., et al., *Domain IV voltage-sensor movement is both sufficient and rate limiting for fast inactivation in sodium channels.* J Gen Physiol, 2013. 142(2): p. 101-12.

43. Ahern, C.A., *What activates inactivation?* Journal of General Physiology, 2013. 142(2): p. 97-100.

44. Ulbricht, W., *Sodium channel inactivation: molecular determinants and modulation.* Physiol Rev, 2005. 85(4): p. 1271-301.

45. Ong, B.H., G.F. Tomaselli, and J.R. Balser, *A structural rearrangement in the sodium channel pore linked to slow inactivation and use dependence.* J Gen Physiol, 2000. 116(5): p. 653-62.

46. Ruff, R.L., L. Simoncini, and W. Stuhmer, *Slow sodium channel inactivation in mammalian muscle: a possible role in regulating excitability.* Muscle Nerve, 1988. 11(5): p. 502-10.

47. Catterall, W.A., A.L. Goldin, and S.G. Waxman, *International Union of Pharmacology. XLVII. Nomenclature and structure-function relationships of voltage-gated sodium channels.* Pharmacol Rev, 2005. 57(4): p. 397-409.

48. Gershon, E., et al., *Protein kinase A reduces voltage-dependent Na+ current in Xenopus oocytes.* J Neurosci, 1992. 12(10): p. 3743-52.

49. Li, M., et al., *Functional modulation of brain sodium channels by cAMP-dependent phosphorylation.* Neuron, 1992. 8(6): p. 1151-9.

50. Smith, R.D. and A.L. Goldin, *Protein kinase A phosphorylation enhances sodium channel currents in Xenopus oocytes.* Am J Physiol, 1992. 263(3 Pt 1): p. C660-6.

51. Numann, R., W.A. Catterall, and T. Scheuer, *Functional modulation of brain sodium channels by protein kinase C phosphorylation.* Science, 1991. 254(5028): p. 115-8.

52. O'Reilly, J.P., T.R. Cummins, and G.G. Haddad, *Oxygen deprivation inhibits Na+ current in rat hippocampal neurones via protein kinase C.* J Physiol, 1997. 503 (Pt 3): p. 479-88.

53. Ahn, M., et al., *Regulation of Na(v)1.2 channels by brain-derived neurotrophic factor, TrkB, and associated Fyn kinase.* J Neurosci, 2007. 27(43): p. 11533-42.

54. Herren, A.W., D.M. Bers, and E. Grandi, *Post-translational modifications of the cardiac Na channel: contribution of CaMKII-dependent phosphorylation to acquired arrhythmias.* Am J Physiol Heart Circ Physiol, 2013. 305(4): p. H431-45.

55. Scheuer, T., *Regulation of sodium channel activity by phosphorylation.* Semin Cell Dev Biol, 2011. 22(2): p. 160-5.

56. Bosmans, F., M. Milescu, and K.J. Swartz, *Palmitoylation influences the function and pharmacology of sodium channels.* Proc Natl Acad Sci U S A, 2011. 108(50): p. 20213-8.

57. Beltran-Alvarez, P., et al., *Protein arginine methyl transferases-3 and -5 increase cell surface expression of cardiac sodium channel.* FEBS Lett, 2013. 587(19): p. 3159-65.

58. Reddy Chichili, V.P., et al., *Structural basis for the modulation of the neuronal voltage-gated sodium channel NaV1.6 by calmodulin.* Sci Rep, 2013. 3: p. 2435.

59. Kovalevskaya, N.V., et al., *Structural analysis of calmodulin binding to ion channels demonstrates the role of its plasticity in regulation.* Pflugers Arch, 2013. 465(11): p. 1507-19.

60. Van Petegem, F., P.A. Lobo, and C.A. Ahern, *Seeing the forest through the trees: towards a unified view on physiological calcium regulation of voltage-gated sodium channels.* Biophys J, 2012. 103(11): p. 2243-51.

61. Baek, J.H., et al., *Reciprocal changes in phosphorylation and methylation of mammalian brain sodium channels in response to seizures.* J Biol Chem, 2014. 289(22): p. 15363-73.

62. Raman, I.M. and B.P. Bean, *Inactivation and recovery of sodium currents in cerebellar Purkinje neurons: evidence for two mechanisms.* Biophys J, 2001. 80(2): p. 729-37.

63. Grieco, T.M. and I.M. Raman, *Production of resurgent current in NaV1.6-null Purkinje neurons by slowing sodium channel inactivation with beta-pompilidotoxin.* J Neurosci, 2004. 24(1): p. 35-42.

64. Jarecki, B.W., et al., *Human voltage-gated sodium channel mutations that cause inherited neuronal and muscle channelopathies increase resurgent sodium currents.* Journal of Clinical Investigation, 2010. 120(1): p. 369-378.

65. Theile, J.W., et al., *Nav1.7 mutations associated with paroxysmal extreme pain disorder, but not erythromelalgia, enhance Navbeta4 peptide-mediated resurgent sodium currents.* J Physiol, 2011. 589(Pt 3): p. 597-608.

66. Raman, I.M. and B.P. Bean, *Resurgent sodium current and action potential formation in dissociated cerebellar Purkinje neurons.* J Neurosci, 1997. 17(12): p. 4517-26.

67. Miyazaki, H., et al., *Singular localization of sodium channel beta4 subunit in unmyelinated fibres and its role in the striatum.* Nat Commun, 2014. 5: p. 5525.

68. Bant, J.S. and I.M. Raman, *Control of transient, resurgent, and persistent current by open-channel block by Na channel beta4 in cultured cerebellar granule neurons.* Proc Natl Acad Sci U S A, 2010. 107(27): p. 12357-62.

69. Barbosa, C., et al., *Navbeta4 regulates fast resurgent sodium currents and excitability in sensory neurons.* Mol Pain, 2015. 11: p. 60.

70. Grieco, T.M., et al., *Open-channel block by the cytoplasmic tail of sodium channel beta4 as a mechanism for resurgent sodium current.* Neuron, 2005. 45(2): p. 233-44.

71. Burbidge, S.A., et al., *Molecular cloning, distribution and functional analysis of the NA(V)1.6. Voltage-gated sodium channel from human brain.* Molecular Brain Research, 2002. 103(1-2): p. 80-90.

72. Grieco, T.M., F.S. Afshari, and I.M. Raman, *A role for phosphorylation in the maintenance of resurgent sodium current in cerebellar purkinje neurons.* The Journal of neuroscience : the official journal of the Society for Neuroscience, 2002. 22(8): p. 3100-7.

73. Grieco, T.M., F.S. Afshari, and I.M. Raman, *A role for phosphorylation in the maintenance of resurgent sodium current in cerebellar purkinje neurons.* J Neurosci, 2002. 22(8): p. 3100-7.

74. Schiavon, E., et al., *Negative-shift activation, current reduction and resurgent currents induced by beta-toxins from Centruroides scorpions in sodium channels.* Toxicon, 2012. 59(2): p. 283-93.

75. Yan, H., et al., *FGF14 modulates resurgent sodium current in mouse cerebellar Purkinje neurons.* Elife, 2014. 3: p. e04193.

76. Tan, Z.Y., et al., *Tetrodotoxin-Resistant Sodium Channels in Sensory Neurons Generate Slow Resurgent Currents That Are Enhanced by Inflammatory Mediators.* Journal of Neuroscience, 2014. 34(21): p. 7190-7197.

77. Tan, Z.Y., et al., *Protein kinase C enhances human sodium channel hNav1.7 resurgent currents via a serine residue in the domain III-IV linker.* Febs Letters, 2014. 588(21): p. 3964-3969.

78. Liu, P., S. Jo, and B.P. Bean, *Modulation of neuronal sodium channels by the sea anemone peptide BDS-I.* J Neurophysiol, 2012. 107(11): p. 3155-67.

79. Huth, T., et al., *beta-Site APP-cleaving enzyme 1 (BACE1) cleaves cerebellar Na+ channel beta4-subunit and promotes Purkinje cell firing by slowing the decay of resurgent Na+ current.* Pflugers Arch, 2011. 461(3): p. 355-71.

80. Sittl, R., et al., *Anticancer drug oxaliplatin induces acute cooling-aggravated neuropathy via sodium channel subtype Na(V)1.6-resurgent and persistent current.* Proc Natl Acad Sci U S A, 2012. 109(17): p. 6704-9.

81. Theile, J.W. and T.R. Cummins, *Inhibition of Navbeta4 peptide-mediated resurgent sodium currents in Nav1.7 channels by carbamazepine, riluzole, and anandamide.* Mol Pharmacol, 2011. 80(4): p. 724-34.

82. Enomoto, A., et al., *Participation of sodium currents in burst generation and control of membrane excitability in mesencephalic trigeminal neurons.* J Neurosci, 2006. 26(13): p. 3412-22.

83. Raman, I.M. and B.P. Bean, *Ionic currents underlying spontaneous action potentials in isolated cerebellar Purkinje neurons.* J Neurosci, 1999. 19(5): p. 1663-74.

84. Khaliq, Z.M., N.W. Gouwens, and I.M. Raman, *The contribution of resurgent sodium current to high-frequency firing in Purkinje neurons: an experimental and modeling study.* J Neurosci, 2003. 23(12): p. 4899-912.

85. Akemann, W. and T. Knopfel, *Interaction of Kv3 potassium channels and resurgent sodium current influences the rate of spontaneous firing of Purkinje neurons.* J Neurosci, 2006. 26(17): p. 4602-12.

86. Magistretti, J., et al., *Kinetic and functional analysis of transient, persistent and resurgent sodium currents in rat cerebellar granule cells in situ: an electrophysiological and modelling study.* J Physiol, 2006. 573(Pt 1): p. 83-106.

87. Do, M.T. and B.P. Bean, *Sodium currents in subthalamic nucleus neurons from Nav1.6-null mice.* J Neurophysiol, 2004. 92(2): p. 726-33.

88. Osorio, N., et al., *Persistent Nav1.6 current at axon initial segments tunes spike timing of cerebellar granule cells.* J Physiol, 2010. 588(Pt 4): p. 651-70.

89. Pan, F. and K.G. Beam, *The absence of resurgent sodium current in mouse spinal neurons.* Brain Res, 1999. 849(1-2): p. 162-8.

90. Castelli, L., M.J. Nigro, and J. Magistretti, *Analysis of resurgent sodium-current expression in rat parahippocampal cortices and hippocampal formation.* Brain Res, 2007. 1163: p. 44-55.

91. Cummins, T.R., et al., *Nav1.6 channels generate resurgent sodium currents in spinal sensory neurons.* FEBS Lett, 2005. 579(10): p. 2166-70.

92. Lewis, A.H. and I.M. Raman, *Resurgent current of voltage-gated Na(+) channels.* J Physiol, 2014. 592(Pt 22): p. 4825-38.

93. Westenbroek, R.E., D.K. Merrick, and W.A. Catterall, *Differential Subcellular-Localization of the Ri and Rii Na+ Channel Subtypes in Central Neurons.* Neuron, 1989. 3(6): p. 695-704.

94. Gong, B., et al., *Type I and type II Na(+) channel alpha-subunit polypeptides exhibit distinct spatial and temporal patterning, and association with auxiliary subunits in rat brain.* J Comp Neurol, 1999. 412(2): p. 342-52.

95. Whitaker, W.R., et al., *Comparative distribution of voltage-gated sodium channel proteins in human brain.* Brain Res Mol Brain Res, 2001. 88(1-2): p. 37-53.

96. Schaller, K.L. and J.H. Caldwell, *Expression and distribution of voltage-gated sodium channels in the cerebellum.* Cerebellum, 2003. 2(1): p. 2-9.

97. Lorincz, A. and Z. Nusser, *Cell-Type-Dependent Molecular Composition of the Axon Initial Segment.* Journal of Neuroscience, 2008. 28(53): p. 14329-14340.

98. Van Wart, A., J.S. Trimmer, and G. Matthews, *Polarized distribution of ion channels within microdomains of the axon initial segment.* Journal of Comparative Neurology, 2007. 500(2): p. 339-352.

99. Duflocq, A., et al., *Nav1.1 is predominantly expressed in nodes of Ranvier and axon initial segments.* Molecular and Cellular Neuroscience, 2008. 39(2): p. 180-192.

100. Ogiwara, I., et al., *Na(v)1.1 localizes to axons of parvalbumin-positive inhibitory interneurons: A circuit basis for epileptic seizures in mice carrying an Scn1a gene mutation.* Journal of Neuroscience, 2007. 27(22): p. 5903-5914.

101. Boiko, T., et al., *Functional specialization of the axon initial segment by isoform-specific sodium channel targeting.* J Neurosci, 2003. 23(6): p. 2306-13.

102. Boiko, T., et al., *Compact myelin dictates the differential targeting of two sodium channel isoforms in the same axon.* Neuron, 2001. 30(1): p. 91-104.

103. Liao, Y., et al., *Molecular correlates of age-dependent seizures in an inherited neonatal-infantile epilepsy.* Brain, 2010. 133(Pt 5): p. 1403-14.

104. Martinez-Hernandez, J., et al., *Polarised localisation of the voltage-gated sodium channel Na(v)1.2 in cerebellar granule cells.* Cerebellum, 2013. 12(1): p. 16-26.

105. Li, T., et al., *Action Potential Initiation in Neocortical Inhibitory Interneurons.* Plos Biology, 2014. 12(9).

106. Shah, B.S., et al., *Developmental expression of the novel voltage-gated sodium channel auxiliary subunit beta3, in rat CNS.* J Physiol, 2001. 534(Pt 3): p. 763-76.

107. Whitaker, W.R.J., et al., *Comparative distribution of voltage-gated sodium channel proteins in human brain.* Molecular Brain Research, 2001. 88(1-2): p. 37-53.

108. Guo, F., et al., *Voltage-gated sodium channel Nav1.1, Nav1.3 and beta1 subunit were up-regulated in the hippocampus of spontaneously epileptic rat.* Brain Res Bull, 2008. 75(1): p. 179-87.

109. Aronica, E., et al., *Induction of neonatal sodium channel II and III alpha-isoform mRNAs in neurons and microglia after status epilepticus in the rat hippocampus.* Eur J Neurosci, 2001. 13(6): p. 1261-6.

110. Whitaker, W.R., et al., *Changes in the mRNAs encoding voltage-gated sodium channel types II and III in human epileptic hippocampus.* Neuroscience, 2001. 106(2): p. 275-85.

111. Hains, B.C., et al., *Upregulation of sodium channel Nav1.3 and functional involvement in neuronal hyperexcitability associated with central neuropathic pain after spinal cord injury.* J Neurosci, 2003. 23(26): p. 8881-92.

112. Hains, B.C., C.Y. Saab, and S.G. Waxman, *Changes in electrophysiological properties and sodium channel Nav1.3 expression in thalamic neurons after spinal cord injury.* Brain, 2005. 128(Pt 10): p. 2359-71.

113. Huang, X.J., et al., *Expression of voltage-gated sodium channel Nav1.3 is associated with severity of traumatic brain injury in adult rats.* J Neurotrauma, 2013. 30(1): p. 39-46.

114. Caldwell, J.H., et al., *Sodium channel Na(v)1.6 is localized at nodes of Ranvier, dendrites, and synapses.* Proceedings of the National Academy of Sciences of the United States of America, 2000. 97(10): p. 5616-5620.

115. Jenkins, S.M. and V. Bennett, *Ankyrin-G coordinates assembly of the spectrin-based membrane skeleton, voltage-gated sodium channels, and L1 CAMs at Purkinje neuron initial segments.* Journal of Cell Biology, 2001. 155(5): p. 739-745.

116. Lorincz, A. and Z. Nusser, *Molecular identity of dendritic voltage-gated sodium channels.* Science, 2010. 328(5980): p. 906-9.

117. Catterall, W.A., *Sodium channels, inherited epilepsy, and antiepileptic drugs.* Annu Rev Pharmacol Toxicol, 2014. 54: p. 317-38.

118. Eijkelkamp, N., et al., *Neurological perspectives on voltage-gated sodium channels.* Brain, 2012. 135(Pt 9): p. 2585-612.

119. Catterall, W.A., F. Kalume, and J.C. Oakley, *NaV1.1 channels and epilepsy.* J Physiol, 2010. 588(Pt 11): p. 1849-59.

120. Bender, A.C., et al., *SCN1A mutations in Dravet syndrome: Impact of interneuron dysfunction on neural networks and cognitive outcome.* Epilepsy & Behavior, 2012. 23(3): p. 177-186.

121. Chopra, R. and L.L. Isom, *Untangling the dravet syndrome seizure network: the changing face of a rare genetic epilepsy.* Epilepsy Curr, 2014. 14(2): p. 86-9.

122. Liu, Y., et al., *Dravet syndrome patient-derived neurons suggest a novel epilepsy mechanism.* Ann Neurol, 2013. 74(1): p. 128-39.

123. Veeramah, K.R., et al., *De novo pathogenic SCN8A mutation identified by whole-genome sequencing of a family quartet affected by infantile epileptic encephalopathy and SUDEP.* Am J Hum Genet, 2012. 90(3): p. 502-10.

124. O'Brien, J.E. and M.H. Meisler, *Sodium channel SCN8A (Nav1.6): properties and de novo mutations in epileptic encephalopathy and intellectual disability.* Front Genet, 2013. 4: p. 213.

125. Estacion, M., et al., *A novel de novo mutation of SCN8A (Na(v)1.6) with enhanced channel activation in a child with epileptic encephalopathy.* Neurobiology of Disease, 2014. 69: p. 117-123.

126. Vaher, U., et al., *De novo SCN8A mutation identified by whole-exome sequencing in a boy with neonatal epileptic encephalopathy, multiple congenital anomalies, and movement disorders.* J Child Neurol, 2014. 29(12): p. NP202-6.

127. Ohba, C., et al., *Early onset epileptic encephalopathy caused by de novo SCN8A mutations.* Epilepsia, 2014. 55(7): p. 994-1000.

128. Kong, W.J., et al., *SCN8A mutations in Chinese children with early onset epilepsy and intellectual disability.* Epilepsia, 2015. 56(3): p. 431-438.

129. Boerma, R.S., et al., *Remarkable Phenytoin Sensitivity in 4 Children with SCN8A-related Epilepsy: A Molecular Neuropharmacological Approach.* Neurotherapeutics, 2016. 13(1): p. 192-7.

130. Ragsdale, D.S. and M. Avoli, *Sodium channels as molecular targets for antiepileptic drugs.* Brain Res Brain Res Rev, 1998. 26(1): p. 16-28.

131. Hille, B., *Local anesthetics: hydrophilic and hydrophobic pathways for the drug-receptor reaction.* J Gen Physiol, 1977. 69(4): p. 497-515.

132. Ragsdale, D.S., et al., *Molecular determinants of state-dependent block of Na+ channels by local anesthetics.* Science, 1994. 265(5179): p. 1724-8.

133. Yarov-Yarovoy, V., et al., *Role of amino acid residues in transmembrane segments IS6 and IIS6 of the Na+ channel alpha subunit in voltage-dependent gating and drug block.* J Biol Chem, 2002. 277(38): p. 35393-401.

134. Yarov-Yarovoy, V., et al., *Molecular determinants of voltage-dependent gating and binding of pore-blocking drugs in transmembrane segment IIIS6 of the Na(+) channel alpha subunit.* J Biol Chem, 2001. 276(1): p. 20-7.

135. Bialer, M., *Why are antiepileptic drugs used for nonepileptic conditions?* Epilepsia, 2012. 53 Suppl 7: p. 26-33.

136. Hu, H., J. Gan, and P. Jonas, *Interneurons. Fast-spiking, parvalbumin(+) GABAergic interneurons: from cellular design to microcircuit function.* Science, 2014. 345(6196): p. 1255263.

137. Bean, B.P., *The action potential in mammalian central neurons.* Nat Rev Neurosci, 2007. 8(6): p. 451-65.

138. Buffington, S.A. and M.N. Rasband, *Na+ channel-dependent recruitment of Navbeta4 to axon initial segments and nodes of Ranvier.* J Neurosci, 2013. 33(14): p. 6191-202.

139. Foadi, N., et al., *Inhibition of voltage-gated Na(+) channels by the synthetic cannabinoid ajulemic acid.* Anesth Analg, 2014. 118(6): p. 1238-45.

140. McCormack, K., et al., *Voltage sensor interaction site for selective small molecule inhibitors of voltage-gated sodium channels.* Proc Natl Acad Sci U S A, 2013. 110(29): p. E2724-32.

141. Yu, F.H. and W.A. Catterall, *Overview of the voltage-gated sodium channel family.* Genome biology, 2003. 4(3): p. 207.

142. Fry, M., *Developmental expression of Na+ currents in mouse Purkinje neurons.* Eur J Neurosci, 2006. 24(9): p. 2557-66.

143. Ogiwara, I., et al., *Nav1.1 localizes to axons of parvalbumin-positive inhibitory interneurons: a circuit basis for epileptic seizures in mice carrying an Scn1a gene mutation.* J Neurosci, 2007. 27(22): p. 5903-14.

144. Lorincz, A. and Z. Nusser, *Cell-type-dependent molecular composition of the axon initial segment.* J Neurosci, 2008. 28(53): p. 14329-40.

145. Yu, F.H., et al., *Reduced sodium current in GABAergic interneurons in a mouse model of severe myoclonic epilepsy in infancy.* Nat Neurosci, 2006. 9(9): p. 1142-9.

146. Kole, M.H., et al., *Action potential generation requires a high sodium channel density in the axon initial segment.* Nat Neurosci, 2008. 11(2): p. 178-86.

147. Hu, H. and P. Jonas, *A supercritical density of Na(+) channels ensures fast signaling in GABAergic interneuron axons.* Nature neuroscience, 2014. 17(5): p. 686-93.

148. Stuart, G., et al., *Action potential initiation and backpropagation in neurons of the mammalian CNS.* Trends Neurosci, 1997. 20(3): p. 125-31.

149. Van Wart, A., J.S. Trimmer, and G. Matthews, *Polarized distribution of ion channels within microdomains of the axon initial segment.* J Comp Neurol, 2007. 500(2): p. 339-52.

150. Hu, W., et al., *Distinct contributions of Na(v)1.6 and Na(v)1.2 in action potential initiation and backpropagation.* Nat Neurosci, 2009. 12(8): p. 996-1002.

151. Do, M.T. and B.P. Bean, *Subthreshold sodium currents and pacemaking of subthalamic neurons: modulation by slow inactivation.* Neuron, 2003. 39(1): p. 109-20.

152. Castelli, L., et al., *Resurgent Na+ current in pyramidal neurones of rat perirhinal cortex: axonal location of channels and contribution to depolarizing drive during repetitive firing.* J Physiol, 2007. 582(Pt 3): p. 1179-93.

153. Dubridge, R.B., et al., *Analysis of Mutation in Human-Cells by Using an Epstein-Barr-Virus Shuttle System.* Molecular and Cellular Biology, 1987. 7(1): p. 379-387.

154. Burbidge, S.A., et al., *Molecular cloning, distribution and functional analysis of the NA(V)1.6. Voltage-gated sodium channel from human brain.* Brain Res Mol Brain Res, 2002. 103(1-2): p. 80-90.

155. Carter, B.C. and B.P. Bean, *Sodium entry during action potentials of mammalian neurons: incomplete inactivation and reduced metabolic efficiency in fast-spiking neurons.* Neuron, 2009. 64(6): p. 898-909.

156. McCormick, D.A., et al., *Comparative electrophysiology of pyramidal and sparsely spiny stellate neurons of the neocortex.* J Neurophysiol, 1985. 54(4): p. 782-806.

157. Hines, M.L. and N.T. Carnevale, *The NEURON simulation environment.* Neural Comput, 1997. 9(6): p. 1179-209.

158. Pospischil, M., et al., *Minimal Hodgkin-Huxley type models for different classes of cortical and thalamic neurons.* Biol Cybern, 2008. 99(4-5): p. 427-41.

159. Schwarz, J.R., *The effect of temperature on Na currents in rat myelinated nerve fibres.* Pflugers Arch, 1986. 406(4): p. 397-404.

160. Schwarz, J.R. and G. Eikhof, *Na currents and action potentials in rat myelinated nerve fibres at 20 and 37 degrees C.* Pflugers Arch, 1987. 409(6): p. 569-77.

161. Belluzzi, O. and O. Sacchi, *A quantitative description of the sodium current in the rat sympathetic neurone.* J Physiol, 1986. 380: p. 275-91.

162. Cummins, T.R., J.R. Howe, and S.G. Waxman, *Slow closed-state inactivation: a novel mechanism underlying ramp currents in cells expressing the hNE/PN1 sodium channel.* The Journal of neuroscience : the official journal of the Society for Neuroscience, 1998. 18(23): p. 9607-19.

163. Theile, J.W., et al., *Nav1.7 mutations associated with paroxysmal extreme pain disorder, but not erythromelalgia, enhance Nav beta 4 peptide-mediated resurgent sodium currents.* Journal of Physiology-London, 2011. 589(3): p. 597-608.

164. Aman, T.K., et al., *Regulation of Persistent Na Current by Interactions between beta Subunits of Voltage-Gated Na Channels.* Journal of Neuroscience, 2009. 29(7): p. 2027-2042.

165. Wang, G.K., T. Edrich, and S.Y. Wang, *Time-dependent block and resurgent tail currents induced by mouse beta4(154-167) peptide in cardiac Na+ channels.* J Gen Physiol, 2006. 127(3): p. 277-89.

166. Connors, B.W. and M.J. Gutnick, *Intrinsic Firing Patterns of Diverse Neocortical Neurons.* Trends in Neurosciences, 1990. 13(3): p. 99-104.

167. Aman, T.K. and I.M. Raman, *Subunit dependence of Na channel slow inactivation and open channel block in cerebellar neurons.* Biophys J, 2007. 92(6): p. 1938-51.

168. Carter, B.C. and B.P. Bean, *Incomplete inactivation and rapid recovery of voltage-dependent sodium channels during high-frequency firing in cerebellar Purkinje neurons.* J Neurophysiol, 2011. 105(2): p. 860-71.

169. Gittis, A.H., S.H. Moghadam, and S. du Lac, *Mechanisms of sustained high firing rates in two classes of vestibular nucleus neurons: differential contributions of resurgent Na, Kv3, and BK currents.* J Neurophysiol, 2010. 104(3): p. 1625-34.

170. Rudy, B. and C.J. McBain, *Kv3 channels: voltage-gated K+ channels designed for high-frequency repetitive firing.* Trends in Neurosciences, 2001. 24(9): p. 517-526.

171. He, B. and D.M. Soderlund, *Functional expression of Rat Nav1.6 voltage-gated sodium channels in HEK293 cells: modulation by the auxiliary beta1 subunit.* PLoS One, 2014. 9(1): p. e85188.

172. Enomoto, A., et al., *Sodium currents in mesencephalic trigeminal neurons from Nav1.6 null mice.* J Neurophysiol, 2007. 98(2): p. 710-9.

173. Raman, I.M., et al., *Altered subthreshold sodium currents and disrupted firing patterns in Purkinje neurons of Scn8a mutant mice.* Neuron, 1997. 19(4): p. 881-91.

174. Venkatesan, K., Y. Liu, and M. Goldfarb, *Fast-onset long-term open-state block of sodium channels by A-type FHFs mediates classical spike accommodation in hippocampal pyramidal neurons.* J Neurosci, 2014. 34(48): p. 16126-39.

175. Fleidervish, I.A. and M.J. Gutnick, *Kinetics of slow inactivation of persistent sodium current in layer V neurons of mouse neocortical slices.* J Neurophysiol, 1996. 76(3): p. 2125-30.

176. Ellerkmann, R.K., et al., *Slow recovery from inactivation regulates the availability of voltage-dependent Na(+) channels in hippocampal granule cells, hilar neurons and basket cells.* J Physiol, 2001. 532(Pt 2): p. 385-97.

177. Ogiwara, I., et al., *Nav1.1 localizes to axons of parvalbumin-positive inhibitory interneurons: a circuit basis for epileptic seizures in mice carrying an Scn1a gene mutation.* The Journal of neuroscience : the official journal of the Society for Neuroscience, 2007. 27(22): p. 5903-14.

178. Dutton, S.B., et al., *Preferential inactivation of Scn1a in parvalbumin interneurons increases seizure susceptibility.* Neurobiol Dis, 2013. 49: p. 211-20.

179. Cheah, C.S., et al., *Specific deletion of NaV1.1 sodium channels in inhibitory interneurons causes seizures and premature death in a mouse model of Dravet syndrome.* Proc Natl Acad Sci U S A, 2012. 109(36): p. 14646-51.

180. Hedrich, U.B., et al., *Impaired action potential initiation in GABAergic interneurons causes hyperexcitable networks in an epileptic mouse model carrying a human Na(V)1.1 mutation.* J Neurosci, 2014. 34(45): p. 14874-89.

181. Kalume, F., et al., *Sudden unexpected death in a mouse model of Dravet syndrome.* J Clin Invest, 2013. 123(4): p. 1798-808.

182. Ogiwara, I., et al., *Nav1.1 haploinsufficiency in excitatory neurons ameliorates seizure-associated sudden death in a mouse model of Dravet syndrome.* Hum Mol Genet, 2013. 22(23): p. 4784-804.

183. Han, S., et al., *Autistic-like behaviour in Scn1a+/- mice and rescue by enhanced GABA-mediated neurotransmission.* Nature, 2012. 489(7416): p. 385-90.

184. Higurashi, N., et al., *A human Dravet syndrome model from patient induced pluripotent stem cells.* Mol Brain, 2013. 6: p. 19.

185. Larsen, J., et al., *The phenotypic spectrum of SCN8A encephalopathy.* Neurology, 2015. 84(5): p. 480-9.

186. Carvill, G.L., et al., *Targeted resequencing in epileptic encephalopathies identifies de novo mutations in CHD2 and SYNGAP1.* Nat Genet, 2013. 45(7): p. 825-30.

187. Blanchard, M.G., et al., *De novo gain-of-function and loss-of-function mutations of SCN8A in patients with intellectual disabilities and epilepsy.* J Med Genet, 2015.

188. Kong, W., et al., *SCN8A mutations in Chinese children with early onset epilepsy and intellectual disability.* Epilepsia, 2015. 56(3): p. 431-438.

189. Estacion, M., et al., *A novel de novo mutation of SCN8A (Nav1.6) with enhanced channel activation in a child with epileptic encephalopathy.* Neurobiol Dis, 2014. 69: p. 117-23.

190. de Kovel, C.G., et al., *Characterization of a de novo SCN8A mutation in a patient with epileptic encephalopathy.* Epilepsy Res, 2014. 108(9): p. 1511-8.

191. Blanchard, M.G., et al., *De novo gain-of-function and loss-of-function mutations of SCN8A in patients with intellectual disabilities and epilepsy.* J Med Genet, 2015. 52(5): p. 330-7.

192. Devinsky, O., et al., *Cannabidiol in patients with treatment-resistant epilepsy: an open-label interventional trial.* Lancet Neurol, 2016. 15(3): p. 270-8.

193. Cruz, J.S., et al., *Resurgent Na+ current: a new avenue to neuronal excitability control.* Life Sci, 2011. 89(15-16): p. 564-9.

194. Hargus, N.J., et al., *Evidence for a role of Nav1.6 in facilitating increases in neuronal hyperexcitability during epileptogenesis.* J Neurophysiol, 2013. 110(5): p. 1144-57.

195. Hargus, N.J., et al., *Temporal lobe epilepsy induces intrinsic alterations in Na channel gating in layer II medial entorhinal cortex neurons.* Neurobiology of Disease, 2011. 41(2): p. 361-376.

196. Okura, D., et al., *The endocannabinoid anandamide inhibits voltage-gated sodium channels Nav1.2, Nav1.6, Nav1.7, and Nav1.8 in Xenopus oocytes.* Anesth Analg, 2014. 118(3): p. 554-62.

197. Turkanis, S.A., L.M. Partlow, and R. Karler, *Delta-9-Tetrahydrocannabinol Depresses Inward Sodium Current in Mouse Neuroblastoma-Cells.* Neuropharmacology, 1991. 30(1): p. 73-77.

198. Hill, A.J., et al., *Voltage-gated sodium (NaV) channel blockade by plant cannabinoids does not confer anticonvulsant effects per se.* Neurosci Lett, 2014. 566: p. 269-74.

199. Oliva, M., S.F. Berkovic, and S. Petrou, *Sodium channels and the neurobiology of epilepsy.* Epilepsia, 2012. 53(11): p. 1849-59.

200. Escayg, A., et al., *Mutations of SCN1A, encoding a neuronal sodium channel, in two families with GEFS+2.* Nat Genet, 2000. 24(4): p. 343-5.

201. Spampanato, J., et al., *Functional effects of two voltage-gated sodium channel mutations that cause generalized epilepsy with febrile seizures plus type 2.* Journal of Neuroscience, 2001. 21(19): p. 7481-7490.

202. Vanoye, C.G., et al., *Single-channel properties of human NaV1.1 and mechanism of channel dysfunction in SCN1A-associated epilepsy.* J Gen Physiol, 2006. 127(1): p. 1-14.

203. Kahlig, K.M., S.N. Misra, and A.L. George, Jr., *Impaired inactivation gate stabilization predicts increased persistent current for an epilepsy-associated SCN1A mutation.* J Neurosci, 2006. 26(43): p. 10958-66.

204. Tang, B., et al., *A BAC transgenic mouse model reveals neuron subtype-specific effects of a Generalized Epilepsy with Febrile Seizures Plus (GEFS+) mutation.* Neurobiol Dis, 2009. 35(1): p. 91-102.

205. Martin, M.S., et al., *Altered function of the SCN1A voltage-gated sodium channel leads to gamma-aminobutyric acid-ergic (GABAergic) interneuron abnormalities.* J Biol Chem, 2010. 285(13): p. 9823-34.

206. Crill, W.E., *Persistent sodium current in mammalian central neurons.* Annu Rev Physiol, 1996. 58: p. 349-62.

207. Kiss, T., *Persistent Na-channels: origin and function. A review.* Acta Biol Hung, 2008. 59 Suppl: p. 1-12.

208. Wagnon, J.L. and M.H. Meisler, *Recurrent and Non-Recurrent Mutations of SCN8A in Epileptic Encephalopathy.* Front Neurol, 2015. 6: p. 104.

209. Smith, M.R. and A.L. Goldin, *Interaction between the sodium channel inactivation linker and domain III S4-S5.* Biophysical Journal, 1997. 73(4): p. 1885-1895.

210. Catterall, W.A., *From ionic currents to molecular mechanisms: The structure and function of voltage-gated sodium channels.* Neuron, 2000. 26(1): p. 13-25.

211. Veeramah, K.R., et al., *De novo pathogenic SCN8A mutation identified by whole-genome sequencing of a family quartet affected by infantile epileptic encephalopathy and SUDEP.* American journal of human genetics, 2012. 90(3): p. 502-10.

212. Rusconi, R., et al., *Modulatory proteins can rescue a trafficking defective epileptogenic Na(v)1.1 Na+ channel mutant.* Journal of Neuroscience, 2007. 27(41): p. 11037-11046.

213. Sharkey, L.M., et al., *The ataxia3 mutation in the N-terminal cytoplasmic domain of sodium channel Na(v)1.6 disrupts intracellular trafficking.* J Neurosci, 2009. 29(9): p. 2733-41.

214. Rusconi, R., et al., *A rescuable folding defective Nav1.1 (SCN1A) sodium channel mutant causes GEFS+: common mechanism in Nav1.1 related epilepsies?* Hum Mutat, 2009. 30(7): p. E747-60.

215. Cestele, S., et al., *Nonfunctional Na(V)1.1 familial hemiplegic migraine mutant transformed into gain of function by partial rescue of folding defects.*

Proceedings of the National Academy of Sciences of the United States of America, 2013. 110(43): p. 17546-17551.

216. Depienne, C., et al., *Spectrum of SCN1A gene mutations associated with Dravet syndrome: analysis of 333 patients.* J Med Genet, 2009. 46(3): p. 183-91.

217. Milescu, L.S., B.P. Bean, and J.C. Smith, *Isolation of somatic Na+ currents by selective inactivation of axonal channels with a voltage prepulse.* J Neurosci, 2010. 30(22): p. 7740-8.

218. Alekov, A., et al., *A sodium channel mutation causing epilepsy in man exhibits subtle defects in fast inactivation and activation in vitro.* J Physiol, 2000. 529 Pt 3: p. 533-9.

219. Lossin, C., et al., *Molecular basis of an inherited epilepsy.* Neuron, 2002. 34(6): p. 877-84.

220. Cestele, S., et al., *Divergent effects of the T1174S SCN1A mutation associated with seizures and hemiplegic migraine.* Epilepsia, 2013. 54(5): p. 927-35.

221. Guerrini, R., et al., *Lamotrigine and seizure aggravation in severe myoclonic epilepsy.* Epilepsia, 1998. 39(5): p. 508-12.

222. Liao, W.P., et al., *Partial epilepsy with antecedent febrile seizures and seizure aggravation by antiepileptic drugs: associated with loss of function of Na(v) 1.1.* Epilepsia, 2010. 51(9): p. 1669-78.

223. Boerma, R.S., et al., *Remarkable Phenytoin Sensitivity in 4 Children with SCN8A-related Epilepsy: A Molecular Neuropharmacological Approach.* Neurotherapeutics, 2015.

224. Porter, B.E. and C. Jacobson, *Report of a parent survey of cannabidiol-enriched cannabis use in pediatric treatment-resistant epilepsy.* Epilepsy & Behavior, 2013. 29(3): p. 574-577.

225. Szaflarski, J.P. and E.M. Bebin, *Cannabis, cannabidiol, and epilepsy - From receptors to clinical response.* Epilepsy & Behavior, 2014. 41: p. 277-282.

226. Deiana, S., et al., *Plasma and brain pharmacokinetic profile of cannabidiol (CBD), cannabidivarine (CBDV), Delta(9)-tetrahydrocannabivarin (THCV) and cannabigerol (CBG) in rats and mice following oral and intraperitoneal administration and CBD action on obsessive-compulsive behaviour.* Psychopharmacology (Berl), 2012. 219(3): p. 859-73.

227. Stott, C.G., et al., *A phase I study to assess the single and multiple dose pharmacokinetics of THC/CBD oromucosal spray.* Eur J Clin Pharmacol, 2013. 69(5): p. 1135-47.

228. Xiao, Y., K. Blumenthal, and T.R. Cummins, *Gating-pore currents demonstrate selective and specific modulation of individual sodium channel voltage-sensors by biological toxins.* Mol Pharmacol, 2014. 86(2): p. 159-67.

229. Leweke, F.M., et al., *Cannabidiol enhances anandamide signaling and alleviates psychotic symptoms of schizophrenia.* Transl Psychiatry, 2012. 2: p. e94.

230. Surmeier, D.J., L. Carrillo-Reid, and J. Bargas, *Dopaminergic modulation of striatal neurons, circuits, and assemblies.* Neuroscience, 2011. 198: p. 3-18.

231. Devinsky, O., et al., *Cannabidiol: Pharmacology and potential therapeutic role in epilepsy and other neuropsychiatric disorders.* Epilepsia, 2014. 55(6): p. 791-802.

232. Wang, W., et al., *The developmental changes of Na(v)1.1 and Na(v)1.2 expression in the human hippocampus and temporal lobe.* Brain Res, 2011. 1389: p. 61-70.

233. Li, T., et al., *Action potential initiation in neocortical inhibitory interneurons.* PLoS Biol, 2014. 12(9): p. e1001944.

234. Tai, C., et al., *Impaired excitability of somatostatin- and parvalbumin-expressing cortical interneurons in a mouse model of Dravet syndrome.* Proc Natl Acad Sci U S A, 2014. 111(30): p. E3139-48.

235. Yin, L., et al., *Selective Modulation of Axonal Sodium Channel Subtypes by 5-HT1A Receptor in Cortical Pyramidal Neuron.* Cereb Cortex, 2015.

236. Sprunger, L.K., et al., *Dystonia associated with mutation of the neuronal sodium channel Scn8a and identification of the modifier locus Scnm1 on mouse chromosome 3.* Human Molecular Genetics, 1999. 8(3): p. 471-479.

237. Planells-Cases, R., et al., *Neuronal death and perinatal lethality in voltage-gated sodium channel alpha(II)-deficient mice.* Biophys J, 2000. 78(6): p. 2878-91.

238. Vanoye, C.G., et al., *Novel SCN3A variants associated with focal epilepsy in children.* Neurobiol Dis, 2014. 62: p. 313-22.

239. Shi, X., et al., *Clinical spectrum of SCN2A mutations.* Brain Dev, 2012. 34(7): p. 541-5.

240. Escayg, A. and A.L. Goldin, *Sodium channel SCN1A and epilepsy: mutations and mechanisms.* Epilepsia, 2010. 51(9): p. 1650-8.

241. Wagnon, J.L., et al., *Convulsive seizures and SUDEP in a mouse model of SCN8A epileptic encephalopathy.* Hum Mol Genet, 2015. 24(2): p. 506-15.

242. Martin, M.S., et al., *The voltage-gated sodium channel Scn8a is a genetic modifier of severe myoclonic epilepsy of infancy.* Human Molecular Genetics, 2007. 16(23): p. 2892-2899.

243. Makinson, C.D., et al., *Role of the hippocampus in Nav1.6 (Scn8a) mediated seizure resistance.* Neurobiol Dis, 2014. 68: p. 16-25.

244. Sun, W., et al., *Aberrant sodium channel activity in the complex seizure disorder of Celf4 mutant mice.* J Physiol, 2013. 591(1): p. 241-55.

245. Qiao, X., et al., *Expression of sodium channel alpha subunits 1.1, 1.2 and 1.6 in rat hippocampus after kainic acid-induced epilepsy.* Epilepsy Res, 2013. 106(1-2): p. 17-28.

246. Blumenfeld, H., et al., *Role of hippocampal sodium channel Nav1.6 in kindling epileptogenesis.* Epilepsia, 2009. 50(1): p. 44-55.

247. Avoli, M., et al., *4-Aminopyridine induces a long-lasting depolarizing GABA-ergic potential in human neocortical and hippocampal neurons maintained in vitro.* Neurosci Lett, 1988. 94(3): p. 327-32.

248. Hill, A.J., et al., *Development of multi-electrode array screening for anticonvulsants in acute rat brain slices.* J Neurosci Methods, 2010. 185(2): p. 246-56.

249. Zwart, R., et al., *Perampanel, an Antagonist of alpha-Amino-3-Hydroxy-5-Methyl-4-Isoxazolepropionic Acid Receptors, for the Treatment of Epilepsy: Studies in Human Epileptic Brain and Nonepileptic Brain and in Rodent Models.*

Journal of Pharmacology and Experimental Therapeutics, 2014. 351(1): p. 124-133.

250. Ahuja, S., et al., *Structural basis of Nav1.7 inhibition by an isoform-selective small-molecule antagonist.* Science, 2015. 350(6267): p. aac5464.

251. Mistry, A.M., et al., *Strain- and age-dependent hippocampal neuron sodium currents correlate with epilepsy severity in Dravet syndrome mice.* Neurobiol Dis, 2014. 65: p. 1-11.

252. Dravet, C., et al., *Severe myoclonic epilepsy in infancy: Dravet syndrome.* Adv Neurol, 2005. 95: p. 71-102.

253. Markram, H., et al., *Interneurons of the neocortical inhibitory system.* Nat Rev Neurosci, 2004. 5(10): p. 793-807.

254. Marin, O., *Interneuron dysfunction in psychiatric disorders.* Nat Rev Neurosci, 2012. 13(2): p. 107-20.

255. Sohal, V.S., et al., *Parvalbumin neurons and gamma rhythms enhance cortical circuit performance.* Nature, 2009. 459(7247): p. 698-702.

256. Perreault, P. and M. Avoli, *4-aminopyridine-induced epileptiform activity and a GABA-mediated long-lasting depolarization in the rat hippocampus.* J Neurosci, 1992. 12(1): p. 104-15.

257. Avoli, M., et al., *On the synchronous activity induced by 4-aminopyridine in the CA3 subfield of juvenile rat hippocampus.* J Neurophysiol, 1993. 70(3): p. 1018-29.

258. Avoli, M., et al., *Synchronous GABA-mediated potentials and epileptiform discharges in the rat limbic system in vitro.* J Neurosci, 1996. 16(12): p. 3912-24.

259. Gonzalez-Sulser, A., et al., *Hippocampal neuron firing and local field potentials in the in vitro 4-aminopyridine epilepsy model.* J Neurophysiol, 2012. 108(9): p. 2568-80.

260. Sessolo, M., et al., *Parvalbumin-Positive Inhibitory Interneurons Oppose Propagation But Favor Generation of Focal Epileptiform Activity.* J Neurosci, 2015. 35(26): p. 9544-57.

261. Grosser, S., et al., *Hilar somatostatin interneurons contribute to synchronized GABA activity in an in vitro epilepsy model.* PLoS One, 2014. 9(1): p. e86250.

262. Yekhlef, L., et al., *Selective activation of parvalbumin- or somatostatin-expressing interneurons triggers epileptic seizurelike activity in mouse medial entorhinal cortex.* J Neurophysiol, 2015. 113(5): p. 1616-30.

263. Mattia, D., G.G. Hwa, and M. Avoli, *Epileptiform activity induced by 4-aminopyridine in guinea-pig and rat neocortices.* Neurosci Lett, 1993. 154(1-2): p. 157-60.

264. Misra, S.N., K.M. Kahlig, and A.L. George, Jr., *Impaired NaV1.2 function and reduced cell surface expression in benign familial neonatal-infantile seizures.* Epilepsia, 2008. 49(9): p. 1535-45.

265. Scalmani, P., et al., *Effects in neocortical neurons of mutations of the Na(v)1.2 Na+ channel causing benign familial neonatal-infantile seizures.* J Neurosci, 2006. 26(40): p. 10100-9.

266. Kamiya, K., et al., *A nonsense mutation of the sodium channel gene SCN2A in a patient with intractable epilepsy and mental decline.* J Neurosci, 2004. 24(11): p. 2690-8.

267. Rudy, B., et al., *Three groups of interneurons account for nearly 100% of neocortical GABAergic neurons.* Dev Neurobiol, 2011. 71(1): p. 45-61.

268. Trudeau, M.M., et al., *Heterozygosity for a protein truncation mutation of sodium channel SCN8A in a patient with cerebellar atrophy, ataxia, and mental retardation.* J Med Genet, 2006. 43(6): p. 527-30.

269. Rauch, A., et al., *Range of genetic mutations associated with severe non-syndromic sporadic intellectual disability: an exome sequencing study.* Lancet, 2012. 380(9854): p. 1674-82.

270. Burgess, D.L., et al., *Mutation of a new sodium channel gene, Scn8a, in the mouse mutant 'motor endplate disease'.* Nat Genet, 1995. 10(4): p. 461-5.

271. Papale, L.A., et al., *Heterozygous mutations of the voltage-gated sodium channel SCN8A are associated with spike-wave discharges and absence epilepsy in mice.* Hum Mol Genet, 2009. 18(9): p. 1633-41.

272. Jones, N.A., et al., *Cannabidiol Displays Antiepileptiform and Antiseizure Properties In Vitro and In Vivo.* Journal of Pharmacology and Experimental Therapeutics, 2010. 332(2): p. 569-577.

273. Khaliq, Z.M., N.W. Gouwens, and I.M. Raman, *The contribution of resurgent sodium current to high-frequency firing in Purkinje neurons: An experimental and modeling study.* Journal of Neuroscience, 2003. 23(12): p. 4899-4912.

274. Castelli, L., et al., *Resurgent Na(+) current in pyramidal neurones of rat perirhinal cortex: axonal location of channels and contribution to depolarizing drive during repetitive firing.* Journal of Physiology-London, 2007. 582(3): p. 1179-1193.

275. Xie, W., et al., *Upregulation of the sodium channel NaVbeta4 subunit and its contributions to mechanical hypersensitivity and neuronal hyperexcitability in a rat model of radicular pain induced by local dorsal root ganglion inflammation.* Pain, 2016. 157(4): p. 879-91.

276. Shaw, G., et al., *Preferential transformation of human neuronal cells by human adenoviruses and the origin of HEK 293 cells.* FASEB J, 2002. 16(8): p. 869-71.

277. Bezanilla, F. and R.E. Taylor, *Temperature effects on gating currents in the squid giant axon.* Biophys J, 1978. 23(3): p. 479-84.

278. Volkers, L., et al., *Febrile temperatures unmask biophysical defects in Nav1.1 epilepsy mutations supportive of seizure initiation.* J Gen Physiol, 2013. 142(6): p. 641-53.

279. Thomas, E.A., et al., *Heat opens axon initial segment sodium channels: a febrile seizure mechanism?* Ann Neurol, 2009. 66(2): p. 219-26.

280. Dumaine, R., et al., *Ionic mechanisms responsible for the electrocardiographic phenotype of the Brugada syndrome are temperature dependent.* Circ Res, 1999. 85(9): p. 803-9.

281. Samani, K., et al., *A novel SCN5A mutation V1340I in Brugada syndrome augmenting arrhythmias during febrile illness.* Heart Rhythm, 2009. 6(9): p. 1318-26.

282. Tepper, J.M. and J.P. Bolam, *Functional diversity and specificity of neostriatal interneurons.* Curr Opin Neurobiol, 2004. 14(6): p. 685-92.

283. Bagla, R. and C.T. Skidmore, *Frontal lobe seizures.* Neurologist, 2011. 17(3): p. 125-35.

284. Chauvette, S., et al., *In vivo models of cortical acquired epilepsy.* J Neurosci Methods, 2016. 260: p. 185-201.

285. Avoli, M. and J.G. Jefferys, *Models of drug-induced epileptiform synchronization in vitro.* J Neurosci Methods, 2016. 260: p. 26-32.

286. Fueta, Y. and M. Avoli, *Effects of antiepileptic drugs on 4-aminopyridine-induced epileptiform activity in young and adult rat hippocampus.* Epilepsy Res, 1992. 12(3): p. 207-15.

287. Szente, M. and F. Pongracz, *Aminopyridine-induced seizure activity.* Electroencephalogr Clin Neurophysiol, 1979. 46(5): p. 605-8.

288. Salah, A. and K.L. Perkins, *Persistent ictal-like activity in rat entorhinal/perirhinal cortex following washout of 4-aminopyridine.* Epilepsy Res, 2011. 94(3): p. 163-76.

289. Buzsaki, G., C.A. Anastassiou, and C. Koch, *The origin of extracellular fields and currents--EEG, ECoG, LFP and spikes.* Nat Rev Neurosci, 2012. 13(6): p. 407-20.

290. Yu, S., et al., *Upregulated expression of voltage-gated sodium channel Nav1.3 in cortical lesions of patients with focal cortical dysplasia type IIb.* Neuroreport, 2012. 23(7): p. 407-11.

291. Chen, C., et al., *Mice lacking sodium channel beta1 subunits display defects in neuronal excitability, sodium channel expression, and nodal architecture.* J Neurosci, 2004. 24(16): p. 4030-42.

292. Cummins, T.R., et al., *Nav1.3 sodium channels: rapid repriming and slow closed-state inactivation display quantitative differences after expression in a mammalian cell line and in spinal sensory neurons.* J Neurosci, 2001. 21(16): p. 5952-61.

293. Krook-Magnuson, E., et al., *On-demand optogenetic control of spontaneous seizures in temporal lobe epilepsy.* Nat Commun, 2013. 4: p. 1376.

294. Paz, J.T., et al., *Closed-loop optogenetic control of thalamus as a tool for interrupting seizures after cortical injury.* Nat Neurosci, 2013. 16(1): p. 64-70.

CURRICULUM VITAE

Reesha R. Patel

EDUCATION

Doctor of Philosophy – Indiana University Medical Neuroscience	2010 – 2016
Bachelor of Science – Purdue University Interdisciplinary Studies: Neuroscience	2009 – 2010
Indiana University Bloomington	2006 – 2009

ADDITIONAL EDUCATION

Neural Data Science Course – Cold Spring Harbor Laboratory	July 2015

AWARDS

Larry Kays Fellowship Award	2015
Graduate – Professional Educational Grant	2015
Indiana University School of Medicine Graduate Student Travel Award	2015
Educational Enhancement Grant	2014
American Epilepsy Society: Fellows Award	2014
American Epilepsy Society: Young Investigator Travel Award	2014
Indiana University School of Medicine Graduate Student Travel Award	2014
Bepko Learning Center Physiology Mentor Scholarship	2010

MANUSCRIPTS

Navβ4 regulates fast resurgent sodium currents and excitability in sensory neurons	2015

Cindy Barbosa, Zhi-Yong Tan, Ruizhong Wang, Wenrui Xie, Judith A. Strong, Reesha R. Patel, Michael R. Vasko, Jun-Ming Zhang and Theodore R. Cummins
Molecular Pain, doi: 10.1186/s12990-015-0063-9

Human Nav1.6 generate larger resurgent current than human Nav1.1 channels, but the Navβ4 does not protect either isoform from use-dependent reduction — 2015
Reesha R. Patel, Cindy Barbosa, Yucheng Xiao and Theodore R. Cummins
PLoS One, doi: 10.1371/journal.pone.0133485

MANUSCRIPTS UNDER REVISION

Aberrant epilepsy-associated mutant Nav1.6 sodium channel activity can be targeted with cannabidiol
Reesha R. Patel, Cindy Barbosa, Tatiana Brustovetsky, Nickolay Brustovetsky and Theodore R. Cummins

MANUSCRIPTS IN PREPARATION

Preferential pharmacological inhibition of Nav1.6, but not Nav1.1, abolishes epileptiform activity induced by 4-AP in mouse cortical brain slices
Reesha R. Patel, Xingjie Ping, Shaun R. Patel, Jeffrey L. Krajewski, Jeff S. McDermott, Xiaoming Jin and Theodore R. Cummins

RESEARCH PRESENTATIONS – PODIUM

Enhanced Resurgent Sodium Current Generation by Epilepsy-Associated Mutant Voltage-Gated Sodium Channels can be Targeted with Cannabidiol — Oct 2015, Indianapolis, IN
Reesha R. Patel, Cindy Barbosa, Theodore R. Cummins
Invited Talk – Indiana University School of Medicine

Enhanced Resurgent Sodium Current Generation by Epilepsy-Associated Mutant Voltage-Gated Sodium Channels can be Targeted with Cannabidiol — Nov 2014, Washington, DC
Reesha R. Patel, Cindy Barbosa, Theodore R. Cummins
Society for Neuroscience Meeting

Epilepsy-Associated Mutant Voltage-Gated Sodium Channels alter Resurgent Current Generation that could be Preferentially Targeted with Cannabidiol — July 2014, South Hadley, MA
Reesha R. Patel, Cindy Barbosa, Theodore R. Cummins
Gordon Research Seminar: Ion Channels

RESEARCH PRESENTATIONS – POSTER

Enhanced Resurgent Sodium Current Generation by Epilepsy-Associated Mutant Voltage-Gated Sodium Channels can be Targeted with Cannabidiol — Dec 2014, Seattle, WA
Reesha R. Patel, Cindy Barbosa, Theodore R. Cummins
American Epilepsy Society

Enhanced Resurgent Sodium Current Generation by Epilepsy-Associated Mutant Voltage-Gated Sodium Channels can be Targeted with Cannabidiol — Oct 2014, Bloomington, IN
Reesha R. Patel, Cindy Barbosa, Theodore R. Cummins
Gill Symposium

Enhanced Resurgent Sodium Current Generation by Epilepsy-Associated Mutant Voltage-Gated Sodium Channels can be Targeted with Cannabidiol — Oct 2014, Indianapolis, IN
Reesha R. Patel, Cindy Barbosa, Theodore R. Cummins
Indianapolis Chapter of the Society for Neuroscience Meeting

Epilepsy-Associated Mutant Voltage-Gated Sodium Channels alter Resurgent Current Generation that could be Preferentially Targeted with Cannabidiol — July 2014, South Hadley, MA
Reesha R. Patel, Cindy Barbosa, Theodore R. Cummins
Gordon Research Conference: Ion Channels

RESEARCH SUPPORT

Paul and Carole Stark Neuroscience Research Institute Fellowship — 2011

SOCIETY AFFILIATIONS

American Epilepsy Society — 2014 - 2015

Society for Neuroscience Member — 2011 - Present

American Association for the Advancement of Science Member 2010 – 2011

PROFESSIONAL ACTIVITIES

Member of Central Indiana Science Outreach (CINSO) 2014 - Present